Reduced Rank Filtering in Chaotic Systems with Application in Geophysical Sciences

by

Adel Ahanin

B.Sc. Civil Engineering
Sharif University of Technology, 2000

M.Eng. Civil and Environmental Engineering
Massachusetts Institute of Technology, 2002

Submitted to the Department of Civil and Environmental Engineering
in partial fulfillment of the requirements for the degree of

Doctor of Philosophy

at the

MASSACHUSETTS INSTITUTE OF TECHNOLOGY

September 2008

Signature of Author ……...
Department of Civil and Environmental Engineering
August 15th , 2008

Certified by ……...
Dara Entekhabi
Bacardi and Stockholm Water Foundation Professor of Civil and Environmental Engineering
Thesis Supervisor

Certified by ……...
Dennis B. McLaughlin
H.M. King Bhumibol Professor of Water Resource Management
Thesis Supervisor

Accepted by ……..
Daniele Veneziano
Chairman, Departmental Committee for Graduate Students

Reduced Rank Filtering in Chaotic Systems with Application in Geophysical Sciences

by Adel Ahanin

Submitted to the Department of Civil and Environmental Engineering
on August 15th, 2008 in partial fulfillment of the requirements for
the degree of Doctor of Philosophy in the field of Hydrology

Abstract

Recent technological advancements have enabled us to collect large volumes of geophysical noisy measurements that need to be combined with the model forecasts, which capture all of the known properties of the underlying system. This problem is best formulated in a stochastic optimization framework, which when solved recursively is known as Filtering. Due to the large dimensions of geophysical models, optimal filtering algorithms cannot be implemented within the constraints of available computation resources. As a result, most applications use suboptimal reduced rank algorithms.

Successful implementation of reduced rank filters depends on the dynamical properties of the underlying system. Here, the focus is on geophysical systems with chaotic behavior defined as extreme sensitivity of the dynamics to perturbations in the state or parameters of the system. In particular, uncertainties in a chaotic system experience growth and instability along a particular set of directions in the state space that are continually subject to large and abrupt state-dependent changes. Therefore, any successful reduced rank filter has to continually identify the important direction of uncertainty in order to properly estimate the true state of the system. In this thesis, we introduce two efficient reduced rank filtering algorithms for chaotic system, scalable to large geophysical applications.

Firstly, a geometric approach is taken to identify the growing directions of uncertainty, which translate to the leading singular vectors of the state transition matrix over the forecast period, so long as the linear approximation of the dynamics is valid. The singular vectors are computed via iterations of the linear forward and adjoint models of the system and used in a filter with linear Kalman-based update.

Secondly, the dynamical stability of the estimation error in a filter with linear update is analyzed, assuming that error propagation can be approximated using the state transition matrix of the system over the forecast period. The unstable directions of error dynamics are identified as the Floquet vectors of an auxiliary periodic system that is defined based on the forecast trajectory. These vectors are computed by iterations of the forward nonlinear model and used in a Kalman-based filter.

Both of the filters are tested on a chaotic Lorenz 95 system with dynamic model error against the ensemble Kalman filter. Results show that when enough directions are considered, the filters perform at the optimal level, defined by an ensemble Kalman filter with a very large ensemble size. Additionally, both of the filters perform equally well when the dynamic model error is absence and ensemble filters fail. The number of iterations for computing the vectors can be set a priori based on the available computational resources and desired accuracy.

To investigate scalability of the algorithms, they are implemented in a quasi-geostrophic ocean circulation model. The results are promising for future extensions to realistic geophysical applications, with large models.

Thesis Supervisor: Dara Entekhabi
Title: Bacardi and Stockholm Water Foundation Professor of Civil and Environmental Engineering

Thesis Supervisor: Dennis McLaughlin
Title: H.M. King Bhumibol Professor of Water Resource Management

"As we express our gratitude, we must never forget that the highest appreciation is not to utter words, but to live by them."

– John F. Kennedy

ACKNOWLEDGEMENT

Throughout this research, I was privileged to work with outstanding scholars whose contributions made it possible to successfully complete this thesis. I am deeply indebted to my advisors Professors Dara Entekhabi and Dennis McLaughlin for their continuous support, discerning comments, and probing questions. Moreover, I am grateful to the members of my thesis committee, Professor Paola Malanotte-Rizzoli and Dr. James Hansen for their constructive feedback and invaluable advice. I would like to thank Professors Arnold Heemink and Munther Dahleh for their helpful insight, and also Dr. Steve Meacham for generously providing me with the code for the ocean model. My sincere gratitude goes to the staff at the Parsons lab and the Department of Civil and Environmental Engineering for their commitment to providing the best for innovation and research.

My life in the past six years has been enriched by the many precious moments I shared with individuals I am proud to call friends and family. Without their bounteous support, difficulties during this journey would have been insurmountable.

Finally, I would like to dedicate this thesis to my parents, Soraya and Reza, whose unconditional love and support will always be the keystone of my aspirations.

TABLE OF CONTENTS

LIST OF FIGURE

1 Introduction

1.1 Background and Motivation

Our ability to characterize geophysical systems and to forecast their behavior impacts society in different forms. Decisions to utilize the natural resources are directly influenced by our understanding of the underlying system. In this thesis, we focus on chaotic geophysical systems such as the ocean and the atmosphere, which are characterized by their extreme sensitivity to errors in initial conditions or model parameters. This brings serious difficulties to estimation of the state or the parameters of the system, as well as making predictions about its behavior (Ruelle, 1989; Foale and Thompson, 1991). For example, it was shown that forecasting of the state of atmosphere is limited to two weeks under the most promising conditions (Lorenz, 1963). However, the situation can be considerably improved if frequently available measurements of relevant variables (observations) are combined with the predictions of the model (forecasts) in order to produce improved estimates of the state of the system or its parameters (analysis). Because of the inherent uncertainty in the forecast and observations, this problem is best formulated in a probabilistic framework, widely known as Data Assimilation.

Mathematically speaking, data assimilation solves a Bayesian optimization problem where the expected magnitude of the estimation error, i.e. the distance between the analysis and the truth, is minimized subject to the constraints of the dynamical model of the underlying system and the observation model that relates the observations to the truth. Sequential data assimilation

algorithms aim at solving this optimization problem via recursive assimilation of the observations; thus they are more efficient in assimilating streams of incoming observations (Gelb, 1974). Depending on the time window of the incorporated observations, sequential algorithms are generally categorized as "Smoothing" when the analysis is conditioned on both before and after the estimation time, or "Filtering" when only past observations are used to compute the analysis at a given time. The focus of this thesis is on filtering in geophysical applications, which in general are highly nonlinear and have an enormous state vector with $O(10^6)$ variables. Filtering is particularly appealing for real-time assimilation of the streams of incoming observations and forecasting.

Optimal filtering in linear systems with Gaussian uncertainty is solved by the well-known Kalman Filter (KF). In KF, the analysis is a linear combination of the forecast and the observation, with the linear weights (gain matrix) depending on the forecast error covariance and the observation noise covariance (Gelb, 1974). In the presence of nonlinearity, the uncertainties will not remain Gaussian and higher moments beyond the mean and the error covariance are needed to characterize the distribution of the variables. In fact, finding the optimal solution entails solving the Fokker-Plank equation in order to compute the distribution of the forecast. Generally, this does not have any closed form solutions and is not feasible in large systems (Risken, 1996). Instead, Monte-Carlo-based methods such as the Particle Filter try to solve the optimal Bayesian estimation by approximating the evolved distribution with an ensemble of propagated replicates, model runs with different initial condition, forcing, or parameters drawn from the corresponding distributions (Ristic et al., 2004). However, the large number of replicates needed for the Particle Filter to converge is a practical impediment for its

implementation in large systems. Therefore, optimal filtering in large geophysical systems is not feasible, and the problem must be redefined as solving for a suboptimal solution with reasonable performance.

Because of the simplicity of the linear update scheme in the KF, it has been used in many suboptimal filters mainly designed for quasi-linear systems (Fukumori and Malanotte-Rizzoli, 1995; Cane et al., 1996; Buehner and Malanotte-Rizzoli, 2003; Farrell and Ioannou, 2001; Heemink et al., 2001; Lermusiaux and Robinson, 1999; Pham et al., 1998). In nonlinear systems, again Monte-Carlo-based linear filters such as the Ensemble Kalman Filter (EnKF) are the most popular. In EnKF, an ensemble are random replicates are drawn from the distribution of the initial state and propagated in the nonlinear dynamics. The ensemble's sample mean and covariance are assumed to represent the forecast and its error covariance, and are used in the Kalman linear update scheme (Evensen, 1994, 2003, 2004; Bishop, 2001; Anderson, 2001).

The required number of replicates for convergence of the second order statistics is remarkably smaller than the number needed for the full probability distribution as in the Particle Filter, but implementation of ensemble-based methods in geophysical systems faces some difficulties. Firstly, the required ensemble size for successful implementation of the ensemble methods in geophysical systems with enormous state size is still beyond the capacity of current computational resources. Secondly, it is frequently observed that over a few assimilation cycles the ensemble filter becomes rank deficient in the sense that the ensemble members, which supposedly cover a wide range of possibilities of the truth, start to collapse to a much smaller range than the true uncertainty field (Kalnay, 2003). This is mathematically equivalent to the

loss of mutual independence of the ensemble members and the loss of rank of the ensemble covariance matrix. Rank deficiency is avoided if dynamic model error with enough intensity is added to each replicate to enhance the independence of the ensemble members. Although this will mathematically stabilize the ensemble filters, adding dynamic model error is not a viable option in many geophysical systems such as the ocean and the atmosphere where the dynamics exhibit chaotic behavior. Specifically, additive noise may trigger structural instabilities in such systems, leading to non-physical predictions of the model (Daley, 1991; Fillion, 2002; Neef et al., 2006). A simple demonstration of this issue is given in Appendix A. To avoid this problem, it is common in meteorological and oceanic applications to assume that the dynamic model error is zero, amid ongoing research for appropriate formulation of the dynamic model error.

There are a number of techniques to enhance the rank of the ensemble covariance when dynamic model error is zero. A widely used method is the localization of the correlation information, which is accomplished either by damping the spurious correlations between the distant states (Houtekamer and Mitchell, 2001; Hamill et al., 2001), or by assimilating the observations locally in the physical space (Ott et al., 2006). Localization techniques by construction are suitable only for the spatially extended systems with weak long-range spatial correlations. Otherwise they may eliminate the physically meaningful correlation between distant states. Additionally, localization methods need to be designed for a given system based on its properties and the ensemble size, both of which require an understanding of the system that is often beyond what is available or convenient. Another common technique for resolving the rank deficiency is additive variance inflation, where the variance of different state variables are empirically increased (Anderson, 2007). This approach artificially increases the rank of the ensemble covariance, and

due to its ad hoc nature, is not robust. Thus, although ensemble-based filters provide promising features, they generally face practical limitations in chaotic geophysical systems.

This thesis is motivated by the need for robust filtering algorithms that are designed for chaotic dynamics and are also scaleable to large systems. Two algorithms are introduced that are suitable for such applications. In the first algorithm, the problem is formulated from a geometric point of view and the gain matrix is adaptively computed in a way that the estimation error is continually reduced. The second algorithm focuses on the stability of the error dynamics, leading to a gain matrix that stabilizes the unstable modes of error growth. The computational costs of these methods are also discussed and it is shown that in presence of dynamic model error, their cost is comparable to the cost of the ensemble methods. It is further shown that after a minor modification, both of these algorithms perform well when dynamic model error is zero and ensemble methods fail.

In order to investigate the scalability of the algorithms, both of the algorithms are tested on a chaotic wind-driven reduce-gravity quasi-geostrophic ocean circulation system without dynamic model error. The algorithms are revised modified to enhance the computational efficiency in assimilating a large vector of observations, a common situation in remote sensing applications. Results confirm the ability of the proposed algorithms in tracking the true state of chaotic systems, suggested by experiments on a small Lorenz 95 system.

Additionally, we show in that if the observed states are too few or are not selected properly in the quasi-geostrophic ocean system, an otherwise successful filter will have a poor performance. Our proposed framework for reduced rank filtering provides a mean to a more elaborate analysis

of the observability of the nonlinear systems, which is beyond the scope of this thesis and is left to future research.

In this thesis, performance of the algorithms are demonstrated with models that are structurally stable, meaning that given the convergence of the trajectory of a nominal initial state to an attractor of the system, any perturbed trajectory, whose initial state is slightly different from the nominal initial state will converge to the same attractor. In other words, perturbing the state does not make its trajectory to depart the basin of attraction. The extension to more realistic geophysical systems that may have multiple attractors, possibly exhibiting nonphysical dynamics is an important step, but falls beyond the scope of this work.

1.2 References

Anderson, J. L., 2001: An ensemble adjustment Kalman filter for data assimilation. *Mon. Wea. Rev.*, **129**, pp 2884-2903.

Anderson, J. L., B. Wyman, S. Zhang, and T. Hoar, 2005: Assimilation of surface pressure observations using an ensemble filter in an idealized global atmospheric prediction system. *J. Atmos. Sci.*, **62**, pp 2925-2938.

Anderson, J. L., 2007: An adaptive covariance inflation error correction algorithm for ensemble filters. *Tellus*, **59A**, pp 210-224.

Bishop, C. H., B. J. Etherton, and S. J. Majumdar, 2001: Adaptive Sampling with the Ensemble

Transform Kalman Filter. Part I: Theoretical Aspects. *Mon. Wea. Rev.*, **129**, pp 420-436.

Buehner, M., and P. Malanotte-Rizzoli, 2003: Reduced-rank Kalman filter applied to an idealized model of the wind-driven ocean circulation, *J. Geophys. Res.*, **108**, p 3192

Cane, M., A. Kaplan, R. N. Miller, B. Tang, E. C. Hackert, and A. J. Busalacchi, 1996: Mapping tropical Pacific sea level: Data assimilation via a reduced state space Kalman filter. *J. Geophys. Res.*, **101**, pp 22 599 –22 617.

Daley, R., 1991: *Atmospheric Data Analysis*. Cambridge University Press, UK, p 457.

Evensen, G., 1994: Sequential data assimilation with a nonlinear quasi-geostrophic model using Monte-Carlo methods to forecast error statistics. *J. Geophys. Res.,* **99(C5)**, pp 10 143-10 162.

Evensen, G., 2003: The ensemble Kalman filter: theoretical formulation and practical implementation. *Ocean Dyn.*, **53**, pp 343-367.

Evensen, G., 2004: Sampling strategies and square root analysis schemes for the EnKF. *Ocean Dynamics*, **54**, pp 539-560.

Farrell, B. F., and P. J. Ioannou, 2001: State estimation using a reduced order Kalman filter, *J. Atmos. Sci.*, **58**, pp 3666-3680.

Fillion, L., 2002: Variational Assimilation of precipitation data and gravity wave excitation. *Mon. Wea. Rev.*, **130**, pp 357-371.

Foale, S., and J. M. T. Thompson, 1991: Geometrical concepts and computational techniques of

nonlinear dynamics. *Comp. Methods Appl. Mech. Eng.*, **89**, pp 381-394.

Fukumori, I., and P. Malanotte-Rizzoli, 1995: An approximate Kalman filter for ocean data assimilation: An example with an idealized Gulf stream model, *J. Geophys. Res.*, **100**, pp 6777-6793.

Gelb, A., Ed., 1974: *Applied Optimal Estimation*. The MIT Press, Cambridge, USA.

Hamill, T. M., J. S. Whitaker, and C. Snyder, 2001: Distance-dependent filtering of background error covariance estimates in an ensemble Kalman filter. *Mon. Wea. Rev.*, **129**, pp 2776-2790.

Heemink, A. W., M. Verlaan, and A. J. Segers, 2001: Variance reduced ensemble Kalman filtering. *Mon. Wea. Rev.*, **129**, pp 1718-1728.

Houtekamer, P. L., and H. L. Mitchell, 2001: A sequential ensemble Kalman filter for atmospheric data assimilation. *Mon. Wea. Rev*., **129**, pp 123-137.

Kalnay, E., 2003: *Atmospheric modeling, data assimilation and predictability*. Cambridge University Press, UK, pp 220-248.

Lermusiaux, P. F. J., and A. R. Robinson, 1999: Data assimilation via error subspace statistical estimation. Part I: theory and schemes. *Mon. Wea. Rev.*, **127**, pp 1385-1407.

Lorenz, E. N., 1963: Deterministic non-periodic flow. *J. Atmos. Sci.*, **20**, p 130.

Neef, L. J., S. M. Polavarapu, T. G. Shepherd, 2006: Four-dimensional data assimilation and balanced dynamics. *J. Atmos. Sci.*, **63**, pp 1840-1858.

Ott, E., B. R. Hunt, I. Szunyogh, A. V. Zimin, E. J. Kostelich, M. Corazza, E. Kalnay, D. J. Patil, and J. Yorke, 2006: A local ensemble Kalman filter for atmospheric data assimilation. *Submitted to Mon. Wea. Rev., Revised May 24, 2006.*

Pham, D. T., J. Verron, and M. C. Roubaud, 1998: A singular evolutive extended Kalman filter for data assimilation in oceanography. *J. Marine Sys.*, **16**, pp 323-340.

Risken, H., 1996: *The Fokker-Planck Equation - Methods of Solution and Applications.* Springer, New York, USA.

Ristic, B., S. Arulampalam, and N. Gordon, 2004: *Beyond the Kalman Filter - Particle Filters for Tracking Applications.* Artech House, Boston, USA.

Ruelle, D., 1989: Deterministic Chaos: The Science and the Fiction. *Proc. R. Soc. Lon. Series A, Math. and Phys. Sci.*, **427(1873)**, pp 241-248.

2 A Singular Vector Approach to Suboptimal Filtering in Chaotic Systems

2.1 Introduction

In a wide range of geophysical applications the system under investigation exhibits chaotic behavior, in the sense that two slightly different initial states, such as a true state and a forecast, quickly separate over time, following much different trajectories (Nagashima and Baba, 1999; Ruelle, 1989; Foale and Thompson, 1991). In chaotic systems the true and forecast trajectories will remain inside a bounded region but differences between them may become too large for the forecast to be useful (Lorenz, 1963). These differences may be temporarily reduced if the forecast is updated with measurements, so long as care is taken to insure that the updated states remain physically reasonable. In particular, the update process should be able to identify and deal with rapidly growing errors before they become unacceptably large.

This paper examines some of the distinctive issues that arise in data assimilation for chaotic systems such as a turbulent atmosphere or ocean. Our focus is on computationally efficient reduced rank Kalman filters, which yield updates that are linear combinations of measurements and forecasts. From a geometrical perspective reduced rank filters propagate low rank covariances that are projections of full covariances on a low dimensional subspace of the system state space. These low rank covariances provide a concise characterization of uncertainty. While there are many choices for the reduced rank subspace, some tend to give better performance and

are able to maintain physical constraints better than others. Here we describe a reduced rank filter that projects a portion of the forecast covariance onto a subspace constructed from the leading singular vectors of the state transition matrix (a linearized approximation to the nonlinear state equation). If the measurements used for updating are sufficiently informative and the linearization remains valid the filter updates keep growing errors in check, for both with and without dynamic model error. The subsequent sections describe the singular vector Kalman filter and present some preliminary results obtained for the Lorenz 95 system (Lorenz and Emanuel, 1998).

2.2 Background

2.2.1 Error Growth and Decay in Chaotic Systems

It is useful to begin by considering some of the design constraints encountered in chaotic data assimilation problems We suppose that the system of interest can be completely described by an n-dimensional vector of states represented by $x(t)$ at time t. The state vector $x(t)$ is composed of non-dimensional variables and is related to the vector of dimensional physical variables $\xi(t)$ by the non-singular linear transformation $x(t) = C(t)\xi(t)$. Consequently, the norms used to measure distances in the $x(t)$ and $\xi(t)$ spaces are related as follows:

$$\left\| x(t) \right\| = \sqrt{x^T(t)x(t)} = \sqrt{\xi^T(t)C(t)^T C(t)\xi(t)} = \left\| \xi(t) \right\|_{C^T C} \qquad (2\text{-}1)$$

where $C(t)^T C(t)$ is a positive definite weighting matrix. For simplicity we work with the transformed state $x(t)$ here, recognizing that the choice of the application-specific transformation matrix $C(t)$ has an important influence on the dynamical properties of the state, which will impact the performance of the data assimilation algorithms (Orrell, 2002; Palmer et al., 1998).

We use the superscripts t, f, and a to differentiate the true (unknown), forecast (prior) and analysis (posterior) states. These various states can be viewed geometrically as points in the n-dimensional state space. Differences between states (errors, perturbations, etc.) can be viewed as n-dimensional vectors with characteristic magnitudes and directions. We suppose the true states evolve from time s to time t according to the following state equation:

$$x^t(t) = f\left[x^t(s), t \right] + \omega(t) \tag{2-2}$$

where $f\left[x, t \right]$ is a nonlinear function of the state and $x^t(t)$ represents a multidimensional trajectory through the state space. We assume the initial condition $x^t(t_0)$ at $s = t_0$ is a random vector with a known mean $\overline{x^t(t_0)}$ and covariance $P^t(t_0)$. The dynamic model error $\omega(t)$ is a zero mean temporally uncorrelated random vector with known covariance $Q(t)$. For convenience we assume that $\omega(t)$ and $x^t(t_0)$ are uncorrelated.

Since it is impractical to characterize a full $n \times n$ matrix $Q(t)$ for a large system the dynamic model error covariance is sometimes assumed to have a sparse (e.g. diagonal) structure.

However it can still be difficult to interpret what model error represents if the system of interest is chaotic, especially when this error can generate non-physical trajectories. In such cases $Q(t)$ is often assumed to be zero (i.e. the dynamic model error is zero) and the estimation problem focuses on initial condition uncertainty. Here we consider filtering with and without dynamic model error, represented respectively by a diagonal $Q(t) \neq 0$ and $Q(t) = 0$.

When the nonlinear system defined by (2-2) is chaotic, perturbations around a nominal state may grow or decay. To examine this behavior more precisely we consider points on or near the system attractor A. The attractor is a subset of the state space that has the following properties: 1) $f\left[x(s),t\right]$ is in A if $x(s)$ is in A, 2) there is a neighborhood $B(A)$ of A (commonly called the basin of attraction of A) composed of points that evolve arbitrarily close to A for sufficiently large t, and 3) A is the smallest set that obeys the first two properties.

The neighborhood of a point $x^0(t)$ on the attractor can be divided into stable and unstable manifolds, depending on their long-term temporal behavior (Jaeger and Kantz, 1997). This concept can be adapted to assimilation problems by considering the behavior of small perturbations over the time periods between measurement updates. In particular, consider the evolution between time t and a later time $t+T$ of a perturbation around $x^a(t)$, the updated estimate (or analysis). Suppose that $x^a(t)$ is known at the analysis time t and a forecast $x^f(t+T)$ is derived at the forecast time $t+T$, as follows:

$$x^f(t+T) = f\left[x^a(t), t+T \right] \tag{2-3}$$

In a sequential filtering context the forecast time is the time of the next measurement update.

We define the decaying manifold $W_T^D\left[x^a(t) \right]$ to be the set of perturbations from $x^a(t)$ that decay over the time interval $[t, t+T]$:

$$W_T^D\left[x^a(t) \right] = \left\{ x(t) \in A \,\middle|\, \left\| x(t) - x^a(t) \right\| < \varepsilon, \left\| x(t) - x^a(t) \right\| > \left\| x(t+T) - x^f(t+T) \right\| \right\} \tag{2-4}$$

If the $x(t)$ values in this manifold are interpreted as possible values of the true state $x^t(t)$ the perturbations $x(t) - x^a(t)$ define a set of possible analysis errors $x^t(t) - x^a(t)$ at t.

The manifold of growing forecast errors $W_T^G\left[x^f(t+T) \right]$ is the set of perturbations from $x^f(t+T)$ that have grown over $[t, t+T]$:

$$W_T^G\left[x^f(t+T) \right] = \left\{ x(t+T) \in A \,\middle|\, \left\| x(t+T) - x^f(t+T) \right\| < \varepsilon, \left\| x(t+T) - x^f(t+T) \right\| > \left\| x(t) - x^a(t) \right\| \right\} \tag{2-5}$$

If the $x(t+T)$'s in this manifold are interpreted as possible values of the true state $x^t(t+T)$ the

perturbations $x(t+T)-x^f(t+T)$ define a set of possible forecast errors $x^t(t+T)-x^f(t+T)$ at $t+T$.

It is possible to approximate the manifolds of decaying and growing errors if ε and T are sufficiently small. To do this we divide $[t, t+T]$ into k time steps each of length dt and approximate the forward time evolution as follows:

$$x(t+T)-x^f(t+T)=f\left[x(t),t+T\right]-f\left[x^a(t),t+T\right]\approx F_{t,t+T}\left[x(t)-x^a(t)\right] \tag{2-6}$$

where $F_{t,t+T}$ is an $n\times n$ state transition matrix defined by:

$$F_{t,t+T}=F_{t,t+kdt}=F_{t+(k-1)dt,t+kdt}\times\cdots\times F_{t+dt,t+2dt}\times F_{t,t+dt} \tag{2-7}$$

and each term on the right hand side, $F_{\tau,\tau+dt}=\left.\dfrac{\partial f\left[x(\tau),\tau+dt\right]}{\partial x}\right|_{x(\tau)}$ is an $n\times n$ Jacobian matrix (or propagator) evaluated at $x(\tau)$, the best estimate of the state, which is the forecast except just after an update, when it is the analysis.

The state transition matrix may be characterized by its singular value decomposition:

$$F_{t,t+T}=U_{t,t+T}\Sigma_{t,t+T}V_{t,t+T}^T \tag{2-8}$$

where $U_{t,t+T}$ and $V_{t,t+T}$ are matrices with columns consisting of the left and right singular vectors

of $F_{t,t+T}$, respectively, and $\Sigma_{t,t+T}$ is a diagonal matrix of ordered singular values $\sigma_1 \geq \sigma_2 \geq \cdots \geq \sigma_N \geq 1 > \cdots \geq \sigma_n$. Let the N leading columns of $U_{t,t+T}$ and $V_{t,t+T}$ which correspond to $\sigma_1, \cdots, \sigma_N$ be placed as columns of $U^N_{t,t+T}$ and $V^N_{t,t+T}$, respectively, and the remaining columns of $U_{t,t+T}$ and $V_{t,t+T}$ be placed as columns in $U^{n-N}_{t,t+T}$ and $V^{n-N}_{t,t+T}$. In this case (2-8) can be rewritten as:

$$F_{t,t+T} = \left[U^N_{t,t+T} \middle| U^{n-N}_{t,t+T} \right] \begin{bmatrix} \Sigma^N_{t,t+T} & 0 \\ 0 & \Sigma^{n-N}_{t,t+T} \end{bmatrix} \left[V^N_{t,t+T} \middle| V^{n-N}_{t,t+T} \right]^T \tag{2-9}$$

where $\Sigma^N_{t,t+T}$ and $\Sigma^{n-N}_{t,t+T}$ are diagonal matrixes. In practice the singular vectors and singular values of $F_{t,t+T}$ can be computed following the procedure outlined in Appendix A, without actually forming and storing $F_{t,t+T}$.

In order to facilitate discussion of the geometrical aspects of error growth we define the column space of a matrix as the space spanned by its columns, which can be viewed as vectors in the state space. When the linearization of (2-6) applies perturbations at t lying in the column space E^{n-N}_t of $V^{n-N}_{t,t+T}$ will decay to smaller perturbations at $t+T$ that lie in the column space of $U^{n-N}_{t,t+T}$. Similarly, small perturbations at t lying in the column space of $V^N_{t,t+T}$ will grow to larger perturbations at $t+T$ that lie in the column space E^N_{t+T} of $U^N_{t,t+T}$. These relationships provide a practical characterization of the decaying and growing manifolds. When certain regularity conditions hold E^{n-N}_t is tangent to the manifold $W^D_T\left[x^a(t)\right]$ of decaying analysis errors while

E_{t+T}^{N} is tangent to the manifold $W_T^G[x^f(t+T)]$ of growing forecast errors (Jaeger and Kantz, 1997). The relationships between the singular vectors and the spaces E_t^{n-N} and E_{t+T}^{N} are illustrated in Figure 2-1.

The singular vectors of the state transition matrix provide a convenient characterization of error growth and decay so long as the linear approximations they rely upon are valid (Mukougawa et al., 1991). In chaotic systems the use of singular vectors to describe growing and decaying directions may break down at bifurcations and at certain other points on the attractor (Palis and Takens, 1993; Kraut and Grebogi, 2004; Robert et al., 2000; Schroer et al., 1998). However, singular vectors can provide valuable information about nonlinear dynamical properties in many situations of practical interest. We consider how singular vectors can be used to construct efficient and accurate reduced rank filters after reviewing some of the properties of linear update algorithms.

2.2.2 Properties of Linear Updating Procedures

With the distinctions between growing and decaying errors in mind we can now examine the structure of a sequential data assimilation algorithm that uses a linear update to derive state estimates. We assume that the observations used at update time t are assembled in the m-dimensional vector, $y(t)$ which is a linear function of the true state:

$$y(t) = H(t)\, x^t(t) + \upsilon(t) \tag{2-10}$$

where $H(t)$ is an $m \times n$ observation matrix, the measurement error $\upsilon(t)$ is a zero mean random vectors with known covariance $R(t)$, which is mutually uncorrelated with both $x^t(t_0)$ and $\omega(t)$.

The forecast and analysis equations for a sequential filter with a linear update are:

$$x^f(t+T) = f\left[x^a(t), t+T\right] \tag{2-11}$$

$$x^a(t) = x^f(t) + K(t)\left[y(t) - H(t)x^f(t)\right] \tag{2-12}$$

where $K(t)$ is an $n \times m$ weighting (or gain) matrix and the filter is initialized with $x^a(t_0) = \overline{x^t(t_0)}$.

The algorithm uses the nonlinear function $f\left[x^a(t), s\right]$ in (2-11) to propagate the analysis $x^a(t)$ at time t forward to give a forecast $x^f(s)$ at some time $s > t$. When $s = t + T$ the forecast is updated in (2-12) with the measurement $y(t)$.

The weighting matrix used in a linear filtering algorithm can be derived in a number of different ways. One option is to select the gain to minimize the expected value of the Euclidean norm of the analysis error. When the measurements are linear functions of the states and the system dynamics are also linear, this norm yields the Kalman Filter (KF) (Gelb, 1974), which uses the following gain:

$$K(t) = P^a(t)H(t)^T R(t)^{-1} = P^f(t)H(t)^T \left[H(t)P^f(t)H(t)^T + R(t) \right]^{-1} \quad (2\text{-}13)$$

The analysis error covariance matrix $P^a(t)$ required in (2-13) can be computed from the forecast error covariance $P^f(t)$ as follows:

$$P^a(t) = P^f(t) - P^f(t)H(t)^T \left[H(t)P^f(t)H(t)^T + R(t) \right]^{-1} H(t)P^f(t) \quad (2\text{-}14)$$

and the forecast error covariance is computed from the previous analysis covariance using the following covariance propagation equation:

$$P^f(t+T) = F_{t,t+T}P^a(t)F_{t,t+T}^T + Q(t+T) = \tilde{P}^f(t+T) + Q(t+T) \quad (2\text{-}15)$$

where $P^a(t_0) = P^t(t_0)$, $F_{t,t+T}$ is the state transition matrix over $[t, t+T]$, and we have defined $\tilde{P}^f(t+T) = F_{t,t+T}P^a(t)F_{t,t+T}^T$. The covariance $\tilde{P}^f(t+T)$ may be viewed as the portion of the total forecast covariance due only to uncertainties in the previous analysis. Note that $P^f(t+T)$ includes the effect of model error but $\tilde{P}^f(t+T)$ does not.

When the dynamics and/or the observation operator are nonlinear, the linearized expressions in (2-13)-(2-15) may be adopted as approximations, giving the classical extended Kalman filter (EKF) (Miller et al., 1994; Miller et al., 1999; Picard, 1991, Ide and Ghil, 1997a and 1997b). Here, we assume that the observation operator is linear as in (2-10) and focus only on nonlinear dynamics. The approximation in (2-15) is useful for a chaotic system only if the state transition

matrix $F_{t,t+T}$ is recomputed with a sufficiently small dt to track the continually changing directions of error growth and decay. This can be computationally demanding for the large nonlinear systems of most interest in geophysical applications.

The computational difficulties encountered with covariance propagation and updating can be mitigated if some of the matrices used in the filter algorithm are replaced by reduced rank approximations. Reduced rank versions of Kalman filtering have been described by Fukumori and Malanotte-Rizzoli (1995), Cane et al. (1996), Buehner and Malanotte-Rizzoli (2003), Farrell and Ioannou (2001), Heemink et al. (2001), Lermusiaux and Robinson (1999), Pham et al. (1998), Ubaldi et al. (2005), Ubaldi and Travisan (2006), and Evensen (2003, 2004). Here we use a reduced rank approximation of $F_{t,t+T}$ to compute $\widetilde{P}^f(t+T)$ in (2-15). By contrast, most other reduced rank approaches are based on approximations of $P^f(t+T)$.

It is useful to consider the impact of a reduced rank approximation on the Kalman update both with and without model error. The update from forecast to analysis given in (2-12) must lie in the column space of the Kalman gain $K(t)$. If we assume that $R(t)$ has a full rank of m the column space of $K(t)$ lies in the column space of the product $P^f(t)H(t)^T$. This implies that the space of updates depends on both $P^f(t)$ and $H(t)^T$, but has in any case a dimension no larger than m, the number of measurements. If $P^f(t)$ is full rank only the measurement network described by $H(t)$ constrains the update subspace, which has dimension m. If $P^f(t)$ has rank $r < n$ the update subspace may be further constrained by the rank reduction procedure. When the measurement network is properly matched to the reduced rank forecast covariance the update

subspace dimension attains its maximum value of $\min(r,m)$. By contrast, if the errors accounted for in the reduced rank forecast covariance cannot be observed (e.g. if the columns of $H(t)^T$ are orthogonal to those of $P^f(t)$) the Kalman gain is zero and no updates are made.

If dynamic model error is zero ($Q(t+T)=0$) then $P^f(t+T)=\widetilde{P}^f(t+T)$ and a reduced rank approximation of $\widetilde{P}^f(t)$ has the same impact on the update subspace as a reduced rank approximation of $P^f(t)$. If model error is included, if $Q(t+T)$ is full rank, and if a reduced rank approximation is only applied to $\widetilde{P}^f(t)$ then $P^f(t)$ is full rank and the update subspace will have dimension m. In this case the full rank $P^f(t)$ accounts for uncertainty contributed by all the model errors but it only accounts for uncertainty in the propagated analysis errors that lie in the column space of $\widetilde{P}^f(t)$.

This discussion suggests that it is advisable to reduce the rank of $\widetilde{P}^f(t)$ rather than $P^f(t)$ when model errors are included, so that the filter will be able to correct these errors in the update step. We shall see in Section 2.3 that this can be done without sacrificing the computational benefits of the reduced rank approach. Moreover, since model errors are properly accounted for we can focus on propagated analysis errors when selecting the column space of $\widetilde{P}^f(t)$. A reasonable design criterion is to require that the column vectors of $\widetilde{P}^f(t)$ lie in the space E^N_{t+T} of growing errors described in section 2.1. Then the filter will be able to update all growing analysis errors, provided that $P^f(t)H(t)^T$ has rank $r \geq N$. It should be noted that the growing singular vectors that define E^N_{t+T} are always changing in a chaotic system, so that errors that are growing at one

time may soon decay and vice versa. If transient growing errors are missed in the update the filter may still be able to track the true trajectory. However, since it is difficult to know how large growing errors will become before they may decay, a conservative approach is to design the filter so that it can update all growing errors. This objective will be achieved if $r \geq N$, $m \geq N$, $P^f(t)H(t)^T$ has rank $r \geq N$, the column space of $\widetilde{P}^f(t)$ projects onto E^N_{t+T}, and updates are sufficiently frequent to justify linearization assumptions. These requirements form the basis for the singular vector Kalman filter (SVKF) described in Section 2.3.

In order to introduce some of the issues that arise in applications of reduced rank filtering to chaotic systems it is useful to review one of the most popular reduced rank alternatives, the ensemble Kalman filter (EnKF) (Evensen, 1994, 2003, 2004; Bishop et al., 2001, Anderson, 2001). The EnKF uses (2-2) to propagate through time a set of r random analysis perturbations $x^a(t_0)$ generated at t_0 with the specified initial state mean and covariance. Each replicate is updated according to (2-13) and (2-14) at the analysis times, with $P^a(t)$ estimated from the forecast perturbations. If dynamic model error is included additional random perturbations are added to the forecasts between analysis times. In this case the $r < N$ dimensional update subspace at any given time is random (i.e. it is different for every replicate) (Paul, 2007).

It is important to consider the temporal behavior of the subspace spanned by the forecast perturbations generated by any reduced rank filter, including the ensemble Kalman filter. This can be done by constructing a matrix $L^f(t+T)$ with column j given by $L^{fj}(t+T) = \delta x^{fj}(t+T)$. This matrix is a square root of the reduced rank forecast covariance. A number of investigators

have observed that the rank of $L^f(t+T)$ tends to decrease as T increases if model error is not included (i.e. if $Q(t)=0$), indicating an increase in linear dependence among the propagated vectors. This is true for linear as well as nonlinear systems and can occur even if $L^f(t+T)$ is initially full rank. The loss of rank occurs because independent perturbation vectors propagated through deterministic dynamics eventually all line up with the leading Lyapunov vector (Kalnay, 2003). This convergence to the Lyapunov vector can still occur even if the propagation is interrupted by linear updates that periodically rotate and rescale the vectors, as is done in reduced rank versions of the ensemble Kalman filter.

Loss of rank in an ensemble Kalman filter manifests itself as ensemble collapse -- the tendency for all the random replicates to converge to a single vector. In this case, there is no variability around the ensemble mean and measurements only have an effect in the direction of the single remaining replicate. Ensemble collapse has important implications for ensemble filters that are applied to chaotic systems such as those encountered in meteorology. When there are many independent perturbations and the ensemble subspace has a higher dimension than $W_T^G\left[x^f(t+T)\right]$ it is likely that this subspace contains projections of all growing directions. However, if the perturbations lose their independence and the ensemble collapses the dimension of the ensemble subspace will decrease until one or more growing directions in $W_T^G\left[x^f(t+T)\right]$ are missed (i.e. they no longer project onto the ensemble subspace). As the ensemble collapses further the subspace dimension approaches one and the filter diverges.

Rank loss may usually be prevented if dynamic model error of sufficient intensity is included when the vectors are propagated through (2-2). If the model errors have projections on all directions in the state space propagated vectors that are perturbed with these errors at every time step will not collapse to a single direction. This is one reason why most applications of sequential filtering to non-chaotic systems include dynamic model error in the forecast step.

In an ensemble Kalman filter dynamic model error can be included by adding random perturbations to the state equation. Unfortunately, such perturbations can induce non-physical anomalies or imbalances. This is a serious problem in numerical weather prediction, where small perturbations in model states can generate spurious inertial or gravity waves (Barwell and Bromley, 1988, Daley, 1991, Gauthier and Thépaut, 2001, Fillion, 2002, Neef et al., 2006). In effect, the model error perturbation drives forecast vectors off the attractor into regions of the state space where they follow non-physical trajectories. For this reason, most ensemble filters used in meteorological data assimilation applications do not include dynamic model error and use other methods to deal with ensemble collapse (Houtekamer and Mitchell, 2001; Hamill et al., 2001; Anderson and Anderson, 1999; Pereira and Berre, 2006; Gaspari and Cohn, 1999). While such methods may be effective in certain situations the conflict between ensemble collapse (when model error is ignored) and imbalance (when model error is included) makes the EnKF problematic in some important application areas.

The implementation of a reduced rank filter based on singular vectors depends strongly on the norm used to define the magnitude of perturbations. In some cases, different norms may be specified at the analysis and forecast times. For example, if the analysis and forecast norms are

chosen as described in Ehrendorfer and Tribbia (1997) and there is no dynamic model error the most rapidly growing singular vectors align with the leading eigenvectors of the forecast covariance (the directions of largest uncertainty). These vectors are commonly called the Hessian singular vectors since they can be derived from the Hessian of a variational objective function (Barkmeijer et al., 1999). Fisher (2001) describes a simplified Kalman filter based on Hessian singular vectors.

The new singular vector Kalman filter proposed here is based on the leading singular vectors of the state transition matrix described in Section 2.2.1 rather than the forecast covariance eigenvectors. These singular vectors are used to derive the projection of the forecast covariance is filter is designed to insure that the Kalman update at $t+T$ accounts for uncertainties in the subspace E_{t+T}^{N} of growing errors spanned by the columns of $U_{t,t+T}^{N}$. In addition to focusing on growing errors our SVKF deals explicitly with the rank deficiency problems that arise when dynamic model error is neglected. The SVKF is described in Section 2.3 and tested in a set of computational experiments in Section 2.4.

2.3 The Singular Vector Kalman Filter

In this section, we present the formulation of a reduced rank Kalman Filter that updates in the space of growing errors. We assume that the state vector is already normalized by a chosen positive definite deterministic matrix as discussed in Section 2.2.1 and use a simple Euclidean norm. The forecast and analysis equations are exactly as in (2-11) and (2-12) but the Kalman gain is derived from a low rank approximation to the analysis covariance square root matrix

(Andrews, 1968). The square root approach in our formulation avoids explicit calculation of large analysis and forecast covariance matrices and also has an enhanced numerical precision.

A square root formulation is more attractive when the square roots $\sqrt{R(t)}$ and $\sqrt{Q(t)}$ of the noise covariance matrices $R(t)$ and $Q(t)$ are easy to compute. Here we assume that $Q(t)$ is full rank and diagonal so $\sqrt{Q(t)}$ is an $n \times n$ diagonal matrix. We assume that $m << n$ and that $\sqrt{R(t)}$ may be readily computed from a singular value decomposition of $R(t)$. Both of these assumptions can be relaxed at the expense of complicating the algorithm.

The square root algorithm for computing the Kalman gain can be expressed as a recursion which is initialized at a specified time $t = 0$ and repeated at each subsequent measurement (or analysis) time. For simplicity of notation we assume that the time between measurements is fixed at T. We start by defining rank $N < n$ square roots $L^a(t) = \sqrt{P^a(t)}$ and $L^f(t) = \sqrt{P^f(t)}$ of the analysis and forecast covariance matrices, which have the same column spaces as $P^a(t)$ and $P^f(t)$:

$$\begin{aligned} P^a(t) &= L^a(t)L^a(t)^T \\ P^f(t) &= L^f(t)L^f(t)^T \end{aligned} \qquad \text{(2-16)}$$

With these definitions, we can develop square root versions of the classic update and propagation equations of (2-13) through (2-15), with t indicating the initial time or the most recent analysis time and $t + T$ indicating the next analysis time:

Forecast from time t to $t + T$:

$$L^f(t+T)=\left[\tilde{L}^f(t+T)\middle|\sqrt{Q(t+T)}\right] \tag{2-17}$$

where | indicates concatenation of two dimensionally consistent matrices and

$$\tilde{L}^f(t+T)=\left[U^N_{t,t+T}(U^N_{t,t+T})^T\right]F_{t,t+T}L^a(t)=U^N_{t,t+T}\Sigma^N_{t,t+T}\left(V^N_{t,t+T}\right)^T L^a(t) \tag{2-18}$$

Update at time $t+T$:

$$K(t+T)=L^a(t+T)L^a(t+T)^T H(t+T)^T R(t+T)^{-1} \tag{2-19}$$

where:

$$L^a(t+T)=L^f(t+T)-\Psi(t+T)H(t+T)L^f(t+T) \tag{2-20}$$

$$\Psi(t+T)=L^f(t+T)\left[H(t+T)L^f(t+T)\right]^T\sqrt{Z(t+T)}^{-T}\left[\sqrt{Z(t+T)}+\sqrt{R(t+T)}\right]^{-1} \tag{2-21}$$

$$Z(t+T)=\left[H(t+T)L^f(t+T)\right]\left[H(t+T)L^f(t+T)\right]^T+R(t+T) \tag{2-22}$$

In this algorithm the term $\tilde{L}^f(t+T)$ in (2-17) and (2-18) is the projection of the propagated analysis square root covariance $F_{t,t+T}L^a(t)$ onto the subspace of growing perturbations (the column space of $U^N_{t,t+T}$). The augmented term $\sqrt{Q(t+T)}$ in (2-17) accounts for the effect of dynamic model error and insures that (2-17) and (2-18) are equivalent to (2-15). The resulting

expression for the reduced rank square root forecast covariance $L^f(t+T)$ is consistent with our requirement that all growing perturbations are included in the forecast covariance column space. The rest of the algorithm is compatible with classic Kalman filtering algorithms. In particular, (2-19) is the same as (2-13) and (2-20)-(2-22) are the square root equivalent of (2-14) following Andrews (1968) and also shown in appendix C.

For computational efficiency the above expressions are modified to take advantage of the rank deficiency of several large matrices. This avoids the need to compute or store any matrices with more than $\max(m, N)$ columns (where it is presumed that $N << n$ and $m << n$). The resulting recursion is described by the following equations:

1. Initialization:

   - $f[\cdot]$, $H(t)$, $\sqrt{Q(t)}$, and $\sqrt{R(t)}$ specified for all $t > 0$

   - $x^a(0)$ and $L_0^a = \sqrt{P^a(0)}$ is specified (e.g. as a given diagonal matrix) or derived from a specified set of column vectors (e.g. random ensemble replicates). Number of columns p will generally be less than n.

At each time ($t = 0, T, 2T, \cdots$):

2. Compute the forecast by (2-11):

$$x^f(t+T) = f\left[x^a(t), t+T\right]$$

3. Compute a truncated singular value decomposition (SVD) of the state transition matrix $F_{t,t+T}$, using the procedure described in Appendix A.

   This procedure iterates linear forward and adjoint integrations of the nonlinear model around the forecast trajectory over $[t, t+T]$ to compute the leading singular vectors and associated singular values of the state transition matrix. The matrix $F_{t,t+T}$ does not have to be calculated or stored. The SVD matrices produced at time t are $U^N_{t,t+T}$ $V^N_{t,t+T}$, and $\Sigma^N_{t,t+T}$.

4. Compute the matrix $\Gamma_{t,t+T}$:

   If $t = 0$: $\Gamma_{0,T} = (V^N_{0,T})^T L^a_0$, $Dim[\Gamma_{0,T}] = N \times p$ (2-23)

   p = number of vectors used to construct L^a_0

   If $t > 0$: $\Gamma_{t,t+T} = \left[\left(V^N_{t,t+T}\right)^T \tilde{L}^a(t) \,\middle|\, \Phi(t) \right]$, $Dim[\Gamma_{t,t+T}] = N \times (N+n)$ (2-24)

   $\tilde{L}^a(t), \Phi(t)$ from previous cycle

5. Compute $\tilde{\Gamma}_{t,t+T}$, an equivalent to $\Gamma_{t,t+T}$ in the sense that $\Gamma_{t,t+T}\Gamma_{t,t+T}{}^T = \tilde{\Gamma}_{t,t+T}\tilde{\Gamma}_{t,t+T}{}^T$, based on an SVD of $\Gamma_{t,t+T}$, $Dim[\tilde{\Gamma}_{t,t+T}] = N \times N$.

6. Compute $\tilde{L}^f(t+T)$, $Dim[\tilde{L}^f(t+T)] = n \times N$:

$$\widetilde{L}^{f}(t+T)=U^{N}_{t,t+T}\Sigma^{N}_{t,t+T}\widetilde{\Gamma}_{t,t+T} \tag{2-25}$$

7. Compute $Z(t+T)$ in a revised form of (2-22), $Dim\,[Z(t+T)]=m\times m$:

$$Z(t+T)=\left[H(t+T)\widetilde{L}^{f}(t+T)\right]\left[H(t+T)\widetilde{L}^{f}(t+T)\right]^{T}+$$
$$\left[H(t+T)\sqrt{Q(t+T)}\right]\left[H(t+T)\sqrt{Q(t+T)}\right]^{T}+R(t+T) \tag{2-26}$$

8. Compute $\Psi(t+T)$ in a revised form of (2-21), $Dim\,[\Psi(t+T)]=n\times m$:

$$\Psi(t+T)=\left\{\widetilde{L}^{f}(t+T)\left[H(t+T)\widetilde{L}^{f}(t+T)\right]^{T}+\sqrt{Q(t+T)}\left[H(t+T)\sqrt{Q(t+T)}\right]^{T}\right\}\cdot$$
$$\sqrt{Z(t+T)}^{-T}\left[\sqrt{Z(t+T)}+\sqrt{R(t+T)}\right]^{-1} \tag{2-27}$$

9. Compute $\widetilde{L}^{a}(t+T)$, $Dim\,[\widetilde{L}^{a}(t+T)]=n\times N$:

$$\widetilde{L}^{a}(t+T)=\widetilde{L}^{f}(t+T)-\Psi(t+T)\left[H(t+T)\widetilde{L}^{f}(t+T)\right] \tag{2-28}$$

10. Compute $\Xi(t+T)$, $Dim\,[\Xi(t+T)]=m\times n$:

$$\Xi(t+T)=\left[H(t+T)\sqrt{Q(t+T)}\right]-\left[H(t+T)\Psi(t+T)\right]\left[H(t+T)\sqrt{Q(t+T)}\right] \tag{2-29}$$

11. Compute $K(t+T)$, $Dim\,[K(t+T)] = n \times m$:

$$K(t+T) = \tilde{L}^a(t+T)\left[H(t+T)\tilde{L}^a(t+T) \right]^T R(t+T)^{-1} + \sqrt{Q(t+T)}\Xi(t+T)^T\ R(t+T)^{-1} - \Psi(t+T)H(t+T)\sqrt{Q(t+T)}\Xi(t+T)^T\ R(t+T)^{-1} \quad (2\text{-}30)$$

12. Compute updated estimate (analysis):

$$x^a(t+T) = x^f(t+T) + K(t+T)\left[y(t+T) - H(t+T)x^f(t+T) \right] \quad (2\text{-}31)$$

13. Compute $\Phi(t+T)$ (for next cycle), $Dim\,[\Phi(t+T)] = N \times n$:

$$\Phi(t+T) = \left(V^N_{t+T,t+2T}\right)^T \sqrt{Q(t+T)} - \left(V^N_{t+T,t+2T}\right)^T \Psi(t+T)H(t+T)\sqrt{Q(t+T)} \quad (2\text{-}32)$$

14. Exit or return to Step 2.

Appendix B shows that this recursion gives the same Kalman gain as (2-19).

The recursion algorithm simplifies greatly when model errors can be neglected and $Q(t) = 0$. In that case it becomes:

1. Initialization:

   - $f[\cdot]$, $H(t)$, and $\sqrt{R(t)}$ specified for all $t > 0$.

- $x^a(0)$ and $L_0^a = \sqrt{P^a(0)}$ specified or derived.

At each time ($t = 0, T, 2T, \cdots$):

2. Compute forecast by (2-11):

$$x^f(t+T) = f\left[x^a(t), t+T\right]$$

3. Compute singular value decomposition (SVD) of the state transition matrix $F_{t,t+T}$, using the procedure described in Appendix A. The SVD matrices produced at time t are $U^N_{t,t+T}$, $V^N_{t,t+T}$, and $\Sigma^N_{t,t+T}$.

4. Compute the matrix $\Gamma_{t,t+T}$:

If $t = 0$: $\Gamma_{0,T} = (V^N_{0,T})^T L^a_0$, $Dim[\Gamma_{0,T}] = N \times p$ (2-33)

p = number of vectors used to construct L^a_0

If $t > 0$: $\Gamma_{t,t+T} = \left[\left(V^N_{t,t+T}\right)^T L^a(t) \;\middle|\; \Lambda(t+T)\right]$, $Dim\,[\Gamma_{t,t+T}] = N \times (N+n)$ (2-34)

$L^a(t)$ from previous cycle and $\Lambda(t+T)$ is a correction term explained below. This term, which is not included in the general recursion, accounts for growing errors that are missed in the SVD truncation process in the case without dynamic model error:

$$\Lambda(t+T) = \left(V_{t,t+T}^{N}\right)^{T}\left[I - \Omega(t)\,\Omega(t)^{T} \right] r(t) \tag{2-35}$$

$\Omega(t) =$ an orthogonal matrix with the same column space as $L^{a}(t)$

$r(t) =$ a scalar

5. Compute $\widetilde{\Gamma}_{t,t+T}$, which is equivalent to $\Gamma_{t,t+T}$ in the sense that $\Gamma_{t,t+T}\Gamma_{t,t+T}^{\ T} = \widetilde{\Gamma}_{t,t+T}\widetilde{\Gamma}_{t,t+T}^{\ T}$, based on an SVD of $\Gamma_{t,t+T}$, $Dim\,[\widetilde{\Gamma}_{t,t+T}] = N \times N$.

6. Compute $L^{f}(t+T)$, $Dim\,[L^{f}(t+T)] = n \times N$:

$$L^{f}(t+T) = U_{t,t+T}^{N}\Sigma_{t,t+T}^{N}\widetilde{\Gamma}_{t,t+T} \tag{2-36}$$

7. Compute $Z(t+T)$, $Dim\,[Z(t+T)] = m \times m$:

$$Z(t+T) = \left[H(t+T)L^{f}(t+T) \right]\left[H(t+T)L^{f}(t+T) \right]^{T} + R(t+T)\text{`} \tag{2-37}$$

8. Compute $L^{a}(t+T)$, $Dim\,[L^{a}(t+T)] = n \times N$:

$$L^{a}(t+T) = L^{f}(t+T)\,\Pi^{a}(t+T) \tag{2-38}$$

where $Dim\,[\Pi^{a}(t+T)] = N \times N$ and:

$$\Pi^{a}(t+T) = I_{N\times N} - \left[H(t+T)L^{f}(t+T) \right]^{T}\sqrt{Z(t+T)}^{-T}\left[\sqrt{Z(t+T)} + \sqrt{R(t+T)} \right]^{-1}$$

$$\left[H(t+T)\tilde{L}^f(t+T) \right] \tag{2-39}$$

9. Compute $K(t+T)$, $Dim\,[K(t+T)] = n \times m$:

$$K(t+T) = L^a(t+T)\left[H(t+T)L^a(t+T) \right]^T R(t+T)^{-1} \tag{2-40}$$

10. Compute updated estimate (analysis):

$$x^a(t+T) = x^f(t+T) + K(t+T)\left[y(t+T) - H(t+T)x^f(t+T) \right] \tag{2-41}$$

11. Exit or return to Step 2.

The correction term that appears in (2-34) is needed to account for the fact that errors that were formerly decaying but start to grow can be missed if the model error covariance is zero. To see this it is useful to consider three successive update times $t-T$, t, and $t+T$. The update at time t is able to handle errors that grow between $t-T$ and t and lie in the column space of $U^N_{t-T,t}$. Now consider an error ε that was decaying between $t-T$ and t but starts growing between t and $t+T$. This error lies in the column space of $V^N_{t,t+T}$ at time t (because it is starting to grow) but it also lies in $U^{n-N}_{t-T,t}$ (because it was previously decaying). Since it lies in the column space of $U^{n-N}_{t-T,t}$ the error ε is orthogonal to the column spaces of $U^N_{t-T,t}$, $L^f(t)$ and $L^a(t)$ (note that (2-36) and (2-38) imply that the column space of $L^a(t)$ lies in the column space of $L^f(t)$, which lies in

the column space of $U^N_{t-T,\,t}$). Consequently, $L^a(t)$ has no projection along ε and the filter effectively assumes zero uncertainty in the ε direction.

Between t and $t+T$ the error ε is growing rather than decaying. However, the filter will not correct this error at $t+T$, even though it is known to be growing and to lie in the column spaces of $U^N_{t,\,t+T}$ and $L^f(t+T)$. This is because there is no projection of ε onto $L^a(t)$ and therefore no projection onto $\Gamma_{t,t+T}$ (see (2-34) for $\Lambda(t+T)=0$). If model error were included ε would project onto $L^f(t+T)$ at $t+T$ even though it has zero magnitude at t. The correction term $\Lambda(t+T)$ is designed to compensate for the absence of model error so ε will project onto $\Gamma_{t,t+T}$ at $t+T$ if it is in the column space of $U^N_{t,t+T}$.

To derive $\Lambda(t+T)$ define $\Omega(t)$ to be an orthogonal matrix that has the same column space as $L^a(t)$. Then the expression $\left[I_n-\Omega(t)\Omega(t)^T\right]r(t)$ defines a set of column vectors that lie in the null space of $L^a(t)$ and have magnitudes proportional to the specified scalar $r(t)$. This scalar weighting factor can be viewed as a representative standard deviation for uncertainties that are decaying at t but are not resolved in the reduced rank filter.

When $\left[I_n-\Omega(t)\Omega(t)^T\right]r(t)$ is propagated forward to $t+T$ using the SVD of $F_{t,t+T}$ the result is the augmentation of $\Lambda(t+T)$ from (2-35) in (2-34). Note that the column space of this correction term lies in the column space of $U^N_{t,\,t+T}$ (errors growing between t and $t+T$) but is

proportional to postulated uncertainties in the column space of $U_{t-T,t}^{n-N}$ (errors decaying between $t-T$ and t).

The scalar $r(t)$ should be selected to be large enough to insure that some uncertainty is assigned to decaying errors that may start growing but small enough to insure that the modified filter does not exaggerate the model's uncertainty. In the application discussed here it is reasonable to relate $r(t)$ to the level of measurement error uncertainty, which provides a rough upper bound for the uncertainty in unresolved decaying errors:

$$r(t) = \text{max singular value}\left[H^{+}(t)\sqrt{R(t)}\right] \tag{2-42}$$

where $H^{+}(t)$ is the $n \times m$ pseudo-inverse of $H(t)$. In other applications, a better $r(t)$ based on a stricter bound may be used.

2.4 Assimilation Experiments with the Lorenz 95 system

In this section we test the singular vector Kalman filter (SVKF) on a chaotic Lorenz 95 system (Lorenz and Emanuel, 1998, Hansen, 1998), with and without dynamic model error. The state equation for this system is:

$$\frac{dx_j}{dt} = (x_{j+1} - x_{j-2})x_{j-1} - x_j + \theta \quad , \quad j = 1,\cdots,n \tag{2-43}$$

with boundary conditions $x_{-1} = x_{n-1}, x_0 = x_n, x_1 = x_{n+1}$. The cyclic chain created by these

boundary conditions can be thought of as an unspecified scalar meteorological quantity at n equally spaced locations around a latitudinal circle. The total energy, $\sum_n x_j^2$ is conserved in the first two quadratic advection terms but is dissipated by the negative linear term. The last term on the right hand side is an external forcing that prevents the energy from vanishing. The mean and the standard deviation of x_j, are in the ranges of $[0,\theta]$ and $\left[0,\frac{\theta}{2}\right]$, respectively. Thus each state variable can be assumed to stay within $(-\theta,2\theta)$ for 95% of the time, meaning that the magnitude of the natural variability of each state variable is about 3θ.

Depending on the magnitude of θ the system exhibits a wide range of dynamical properties: completely dissipative, quasi periodic or chaotic. To find the forcing threshold for chaotic behavior we follow the analysis by Lorenz and Emanuel (1998). Perturbations δx_j around the steady solution $x_j = \theta, j = 1,\cdots,n$ can be written as follows:

$$\frac{d}{dt}(\delta x_j) = (\delta x_{j+1} - \delta x_{j-2})\,\theta - \delta x_j \qquad (2\text{-}44)$$

Solving (2-44) for a solution with exponential form $\delta x_j = \sum_k p_k\, e^{i.j.k}$ gives:

$$\frac{dp_k}{dt} = \left[\left(e^{i.k} - e^{-2i.k}\right)\theta - 1\right] p_k \qquad (2\text{-}45)$$

which becomes unstable only if $\mathrm{Re}\left[\left(e^{i.k} - e^{-2i.k}\right)\theta\right] > 1$, i.e. $\left[\cos(k) - \cos(2k)\right] > 1/\theta$. It is easy

to show that the maximum of the expression on the left hand side is $9/8$, which happens at $\cos(k) = 1/4$, i.e. a wave with period of about 4.77. The closest wave with a integer period that is a divisor of the state size $n = 144$, has a period of 6, which makes $k = \pi/3$ and $\left[\cos(k) - \cos(2k)\right] = 1$. Therefore, the threshold forcing that leads to an unstable solution to (2-45) with 144 state variables is $\theta = 1$.

We set $\theta = 8$ because this value is sufficiently large to insure that the system remains in the chaotic regime when random dynamic model errors are added to the state equations. With $\theta = 8$ and $n = 144$, Lorenz 95 model has a positive leading Lyapunov exponent while the sum of the Lyapunov exponents is negative. Therefore, the system is chaotic and the uncertainties grow exponentially, while the resulting trajectory is bounded within a hyper-cube of 3θ along each side. The largest Lyapunov exponent corresponds to an error doubling time of ~0.38 units of model time, equivalent to about 2 days in an atmospheric model.

For numerical integration of (2-43), we use a fourth order Runge Kutta scheme with $dt = 0.01$ (equivalent to 1.2 hrs in an atmospheric model). We may occasionally reduce the time step to avoid numerical instability. At every 10 time steps (12 hrs in an atmospheric model), noisy observations of 108 of the state variables are available. The observed states are chosen randomly but the observation operator in (2-11) does not change over time. The standard deviation of the observation noise is assumed to be 0.10, corresponding to about 1% of the attractor radius. Experiments are conducted over 16 units of model time, equivalent to 80 days in the atmosphere.

Figure 2-2 shows plots ranked singular values (from largest to smallest) vs. rank for the 144D Chaotic Lorenz 95 model. These singular values were obtained from linearizations of the model about the open loop value of the state at 2000 typical times, representing points distributed throughout the attractor. This plot indicates that the number of growing directions (singular values greater than 1.0) is typically 50 - 70.

We measure the performance in terms of the root mean square analysis error (RMSE) defined as follows for a given true trajectory $x^t(t)$ (which is known in our synthetic experiments):

$$RMSE(N,t,x^t)=\sqrt{\frac{1}{n}\left[x^a(t)-x^t(t)\right]^T\left[x^a(t)-x^t(t)\right]} \tag{2-46}$$

For the SVKF $x^a(t)$ is the analysis computed at t from (2-12). For the ensemble Kalman filer $x^a(t)$ is the mean over all the analysis replicates at t. The analysis RMSE can be bounded from above with the RMSE of $x^a(t)$ values obtained from a forward integration of the model, with the initial states set to mean values and with no updates (OpenLoop). The lower bound is achieved with the $x^a(t)$ values computed by a full rank EnKF with updates included and the number of replicates set at $N >> n$ (Optimal). In order to obtain this lower bound for the case with model error present we use the analysis produced by a square root version of the ensemble Kalman filter (Evensen, 2004) with $N = 1440$ replicates. The EnKF is not run for the no-model error case because it suffers from the problem of ensemble collapse discussed earlier. However, the SVKF is tested for both the model error and no model error cases. For a given rank N we propagate N singular vectors (for the SVKF) or $N+1$ replicates (for the EnKF).

In our first experiment we include dynamic model error with a constant covariance diagonal $\sqrt{q(t)} = 0.05$. When this level of model error is added to Lorenz 95 the EnKF does not experience any of the structural instabilities that can cause problems when dynamic error is added to numerical weather prediction models. Figure 2-3 shows the $RMSE(N,t,x^t)$ time series obtained from the SVKF and EnKF with different values of N for a typical "true" trajectory generated as an open loop solution with a particular set of random initial conditions. The OpenLoop trajectory obtained for mean initial conditions is also shown provided for comparison. The RMSE values for both the SVKF and EnKF decrease as N grows. For a given N, the SVKF gives lower RMSE than the EnKF because its reduced rank subspace is more efficient in capturing growing errors. As N increases the SVKF converges more quickly than the EnKF to the Optimal lower RMSE bound.

The results shown in Figure 2-3 apply only to a particular true trajectory. To obtain a more general performance assessment we evaluated the filter RMSE over many different possible true trajectories. In this case aggregate performance is measured by $Err(N)$, the average of the asymptotic level of $RMSE(N,t,x^t)$ over the I true values $x_1^t, x_2^t, \ldots, x_I^t$:

$$Err(N) = \frac{1}{I}\sum_{i=1}^{I} \lim_{t\to\infty}\left[RMSE(N,t,x_i^t)\right] \tag{2-47}$$

In our experiments, first we approximate $\lim_{t\to\infty}\left[RMSE(N,t,x_i^t)\right]$ by the temporal mean of $RMSE(N,t,x^t)$ over all times after a transient period of 8 units of model time. Then we

compute $Err(N)$ by averaging this asymptotic level of the analysis error over $I = 80$ different truths.

Figure 2-4 shows $Err(N)$ for the SVKF, EnKF, OpenLoop, and Optimal cases. As expected, $Err(N)$ for both filters improves as N grows, while it remains bounded from above and below by the OpenLoop and Optimal results, respectively. The $Err(N)$ of SVKF converges to the Optimal for $N > 70$, which is the point where enough singular vectors are retained to insure that the reduced rank subspace is the same as E_{t+T}^{N}. In this case all of the growing errors are captured in the update process (See Figure 2-2).

This is confirmed in Figure 2-5, where we have plotted the number of growing directions captured in the reduced rank subspace as a function of the dimension of this subspace (number of singular vectors retained). Note that the EnKF is less efficient in capturing these directions since it works in a random subspace that need not capture all growing directions even if the number of replicates exceeds the dimension of $E_T^G\left[x^f(t+T) \right]$. For example, Figure 2-3 shows that the EnKF needs about $N \sim 140$ replicates to give $Err(N)$ values as small as those obtained with the SVKF with a much smaller N.

In order to compare reduced rank filters for different size problems, we define an Asymptotic Optimality Index (AOI), which is the ratio of the log error reduction achieved to the maximum possible log error reduction:

$$AOI(N) = \frac{\log\left[Err_{OpenLoop}\right] - \log\left[Err(N)\right]}{\log\left[Err_{OpenLoop}\right] - \log\left[Err_{Optimal}\right]}, \quad 0 \le AOI(N) \le 1 \tag{2-48}$$

An AOI close to 1 means that the asymptotic performance of the reduced rank filter is nearly Optimal, while a small AOI shows that the filter is not providing any significant improvement over the OpenLoop case. Figure 2-6 shows the AOI for the SVKF and EnKF as a function of $\frac{N}{n}$, the ratio of the reduced rank filter size to the size of a full rank filter. Here, the superiority of SVKF to EnKF is evident, reflecting the efficiency achieved by focusing on growing modes. In particular, when the rank of the filter is just 20% of the state size, the SVKF is nearly identical to Optimal. In order to check that this observation is independent of the state size we repeated the experiments used to obtain Figure 2-6 with state sizes of 18, 36, 72, 216, and 288, with the number of observed states scaled proportionally. The results were all essentially the same as in Figure 2-6.

To test the SVKF in absence of dynamic model error, we repeated all of the above experiments, setting $Q(t) = 0$. As we discussed earlier, the EnKF suffers from rank deficiency and does not perform well when dynamic model error is zero. This can be seen in Figure 2-7, where RMSE time series of EnKF are plotted for three different N's along with the rank of the error covariance. We have also plotted the RMSE time series of an EnKF with $N = 2880$ before it begins to become rank deficient as the expected Optimal. It can be seen that performance of EnKF improves initially with a larger ensemble size. However, ensemble members quickly

loose their independence in absence of dynamic model error as seen in the rank time series, amid the loss of performance of EnKF.

For the SVKF we have used the algorithm in absence of dynamic model error. Figure 2-8 shows the $RMSE(x^t, N, t)$ time series for SVKF over a typical truth similar to Figure 2-3. When dynamic model error is zero, SVKF performs almost the same as before.

Figure 2-9 and Figure 2-10 show $err(N)$ and the average number of captured growing modes in absence of the dynamic model error, analogous to Figure 2-4 and Figure 2-5, respectively. It can be seen that performance of the SVKF improves as N grows and stays constant for $N > 50$, which according to Figure 2-10 is the point where all of the growing modes of the system are captured. The plot of AOI in Figure 2-11 shows that the SVKF again converges to the Optimal when the rank of the filter is just 20 % of the state size. Figure 2-11 is also independent of the state size and remains the same when n is varied.

2.5 Conclusions

Practical geophysical data assimilation techniques need to contend with high dimensional problems and with nonlinearities. In combination, these characteristics pose some challenging implementation problems since fully nonlinear methods tend to be computationally demanding, while computationally feasible methods tend to rely on linear approximations. The need to account for nonlinearities in an efficient way is particularly important for applications involving chaotic systems. In such systems measurement updates are needed to compensate for the effects

of uncertain initial conditions, which cause estimates to diverge from the true state. When measurements are sufficiently accurate and sufficiently abundant they can be used to identify and correct the growing errors that lead to divergent predictions.

Reduced rank sequential estimators provide a convenient and relatively efficient way to apply linear estimation concepts to chaotic problems. Reduced rank filters use low rank approximations to error covariances (or their square roots) to describe estimation uncertainties. These filters update estimates only in subspaces of the complete state space and do not require the construction or storage of full rank covariance matrices. The update subspace used in a reduced rank filtering application needs to be carefully chosen to insure acceptable performance. One option is to require that the subspace should include directions corresponding to all errors that are growing at the update time. Since these directions are continually changing in a chaotic system the reduced rank subspace needs to be continually adjusted. Also, the estimation procedure must include enough measurements to insure that growing errors can be constrained in the update, for at least most of the update times.

The singular vector Kalman filter (SVKF) described in this paper is a reduced rank estimation procedure that performs updates in a subspace defined by the growing singular vectors of a linearized approximation to the nonlinear state equation. The update is derived from a reduced rank square root covariance that is a projection of the full rank square root covariance onto the selected subspace. The singular vectors of interest are obtained from an iterative procedure that relies on tangent linear and adjoint models. There is no need to compute a full Jacobian matrix.

The structure of our singular vector Kalman filter depends on whether or not dynamic model

error is considered. The general version of the filter accounts for such errors by explicitly including their covariance in the forecast error covariance propagation equation. When the model error covariance is full rank this has the effect of insuring that uncertainty is continually injected in all directions of the update subspace. When dynamic model error is zero errors in directions that were decaying in the past but start to grow will not be updated since their projected uncertainties are zero. This difficulty is overcome in the SVKF by assigning uncertainty to the null-space of the subspace of growing errors. This makes it possible to keep the dynamic model error zero while accounting for the possibility that changing conditions can transfer the past decaying directions to future growing directions.

The SVKF is formulated for both cases with and without dynamic model error such that it takes advantages of the computational efficiencies of the reduced rank approach. This is achieved by using singular value decompositions to replace large rank-deficient matrices by their smaller full rank equivalents. When combined with the use of an adjoint-based method for computing singular vectors this permits the SVKF to provide good performance for chaotic problems with computational effort that is quite competitive with alternatives such as the ensemble Kalman filter.

Results presented for a chaotic Lorenz 95 model with 144 variables indicate that the SVKF works well both with and without dynamic model error, with root mean squared errors (differences between true and estimated states) reduced far below the error level without update. This result applies, in a probabilistic sense, over a population of many alternative “true” state trajectories as well as for individual trajectories.

The satisfactory performance of the SVKF for this chaotic test problem is to be compared to that for the ensemble Kalman filter (EnKF), especially when dynamic model error is zero. The EnKF deals with additive dynamic model error by adding random perturbations to the state equation. This can be problematic is certain applications (most notably numerical weather prediction) where such random perturbations can induce non-physical imbalances (e.g. gravity waves) in model predictions. This is one reason why dynamic model error is often omitted in numerical weather prediction applications of ensemble Kalman filtering.

However, if model errors are omitted the EnKF ensemble eventually collapses (i.e. the error covariance rank decreases to one), as all ensemble members gradually converge to the leading Lyapunov vector of the deterministic model equation. The collapse takes longer when there are more replicates but it is eventually expected to occur, with resulting divergence of the EnKF estimate. When dynamic model error is zero covariance inflation or localization methods are required to prevent the ensemble collapse. By contrast, the SVKF can accommodate either case with or without dynamic model error. When dynamic model error is not zero, SVKF accounts for it by augmenting the forecast square root covariance expression with a deterministic model error square root covariance term, without introducing ant perturbations to the forecast trajectory. When dynamic model error is zero the filter accounts for uncertainties in the null space of the space of growing errors, which cause divergence.

The results and analysis provided here suggest that the SVKF provides an attractive and efficient alternative to the ensemble Kalman filter and to other reduced rank estimation algorithms, especially for chaotic systems where special considerations are needed for imbalances and

ensemble collapse. A definitive assessment of the capabilities and limitations of the SVKF will require more extensive tests, especially on larger and more realistic problems.

2.6 References

Anderson, J. L., and S. L. Anderson, 1999: A Monte Carlo implementation of the nonlinear filtering problem to produce ensemble assimilations and forecasts. *Mon. Wea. Rev.*, **127**, pp 2741-2758.

Anderson, J. L., 2001: An ensemble adjustment Kalman filter for data assimilation. *Mon. Wea. Rev.*, **129**, pp 2884-2903.

Andrews, A., 1968: A square root formulation of the Kalman covariance equations. *AIAA Journal*, **6**, pp 1165-1166.

Barkmeijer J., M. V. Gijzen, and F. Bouttier, 1998: Singular vectors and estimates of analysis-error covariance metric. *Q. J. R. Meteorol. Soc.*, **124**, pp 1695-1713.

Barwell, B. R., and R. A. Bromley, 1988: The adjustment of numerical weather prediction models to local perturbations. *Q. J. R. Meteorol. Soc.*, **114**, pp 665-689.

Bishop, C. H., B. J. Etherton, and S. J. Majumdar, 2001: Adaptive Sampling with the Ensemble Transform Kalman Filter. Part I: Theoretical Aspects. *Mon. Wea. Rev.*, **129**, pp 420-436.

Buehner, M., and P. Malanotte-Rizzoli, 2003: Reduced-rank Kalman filter applied to an

idealized model of the wind-driven ocean circulation, *J. Geophys. Res.*, **108(C6)**, 3192.

Cane, M., A. Kaplan, R. N. Miller, B. Tang, E. C. Hackert, and A. J. Busalacchi, 1996: Mapping tropical Pacific sea level: Data assimilation via a reduced state space Kalman filter. *J. Geophys. Res.*, **101(C10)**, pp 22 599 –22 617.

Daley, R., 1991: *Atmospheric Data Analysis*. Cambridge University Press, UK, p 457.

Ehrendorfer M., and J. J. Tribbia, 1997: Optimal prediction of forecast error covariance through singular vectors. *J. Atmos. Sci.* **54**, pp 286-313.

Evensen, G., 1994: Sequential data assimilation with a nonlinear quasi-geostrophic model using Monte-Carlo methods to forecast error statistics. *J. Geophys. Res.,* **99(C5)**, pp 10 143-10 162.

Evensen, G., 2003: The ensemble Kalman filter: theoretical formulation and practical implementation. *Ocean Dynamics*, **53**, pp 343-367.

Evensen, G., 2004: Sampling strategies and square root analysis schemes for the EnKF. *Ocean Dynamics*, **54**, pp 539-560.

Farrell, B. F., and P. J. Ioannou, 2001: State estimation using a reduced order Kalman filter, *J. Atmos. Sci.*, **58**, pp 3666-3680.

Fillion, L., 2002: Variational Assimilation of precipitation data and gravity wave excitation. *Mon. Wea. Rev.*, **130**, pp 357-371.

Fisher, M. and E. Andersson, 2001: Developments in 4D-Var and Kalman Filtering. *ECMWF*

Tech. Memo. 347.

Foale, S., and J. M. T. Thompson, 1991: Geometrical concepts and computational techniques of nonlinear dynamics. *Comp. Methods Appl. Mech. Eng.*, **89**, pp 381-394.

Fukumori, I., and P. Malanotte-Rizzoli, 1995: An approximate Kalman filter for ocean data assimilation: An example with an idealized Gulf stream model, *J. Geophys. Res.*, **100(C5)**, pp 6777-6793.

Gaspari, G. and S. E. Cohn, 1999: Construction of correlation functions in two and three dimensions. *Quart. J. Roy. Meteor. Soc.*, **125**, pp 723-757.

Gauthier, P., and J. N. Thépaut, 2001: Impact of the digital filter as a weak constraint in the preoperational 4dVar assimilation system of Météo-France. *Mon. Wea. Rev.*, **129**, pp 2089-2102.

Gelb, A., Ed., 1974: *Applied Optimal Estimation*. The MIT Press, p 306.

Hamill, T. M., and J. S. Whitaker, 2005: Accounting for the error due to unresolved scales in ensemble data assimilation: A comparison of different approaches. *Mon. Wea. Rev.*, **133**, pp 3132-3147.

Hansen, J. A., 1998: *Adaptive observations in spatially extended, nonlinear dynamical systems*, Ph.D. thesis, Oxford University, UK, p 207.

Heemink, A., M. Verlaan, and A. J. Segers, 2001: Variance reduced ensemble Kalman filtering. *Mon. Wea. Rev.*, **129**, pp 1718-1728.

Houtekamer, P. L., and H. L. Mitchell, 2001: A sequential ensemble Kalman filter for atmospheric data assimilation. *Mon. Wea. Rev*., **129**, pp 123-137.

Ide, K., and M. Ghil, 1997a: Extended Kalman filtering for vortex systems. Part I: Methodology and point vortices. *Dyn. Atmos. Ocean.*, **27**, pp 301-332.

Ide, K., and M. Ghil, 1997b: Extended Kalman filtering for vortex systems. Part II: Rankine vortices and observing-system design. *Dyn. Atmos. Oceans*, **27**, pp 333–350.

Jaeger, L., and H. Kantz, 1997: Homoclinic tangencies and non-normal Jacobians - Effects of noise in nonhyperbolic chaotic systems. *Physica D*, **105**, pp 79-96.

Kalnay, E., 2003: *Atmospheric modeling, data assimilation and predictability*. Cambridge University Press, UK, pp 220-248.

Kraut, S., and C. Grebogi, 2004: Escaping from nonhyperbolic chaotic attractors. *Phys. Rev. Lett.*, **92(23)**, 234101.

Lermusiaux, P. F. J., A. R. Robinson, 1999: Data assimilation via error subspace statistical estimation. Part I: theory and schemes. *Mon. Wea. Rev.*, **127**, pp 1385-1407.

Lorenz, E. N., 1963: Deterministic non-periodic flow. *J. Atmos. Sci.*, **20**, p 130.

Lorenz, E., and K. Emanuel, 1998: Optimal sites for supplementary weather observations: Simulation with a small model, *J. Atmos. Sci.*, **55**, pp 399-414.

Miller, R., Ghil, M., Gauthiez, F., 1994: Advanced data assimilation in strongly nonlinear

dynamical systems. *J. Atmos. Sci.*, **51**, pp 1037-1056.

Miller, R. N., E. F. Carter, and S. T. Blue, 1999: Data assimilation into nonlinear stochastic models, *Tellus*, **51A**, pp 167-194.

Mukougawa, H., M. Kimoto, and S. Yoden, 1991: A relationship between local error growth and quasi-stationary states: Case study in the Lorenz system. *J. Atmos. Sci.*, **48**, pp 1231-1237.

Nagashima, H. and Y. Baba, 1999: Introduction to Chaos, Physics and Mathematics of chaotic phenomena. *IOP Publishing Ltd*, Bristol, UK. pp 13-40.

Neef, L. J., S. M. Polavarapu, T. G. Shepherd, 2006: Four-dimensional data assimilation and balanced dynamics. *J. Atmos. Sci.*, **63**, pp 1840-1858.

Orrell, D., 2002: Role of the metric in forecast error growth: how chaotic is the weather? *Tellus*, **54A**, pp 350-362.

Palis, J., and F. Takens, 1993: *Hyperbolicity and Sensitive-Chaotic Dynamics at Homoclinic Bifurcations, Fractal Dimensions and Infinitely Many Attractors*. Cambridge Univ. Press.

Palmer, T. N., R. Gelaro, J. Barkmeijer, and R. Buizza,1998: Singular vectors, metrics and adaptive observations. *J. Atmos. Sci.*, **55**, pp 633-653.

Paul, D., 2007: Asymptotics of sample eigenstructure for a large dimensional spiked covariance model. *Statistica Sinica*, **17**, pp 1617-1642.

Pereira, M. B., and L. Berre, 2006: The use of an ensemble approach to study the background

error covariances in a global NWP model. *Mon. Wea. Rev.*, **134**, pp 2466-2489.

Pham, D. T., J. Verron, and M. C. Roubaud, 1998: A singular evolutive extended Kalman filter for data assimilation in oceanography. *J. Marine Sys.*, **16**, pp 323-340.

Picard, J., 1991: Efficiency of the extended Kalman filter for nonlinear systems with small noise. *SIAM J. on Applied Math.*, **51(3)**, pp 843-885.

Robert, C., K. T. Alligood, E. Ott, and J. A. Yorke, 2000: Explosions of chaotic sets. *Physica D*, **144**, pp 44-61.

Ruelle, D., 1989: Deterministic Chaos: The Science and the Fiction. *Proc. R. Soc. Lon. Series A, Math. and Phys. Sci.*, **427(1873)**, pp 241-248.

Saad, Y., 1992: *Numerical methods for large eigenvalue problems*. Manchester University Press, UK, pp 183-185.

Schroer, C. G., E. Ott, and J. A. Yorke, 1998: Effect of noise on nonhyperbolic chaotic attractors. *Phys. Rev. Lett.*, **81**, pp 1397-1400.

Ubaldi, F., A. Travisan, and A. Carrassi, 2005: Developing a dynamically based assimilation method for targeted and standard observations. *Nonlin. Proc. in Geophys.*, **12**, pp 149-156.

Ubaldi, F., and A. Travisan, 2006: Detecting unstable structures and controlling error growth by assimilation of standard and adaptive observations in a primitive equation ocean model. *Nonlin. Proc. in Geophys.*, **13**, pp 67-81.

2.7 Figures

Figure 2-1: Schematic presentation of growing singular and decaying singular vectors over the time interval $[t, t+T]$. Column space E^N_{t+T} of $U^N_{t,t+T}$ contains errors that have grown over $[t, t+T]$.

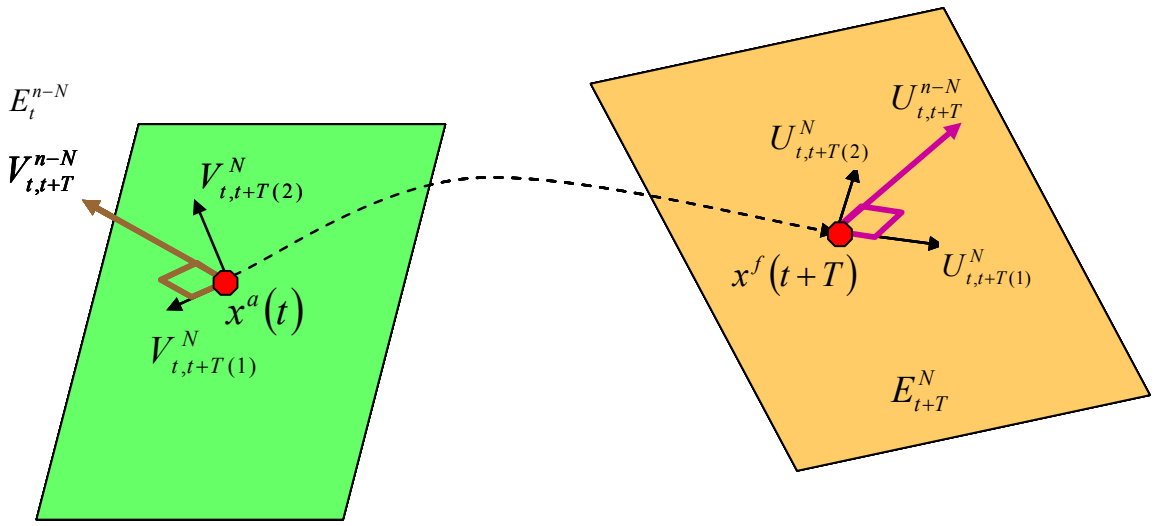

Figure 2-2: Singular value spectra for the 144D Chaotic Lorenz 95 for 2000 typical times, indicating that number of growing directions is typically 50 - 70.

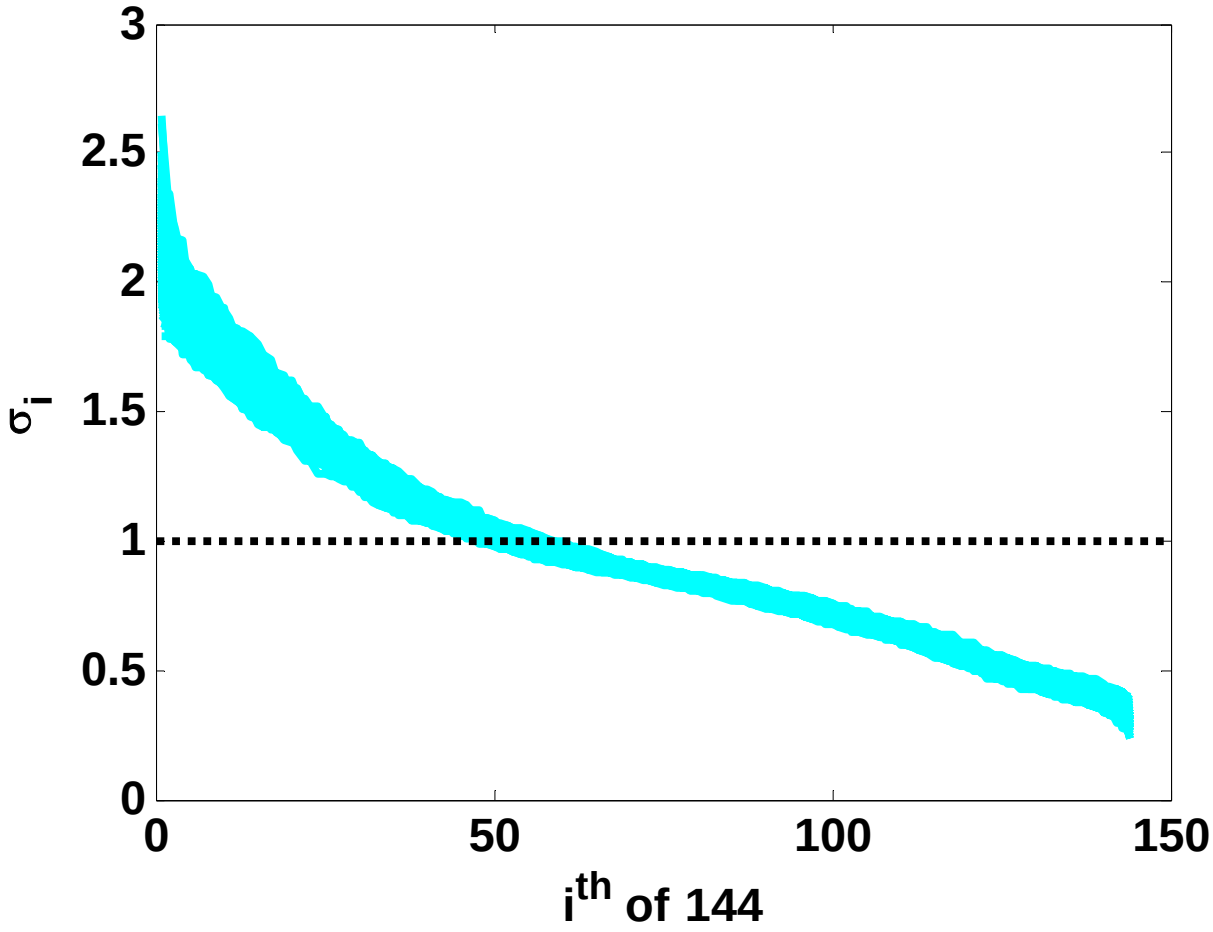

Figure 2-3: RMSE series for a typical truth, 144D Chaotic Lorenz 95 with dynamic model error

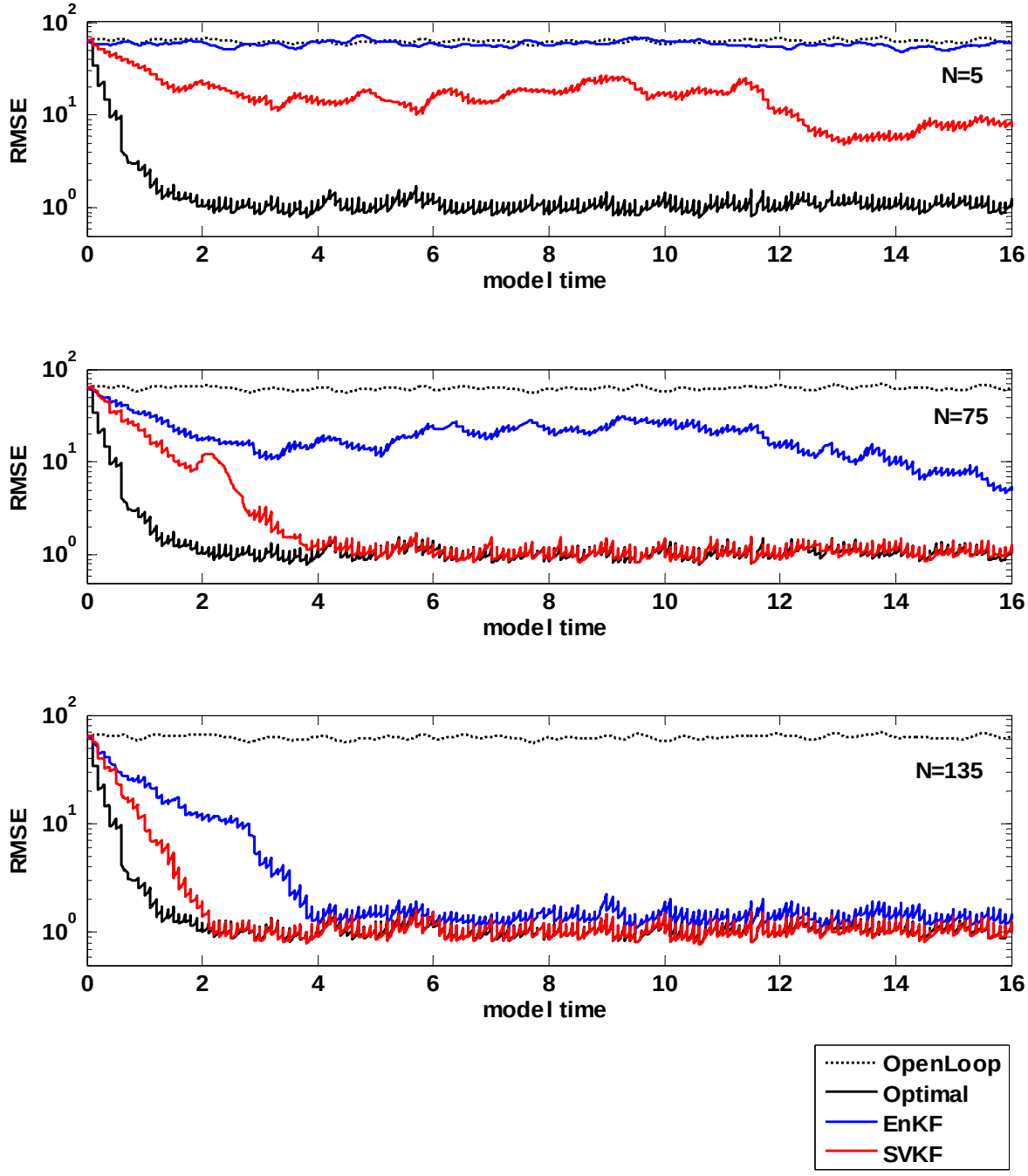

Figure 2-4: Err(N) for EnKF and SVKF, 144D Chaotic Lorenz 95 with dynamic model error

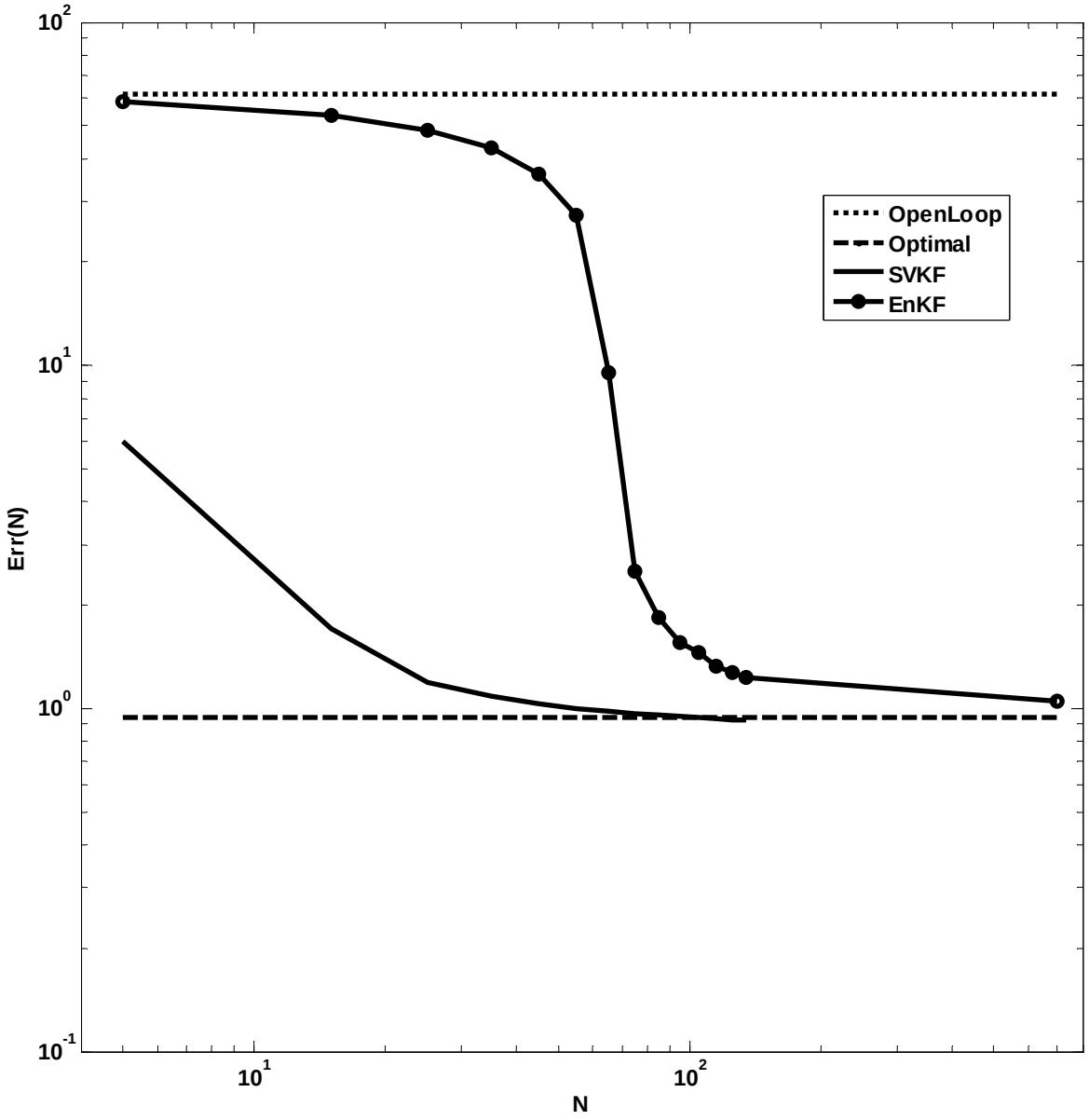

Figure 2-5: Number of captured growing modes for EnKF and SVKF, 144D Chaotic Lorenz 95 with dynamic model error

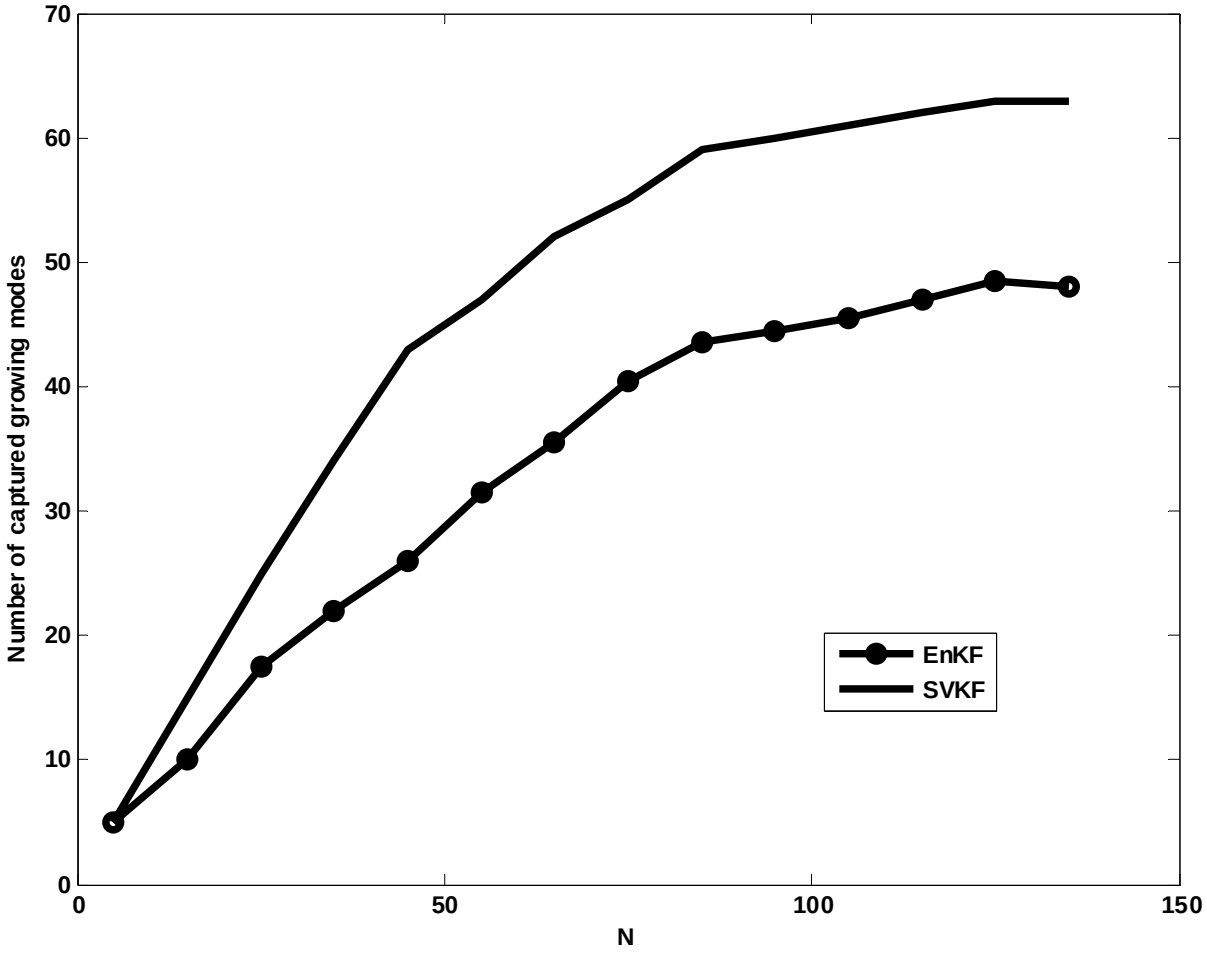

Figure 2-6: AOI(N) for EnKF and SVKF, 144D Chaotic Lorenz 95 with dynamic model error

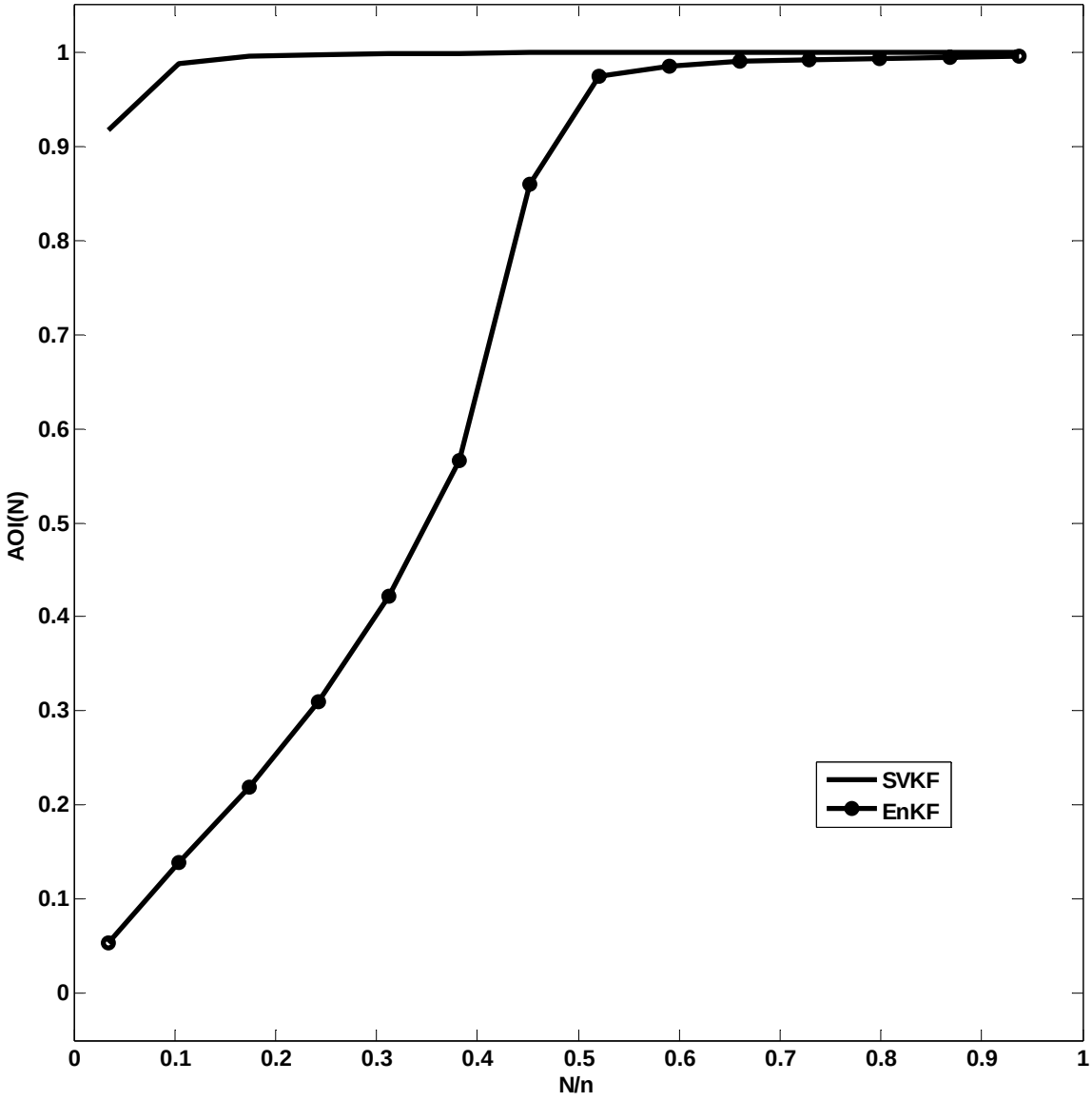

Figure 2-7: RMSE and rank series for EnKF over a typical truth, 144D Chaotic Lorenz 95 without dynamic model error

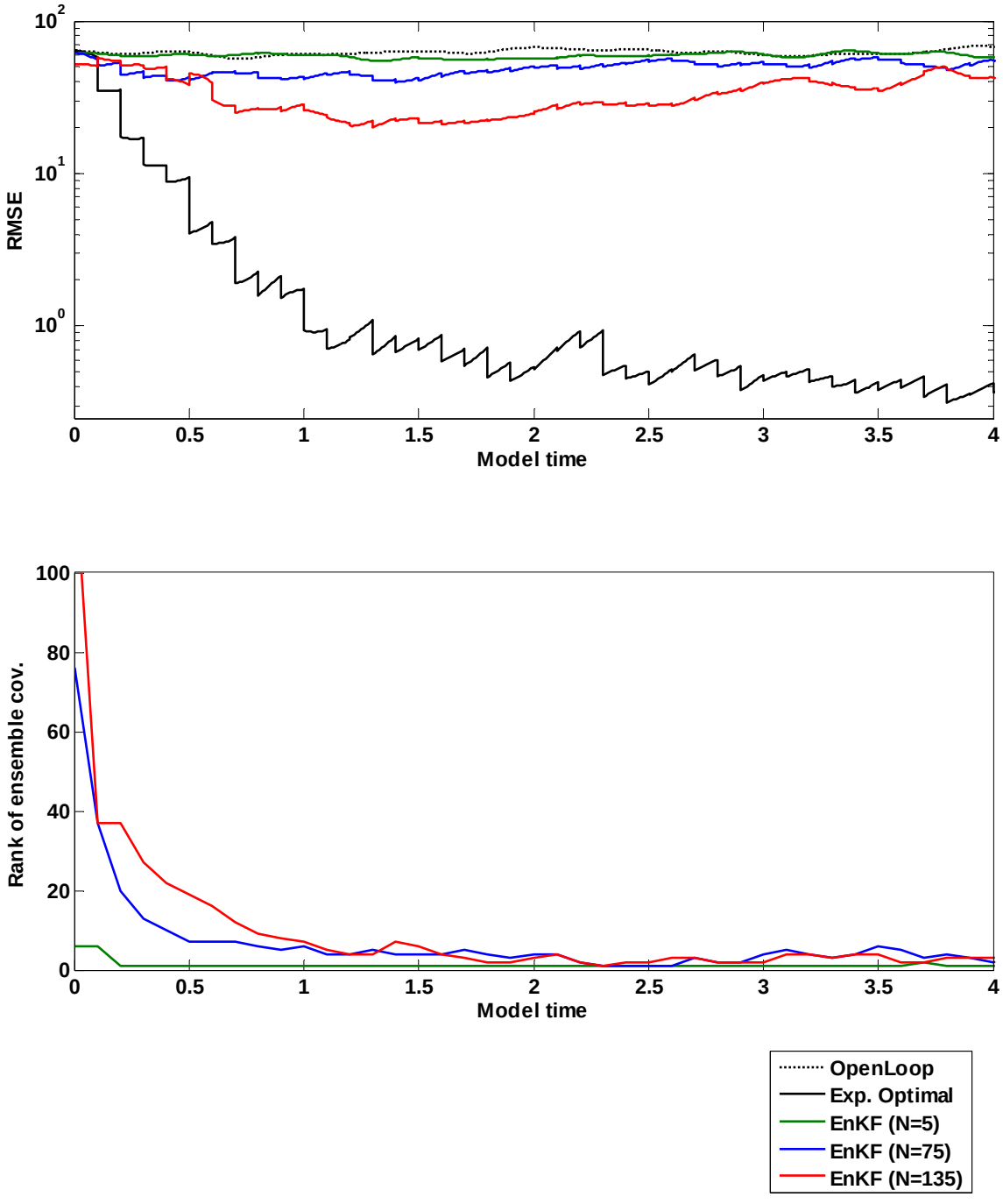

Figure 2-8: RMSE series for SVKF a typical truth 144D Chaotic Lorenz 95 without dynamic model error

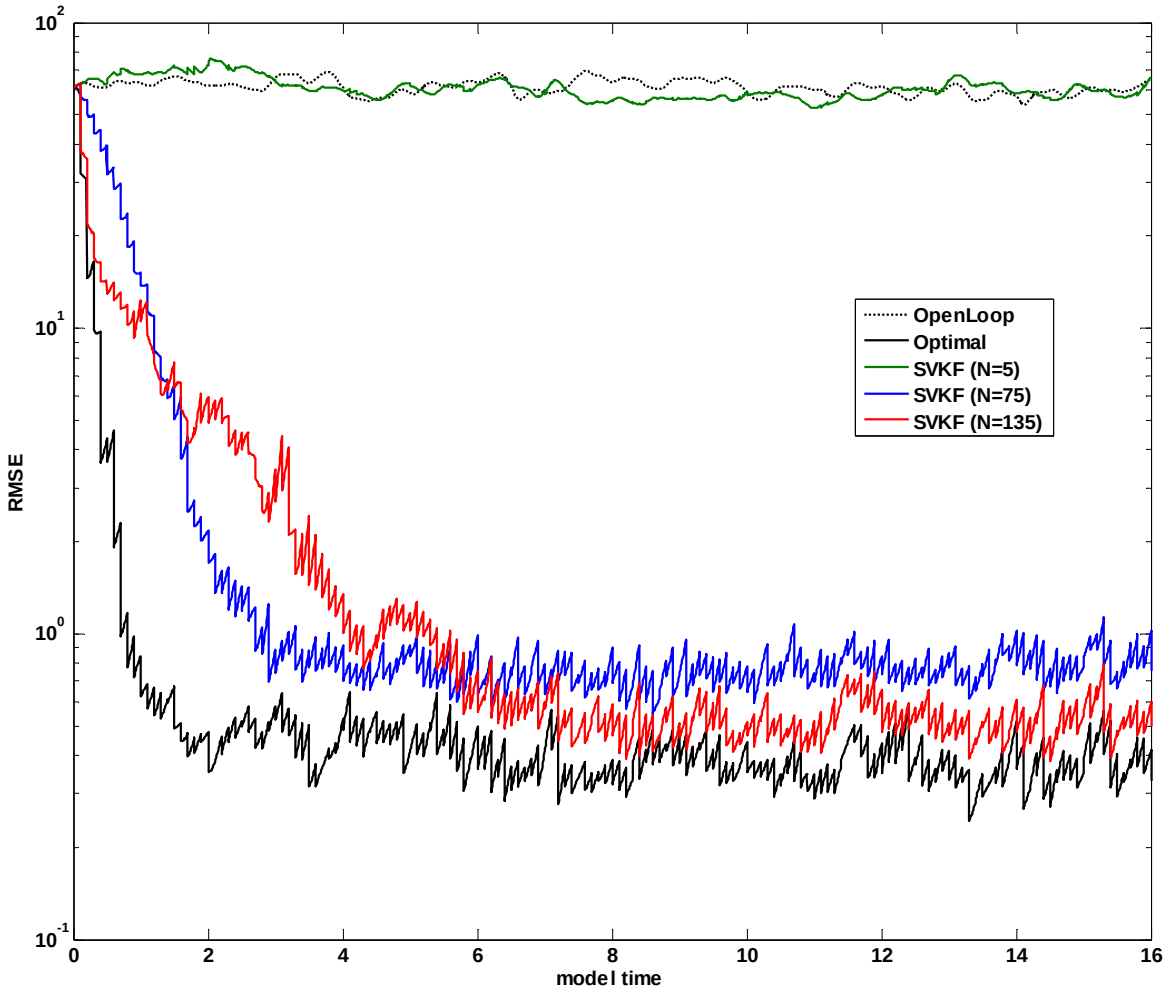

Figure 2-9: Err(N) for SVKF, 144D Chaotic Lorenz 95 without dynamic model error

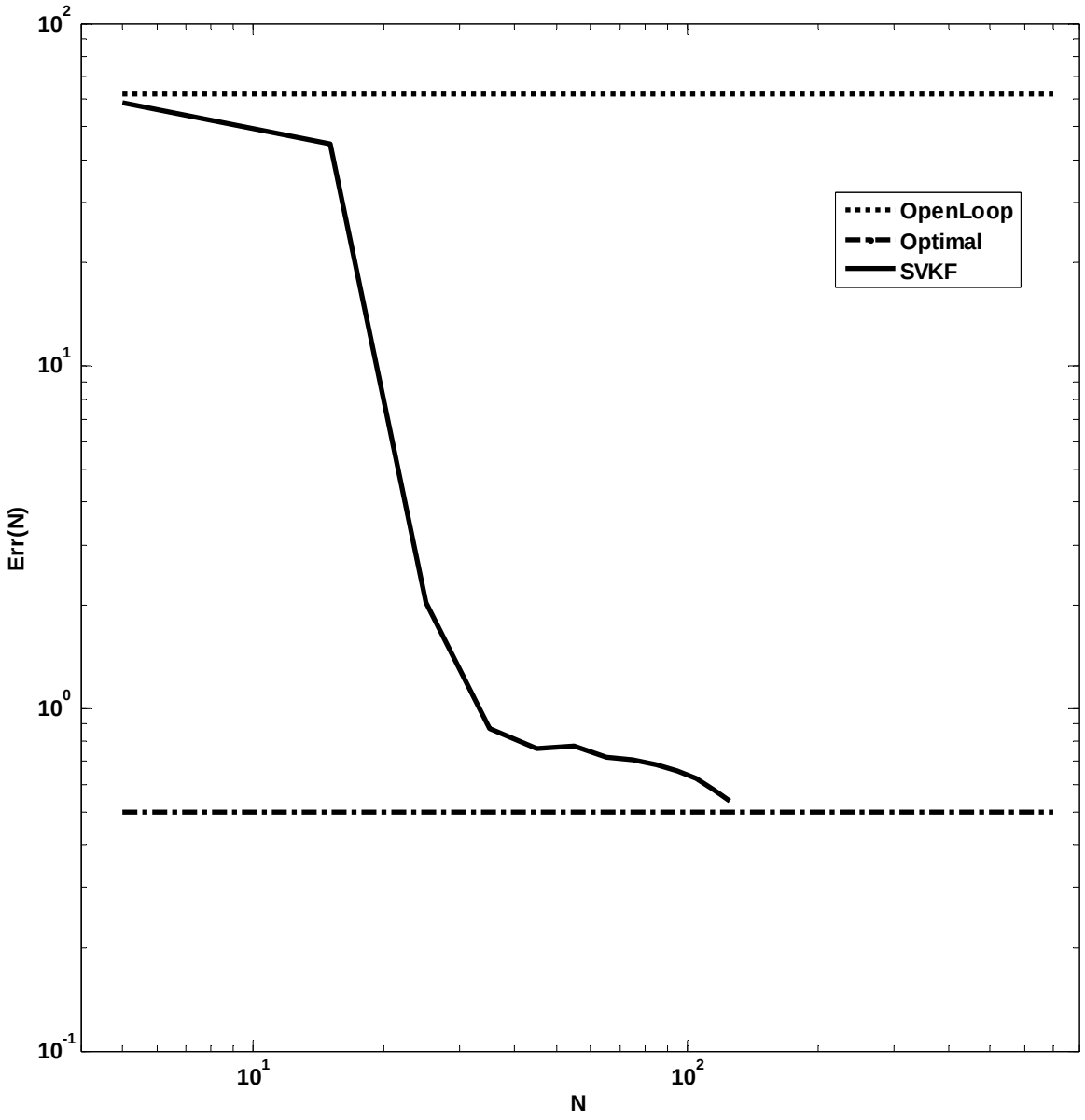

Figure 2-10: Number of captured growing modes for SVKF 144D Chaotic Lorenz 95 without dynamic model error

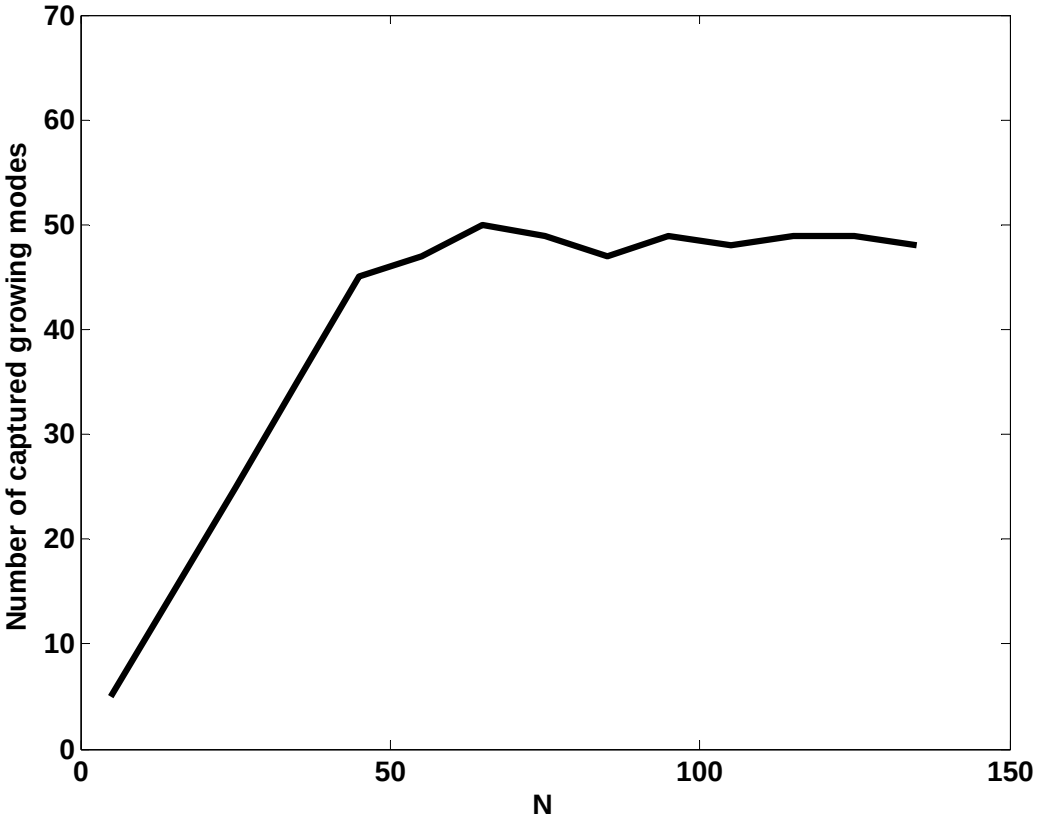

Figure 2-11: AOI(N) for SVKF, 144D Chaotic Lorenz 95 without dynamic model error

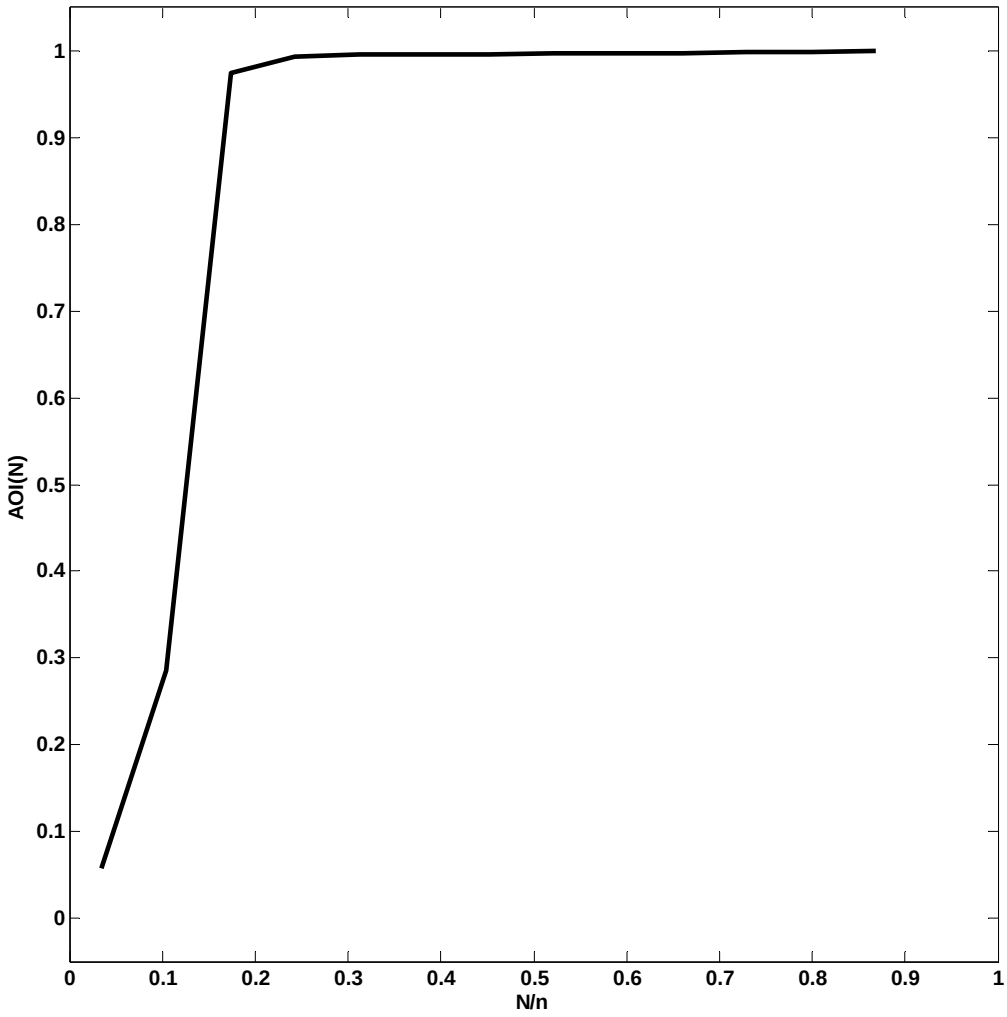

3 Stabilizing Error Dynamics in Chaotic Systems by Filtering

3.1 Introduction

In this chapter, we approach suboptimal filtering in chaotic systems from the point of view of stabilizing the short term dynamics of the estimation error. We use a linear approximation of the error dynamics and show that capturing the locally unstable directions of error growth is essential for the performance of any reduced rank filter. We identify these unstable directions via an iterative procedure that requires only forward integrations of the nonlinear dynamical model. We follow a square root approach to formulate a filter that aims at resolving the uncertainty along these unstable directions. We use a chaotic Lorenz 95 system to examine the performance of the filter both in presence of additive dynamic model error and when the dynamic model error is zero.

3.2 Background

In a geophysical system, approximations in the model and uncertainty in the modeling parameters, inputs, initial condition, and boundary conditions lead to undesirable inaccuracies in the forecast. Recent technological advances have provided us with numerous direct and remotely sensed observations to improve our forecast or estimated parameters of the system.

Data assimilation techniques are methods for utilizing these observations in a probabilistic framework to reduce the uncertainty in the forecast or model parameters. In this paper, we focus on filtering defined as a problem where observations are assimilated recursively as they are collected, thus only past observations are used in the analysis at any given time. Filtering is particularly attractive for its efficiency in real-time assimilation of the incoming streams of observation data.

In a filter, when a new observation is available, it is combined with the current best estimate of the state that is usually computed from a model (forecast) in a Bayesian framework to minimize the expected error of the estimated state (analysis), subject to the constraints of the dynamical model and the observation operator. The analysis will then be used for forecasting during the subsequent time interval until the next observation is available. In linear systems with Gaussian uncertainties, Kalman Filter (KF) solves the filtering problem by calculating the analysis as a linear combination of the forecast and the observation according to an optimal weighing matrix (the Kalman gain), which is computed from the forecast error and observation noise covariance matrices.

In most of the geophysical applications, the dynamical model or the observation operator is nonlinear and the distributions of uncertainties are not Gaussian any more, meaning that higher moments beyond the mean and error covariance are needed to characterize them. The KF is no longer optimal and the optimal filtering needs solving the Fokker–Planck equation for the evolution of the probability distributions, which does not have any closed-form solutions (Risken, 1996). Monte Carlo based methods such as the Particle Filter aim at approximating the

optimal solution by constructing the higher moments based on the statistics of a set of replicates (Ristic et al, 2004). However, the large number of replicates that are needed for the convergence of these methods is a major impediment for application of these algorithms in large geophysical systems such as the ocean and the atmosphere with $O(10^6)$ state variables (Nakano, 2007). Therefore, the optimal solution cannot be found in these applications within the limits of our computational resources.

Because of the simplicity of the linear update scheme in the KF and its known properties, a number of suboptimal filters have been developed that are based on the Kalman formulation of the gain matrix. For example, when the nonlinearities are not strong, the dynamical model and the observation operator can be linearized around the best estimate of the state, and used in a KF formulation. Unfortunately, this approach, which is known as the Extended Kalman Filter (EKF) (Gelb, 1974; Verron et al., 1999) is not computationally feasible in many applications with large state because propagation of the covariance matrix entails constructing a linear model or conducting as many forward integrations of the nonlinear model as the size of the state. Consequently, further suboptimal methods are proposed to approximate the gain matrix of the EKF. For example, the Reduced Rank extended Kalman Filter (RRKF) relies on a reduced rank approximation of the forecast error covariance that is computed by propagating only the leading eigenvectors of the most recent analysis error covariance. In RRKF, it is implied that the leading eigenvectors of the analysis error covariance, which summarize the dominant directions of uncertainty at a given time, evolve to the leading directions of uncertainty in the future. Although RRKF has a reasonable performance in weakly nonlinear systems, in presence of strong nonlinearities or chaotic behavior the linearity assumption in propagating the analysis

error covariance is easily violated, leading to failure of the RRKF (Fukumori and Malanotte-Rizzoli, 1995, Cane et al., 1996, Buehner and Malanotte-Rizzoli, 2003, Farrell and Ioannou, 2001).

Ensemble-based methods such as the Ensemble Kalman Filter (EnKF) (Evensen, 1994; Evensen, 2001; Zang and Malanotte-Rizzoli, 2003) and its so-called deterministic flavors such as the Ensemble Transform Kalman Filter (Bishop, 2001; Anderson, 2001), have been the popular alternatives in nonlinear applications. In these filters, an ensemble of random replicates are propagated by the fully nonlinear model and updated via a linear Kalman scheme, assuming that the covariance of the propagated replicates represents the forecast error covariance. The initial replicates are drawn randomly from the initial distribution of the truth that is assumed to be given.

Performance of the ensemble methods depends greatly on the number of the propagated replicates. In most of the applications of interest, the rank of the ensemble covariance, N, is much smaller than the dimension of the state space, n. Consequently, the column space of the ensemble covariance matrix is an N-dimensional random subspace (Paul, 2007) in a larger n-dimensional state space. Since the update by a Kalman-based gain can correct the forecast only in the column space of the forecast error covariance, ensemble filters can correct the forecast along the directions with significant uncertainty, only if the N-dimensional subspace of the ensemble members span all of those directions. Additionally, effectiveness of the gain matrix to reduce the uncertainty along a particular direction is greatly influenced by the estimated forecast uncertainty along that direction, which is computed based on the alignment of the ensemble

members. This explains why the required ensemble size grows so rapidly with the size of the state, where uncertainties along many directions need to be resolved.

Focus of this paper is on systems that exhibit chaotic behavior. In these systems, dynamics amplify the errors along a few directions, while the rest of uncertainties are attenuated. However, the directions of growing errors change rapidly over time and state space. This has important implications for Kalman-based filters because the forecast error covariance has to specify proper uncertainty along the growing directions to allow robust reduction of the forecast error. As we discussed in chapter 2, the inherent randomness in the ensemble members makes the ensemble-based methods inefficient in capturing the largest number of growing directions with a given ensemble size.

Another drawback of the ensemble methods is related to incorporation of dynamic model error in the form of adding random perturbations to the forecast trajectory. In many oceanic and atmospheric applications, this may excite structural instabilities, leading to non-physical model predictions. Therefore, it is common in geophysical chaotic applications to assume that the dynamic model error is zero (Daley, 1991, Houtekamer et al., 1996, Fillion, 2002, Anderson et al., 2005, Neef et al., 2006). It is frequently reported that in absence of dynamic model error, the ensemble members tend to loose their independence over a few assimilation cycles and the rank of the ensemble covariance decreases over time. Therefore, as the rank of the ensemble covariance approaches one, some of the directions that require correction fall in the null-space of the filter and cannot be corrected. This problem is widely known as the rank deficiency of the filter. Regardless of the number of ensemble members, ensemble filters will eventually become

rank deficient in absence of dynamic model error, unless the algorithm has explicit provisions to enhance the independence of the ensemble members and the rank of the ensemble covariance, for example by localization or variance inflation techniques (Houtekamer and Mitchell, 2001; Hamill et al., 2001; Anderson and Anderson, 1999). Since correct parameterizations of these techniques depend on the specifics of the underlying system and are mostly ad hoc, ensemble methods face practical challenges in some important application areas.

Here, we approach the problem of suboptimal filtering from the point of view of stabilizing the locally unstable error dynamics as discussed by Farrell and Ioannou (1996). Pham et al. (1998) formulated the Singular Evolutive Extended Kalman filter (SEEK) that aimed at computing the unstable directions of error growth. The SEEK was successfully implemented on linear or slightly nonlinear systems, where the unstable directions of the state transition matrix did not change rapidly. However, it was observed that performance of the SEEK filter deteriorated over a few assimilation cycles unless a forgetting factor was introduced to compensate for the underestimation of the forecast error. Pham et al. (1998) showed that choosing a correct forgetting factor was essential for the performance of the SEEK filter.

Carme et al. (2001) showed that the SEEK filter do not perform well in chaotic systems with rapidly changing state transition matrix, unless the unstable directions are computed frequently. They proposed a modified SEEK filter that tracked the changes in the state transition matrix by computing its time derivative. They successfully implemented this modified SEEK filter in a small chaotic system, confirming that a filter's ability to stabilize the locally unstable directions of error dynamics results in a good performance of the filter in chaotic applications. However

the modified SEEK filter requires computing the time derivative of the state transition matrix, which is difficult and computationally demanding in large systems.

In chapter 2, we introduced a suboptimal filter that captured the growing directions of uncertainty in chaotic dynamics by computing the leading singular vectors of the state transition matrix over the forecast period. We implemented this singular vector Kalman filter (SVKF) on a chaotic Lorenz 95 system and showed that it performed well when all of the growing directions were retained in the filter. As we will discuss in section 3.3, from the point of view of the error dynamics a successful implementation of the SVKF, like in any suboptimal Kalman-based filter is possible only if all of the unstable directions of the error growth are properly stabilized by the filter. The remarkable performance of the SVKF suggests that retaining all of the growing directions enables the filter to stabilize all of the locally unstable directions of error dynamics. Although the preliminary results of SVKF were promising, the leading singular vectors of the system can be computed only if its state transition matrix is explicitly calculated or the adjoint of the model is built. This can be a drawback in many geophysical applications where forming the state transition matrix is not feasible and the adjoint model is difficult or costly to build.

In this chapter, we formulate a filter that directly aims at stabilizing the locally unstable directions of error dynamics. In section 3.4, we introduce a method for computing the locally unstable directions of the error dynamics that requires only forward integrations of the nonlinear model. In section 3.5, we formulate the filter that stabilizes these unstable directions. Similar to chapter 2, a chaotic Lorenz 95 system is used to test this filter in section 3.6 followed by a discussion of the results.

3.3 Local instability of the error dynamics

In this section, we review the stability criteria for the dynamics of the estimation error when observations are assimilated via a linear update scheme. Let $x(t)$ be the non-dimensional state vector of size n, which is related to the n-dimensional vector of physical variables $\zeta(t)$ via a non-singular linear transformation $x(t) = C(t)\zeta(t)$. We use the Euclidean norm to measure distances in the state space, which is related to the norm in the physical space as follows:

$$\| x(t) \| = \sqrt{x(t)^T x(t)} = \sqrt{\zeta(t)^T C(t)^T C(t) \zeta(t)} = \| \zeta(t) \|_{C^T C} \tag{3-1}$$

where $C(t)^T C(t)$ is a positive definite matrix. We work with the transformed state $x(t)$, recognizing that the choice of the transformation matrix $C(t)$ is application-specific and has important effects on the performance of the data assimilation algorithm. We use superscripts t, f, and a on $x(t)$ to differentiate the true, forecast, and analysis variables, respectively.

Let the nonlinear model for propagating the true state from time τ to time t be written as:

$$x^t(t) = f\left(x^t(\tau), t \right) + \omega(t) \tag{3-2}$$

where $f(x,t)$ is an n-dimensional nonlinear function of the state. (3-2) is initialized at $\tau = t_0$ by $x^t(t_0)$, a random vector with a known mean $\overline{x^t(t_0)}$ and covariance $P^t(t_0)$. $\omega(t)$ is the dynamic model error, that is added only at the end of the forecast period and is assumed to be a

random vector that is zero mean and uncorrelated with $x^t(t_0)$, and has a known covariance $Q(t)$. In a typical geophysical system with O(10^6) state variables, working with a full $n \times n$ $Q(t)$ is not possible. However, it is commonly assumed that $Q(t)$ is either low rank and can be characterized by its relatively manageable square root, or has a particular structure such as diagonal. Here we assume that $Q(t)$ is diagonal and full-rank, so that only the variances are needed to be declared. A general $Q(t)$ can be turned to the diagonal form by means of a rotation of the coordinates. The system without dynamic model error can also be considered as a special case with $Q(t) = 0$.

Without loss of generality, we assume that observations are available at times with regular intervals of T. We consider a simple linear observation model and leave investigation of more elaborated observation models to future research. The observation vector $y(t)$ of size m is written as a linear function of the true state:

$$y(t) = H(t)\, x^t(t) + \upsilon(t) \qquad (3\text{-}3)$$

with an $m \times n$ observation matrix $H(t)$. The measurement error $\upsilon(t)$ is assumed to be zero mean and uncorrelated with both $\omega(t)$ and $x^t(t_0)$, with a known covariance $R(t)$.

In a filter with linear analysis scheme, the forecast and analysis equations are written as

$$
\begin{aligned}
x^f(t+T) &= f\left(x^a(t), t+T\right) \\
x^a(t+T) &= x^f(t+T) + K(t+T)\left[y(t+T) - H(t+T)\,x^f(t+T)\right]
\end{aligned}
\tag{3-4}
$$

where $K(t+T)$ is an $n \times m$ weighting (or gain) matrix. The filter is initialized at $t = 0$ with $x^a(t_0) = \overline{x^t(t_0)}$. Defining the analysis error as $\varepsilon^a(t+T) = x^a(t+T) - x^t(t+T)$, and substituting from (3-2) and (3-4), we have:

$$
\begin{aligned}
\varepsilon^a(t+T) &= x^f(t+T) + K(t+T)\left[y(t+T) - H(t+T)x^f(t+T)\right] - x^t(t+T) \\
&= x^f(t+T) - x^t(t+T) + K(t+T)H(t+T)\left[x^t(t+T) - x^f(t+T)\right] + K(t+T)\upsilon(t+T) \\
&= \left[I - K(t+T)H(t+T)\right]\left[x^f(t+T) - x^t(t+T)\right] + K(t+T)\upsilon(t+T) \\
&= \left[I - K(t+T)H(t+T)\right]\varepsilon^f(t+T) + K(t+T)\upsilon(t+T)
\end{aligned}
\tag{3-5}
$$

where we have defined $\varepsilon^f(t+T) = x^f(t+T) - x^t(t+T)$. (3-4) and (3-5) are useful for explaining the behavior of the analysis error in response to different choices of $K(t+T)$. For simplicity consider a case where all of the states are observed and $H(t+T) = I$. If $K(t+T)$ is very close to the identity matrix, (3-4) essentially discards the forecast and $x^a(t+T)$ is almost identical to the observation. From the point of view of the analysis error in (3-5), $\varepsilon^f(t+T)$ is strongly attenuated, while $\varepsilon^a(t+T)$ is to a large extent influenced by the observation noise $\upsilon(t+T)$. Consequently, with such a large $K(t+T)$, the analysis error will approach the level of

observation noise. On the other extreme, with a very small $K(t+T)$, $x^a(t)$ in (3-4) ignores the observation and remains very close to $x^f(t+T)$. From the perspective of (3-5), $\varepsilon^a(t+T) \approx \varepsilon^f(t+T)$ and the effect of $\upsilon(t+T)$ on $\varepsilon^a(t+T)$ is negligible, amid dynamics of $x^a(t+T)$ almost resembling a trajectory without analysis. This quickly leads to complete loss of forecast skill in chaotic applications.

An important consideration in choosing the gain matrix is that $\upsilon(t+T)$ in the last term on the right hand side of (3-5) may enhance the analysis error along the directions that are in the column space of $K(t+T)$. Therefore, if the intensity of observation noise is not reflected in $K(t+T)$, the correction to $\varepsilon^f(t+T)$ may be completely countered by the amplification of the observation noise. This shows that a proper gain matrix should consider the relative uncertainty in the forecast and the observations, the principal behind the formulation of the Kalman gain. Although Kalman gain is suboptimal under nonlinearities and does not minimize the analysis error, it can still be computed and used to reduce the analysis error.

If $\varepsilon^a(t+T)$ is small enough such that its propagation is almost linear, we have:

$$\begin{aligned}
\varepsilon^f(t+T) &= x^f(t+T) - x^t(t+T) \\
&= f\left(x^a(t), t+T\right) - f\left(x^t(t), t+T\right) - \omega(t+T) \\
&\approx F_{t,t+T}\left[x^a(t) - x^t(t)\right] - \omega(t+T) \\
&= F_{t,t+T}\,\varepsilon^a(t) - \omega(t+T) \qquad (3\text{-}6)
\end{aligned}$$

where $F_{t,t+T}$ is the $n \times n$ state transition matrix over the forecast window $[t, t+T]$. If the forecast window is divided up to k time steps, each of small length dt, $F_{t,t+T}$ can be expressed as follows:

$$F_{t,t+T} = F_{t+T-dt,t+T} \times \cdots \times F_{t+dt,t+2dt} \times F_{t,t+dt} \tag{3-7}$$

where each term on the right hand side is an $n \times n$ Jacobian matrix of $f(\cdot)$ evaluated at $x(\tau)$:

$$F_{\tau,\tau+dt} = \left. \frac{\partial f\Big(x(\tau), \tau + dt \Big)}{\partial x} \right|_{x(\tau)} \tag{3-8}$$

$x(\tau)$ is the best estimate of the state at time τ, i.e. the analysis estimate right after an update step, and the forecast estimate otherwise.

By substituting (3-6) in (3-5) we get a recursion for the analysis error:

$$\begin{aligned} \varepsilon^a(t+T) = & \left\{ \Big[I - K(t+T)H(t+T) \Big] F_{t,t+T} \right\} \varepsilon^a(t) - \Big[I - K(t+T)H(t+T) \Big] \omega(t+T) \\ & + K(t+T)\upsilon(t+T) \end{aligned} \tag{3-9}$$

which is initialized at $t = 0$ with $\varepsilon^a(0) = x^t(t_0) - \overline{x^t(t_0)}$, a zero mean random vector with covariance $P^t(t_0)$.

In a chaotic system, $F_{t,t+T}$ has a few unstable directions whose growth factors are very sensitive

to the state around which the system is linearized. Missing any of these unstable modes for an extended time will adversely impact the performance of the filter. In particular, the estimation error will be strongly amplified along the missing unstable direction and adversely impact the performance of the filter. A conservative approach is to formulate $K(t+T)$ in a way that all of the unstable directions of error dynamics are stabilized. From the point of view of the feedback pole placement, the analysis step should be able to stabilize all of the unstable direction of $F_{t,t+T}$. This is accomplished only if $K(t+T)H(t+T)$ has sufficient projection along all of the unstable directions.

In a Kalman-based update scheme, $K(t+T)$ is computed from the analysis error covariance, $P^a(t+T)$, as follows (Gelb, 1974):

$$K(t+T) = L^a(t+T)L^a(t+T)^T H(t+T)^T R(t+T)^{-1} \tag{3-10}$$

where $L^a(t+T)$ is a square-root of the analysis error covariance, such that $P^a(t+T) = L^a(t+T)L^a(t+T)^T$. The $n \times n$ matrix $K(t+T)H(t+T)$ can be written as:

$$K(t+T)H(t+T) = L^a(t+T)L^a(t+T)^T H(t+T)^T R(t+T)^{-1} H(t+T) \tag{3-11}$$

According to (3-11), the analysis step can stabilize $F_{t,t+T}$ only if both $H(t+T)^T R(t+T)^{-1} H(t+T)$ and $L^a(t+T)L^a(t+T)^T$ project on all of its unstable directions. Firstly, the observation operator $H(t+T)$ has to have projection along all of the unstable modes. This is a question of observability of the system, which we assume it to be resolved in this

chapter by observing a large number of states. Secondly, the second factor $L^a(t+T)L^a(t+T)^T$ has to have certain properties as we discuss below.

Following the assumption that the propagation of the analysis error is almost linear, the reduced rank propagation of the forecast error covariance can be written as

$$L^f(t+T)=\left[F_{t,t+T}\left[\Xi^{(N)}_{t,t+T}\Xi^{(N)}_{t,t+T}{}^T\right]L^a(t)\middle|\sqrt{Q(t+T)}\right] \tag{3-12}$$

which is an augmentation of the propagation of $L^a(t)$ with the square-root of the dynamic model error covariance $\sqrt{Q(t+T)}$. $\Xi^{(N)}_{t,t+T}$ is an $n\times N$ matrix whose columns $\xi_i, i=1,\cdots,N$ form an orthogonal basis. The reduced rank approximation is only made in the propagation of $L^a(t)$ over the forecast window $[t,t+T]$, by projecting $L^a(t)$ on the subspace that is spanned by $\Xi^{(N)}_{t,t+T}$. The filter becomes identical to the Extended Kalman Filter when $N=n$.

The square-root of the analysis error covariance may be written as:

$$L^a(t+T)=L^f(t+T)\sqrt{\begin{array}{l}I-L^f(t+T)^T\,H(t+T)^T\\ \quad\left[H(t+T)\,L^f(t+T)L^f(t+T)^T\,H(t+T)^T+R(t+T)\right]^{-1}\\ \quad H(t+T)\,L^f(t+T)\end{array}} \tag{3-13}$$

The recursion of (3-12) and (3-13) is initialized by $L^a(t_0)$ defined as $P^t(t_0)=L^a(t_0)L^a(t_0)^T$.

(3-12) and (3-13) show that the uncertainties in $L^f(t+T)$ will be properly reduced only if they

are properly captured by $H(t+T)L^f(t+T)$. When the system is observable, a proper update is solely dependent on the estimated uncertainties in $L^f(t+T)$. If the filter is supposed to properly reduce the estimation error along the locally unstable directions, this has to be reflected in the choice of $\Xi_{t,t+T}^{(N)}$. In particular from the perspective of error stability, if $\Xi_{t,t+T}^{(N)}$ is continually chosen to project on the subspace of unstable modes of $F_{t,t+T}$, the subsequent analysis step is guaranteed to stabilize the error growth, because such a $\Xi_{t,t+T}^{(N)}$ will allow $L^f(t+T)$ to have appropriate projection on all of the unstable directions of $F_{t,t+T}$.

In chapter 2 we showed that when uncertainties along the growing directions were properly captured in the SVKF, the forecast was corrected in the growing subspace. The above discussion suggests that SVKF has to be able to also stabilize the error dynamics. As the following theorem suggests, when all of the growing directions were included in the SVKF, the computed forecast covariance will also resolve some of the uncertainty along all of the unstable directions (see the proof in appendix E):

> *Theorem:* If the state transition matrix in a discreet-time system has p unstable eigenvalues, no unstable right eigenvectors are orthogonal to the subspace of the p leading right (initial) or left (final) singular vectors.

Note that in most of the applications, the equations of dynamics are practically solved discreetly in time, and this theorem applies.

Here, we aim at identifying the locally unstable directions directly. This is beneficial because

the unstable directions can be computed via an iterative eigen-decomposition algorithm as explained in the next section.

3.4 Locally unstable directions and Floquet vectors

The iterative algorithm for computing a basis for the N leading unstable modes of $F_{t,t+T}$ can be summarized as follows:

1. Choose N mutually independent but otherwise arbitrary perturbations of unit length, $\xi^{i,0}, i = 1, \cdots, N$, and set $k = 0$.

2. Compute $\widetilde{\xi}^{i,k+1} = F_{t,t+T}\ \xi^{i,k}$ by propagating $\xi^{i,k}$'s via

$$\widetilde{\xi}^{i,k+1} = F_{t,t+T}\xi^{i,k} \approx \frac{f\left(x^a(t) + \delta\ \xi^{i,k}\ , t+T\right) - f\left(x^a(t), t+T\right)}{\delta} \qquad (3\text{-}14)$$

   where δ is the magnitude of the perturbation that are added to $x^a(t)$. δ should be small enough to maintain the validity of the approximation.

3. Re-orthogonalize $\widetilde{\xi}^{i,k+1}$'s by Gram-Schmidt method, rescale them to unit length, and set $k = k+1$:

$$\xi^{i,k+1}, i = 1, \cdots, N \quad \xleftarrow{\text{Gram-Schmidt}} \quad \widetilde{\xi}^{i,k+1}, i = 1, \cdots, N$$

4. Repeat steps 2 and 3 until the subspace of perturbations becomes invariant under

propagation. The converged perturbations are columns of $\Xi_{t,t+T}^{(N)}$.

In this section we look at the above procedure from the perspective of a dynamical system. At this point we just mention that the above procedure is a straightforward and reliable method for computing the unstable directions even in nonlinear systems, and only requires an optimal number of forward integrations of the model within a Lanczos algorithm. In most of the applications, the maximum allowed number of forward runs can be set a priori in accordance with the available computational resources and the desired accuracy. We will come back to this point when discussing the experiments.

Now consider a forecast trajectory between two consecutive observations at t and $t+T$. Rewrite (3-4) in discreet time with time step dt:

$$x^f(\tau+dt) = f\left(x^f(\tau), \tau+dt\right) \quad , \ \tau \in [t, t+T), \ x^f(t) = x^a(t) \tag{3-15}$$

and define the following auxiliary system:

$$x^p(s) = \begin{cases} x^a(t) & , \ \mathrm{mod}(s,T) = 0 \\ f\left(x^p(s), s+dt\right) & , \ \text{otherwise} \end{cases} \tag{3-16}$$

where $x^p(s)$ is the auxiliary state and s shows the time in the auxiliary system to avoid confusions. $x^p(s)$ in (3-16) starts at $x^a(t)$ and evolves to $x^f(t+T)$ by following the forecast trajectory between t and $t+T$ in (3-15), then jumps back to $x^a(t)$ and repeats its trajectory. In

essence, (3-16) is a periodic and piecewise continuous system. Floquet theory for periodic systems states that if the output of such a system is sampled regularly at the period of the system, it will be equivalent to the output of a linear and time invariant (LTI) system (Yakubovich and Starzhinskii, 1975). Therefore, the concepts of stable and unstable modes of error growth in LTI systems can be expanded to this auxiliary periodic system, which in fact characterizes the dynamical properties of the original chaotic system over the forecast window.

In particular, consider the initial vectors in step 1 of the above procedure, and place infinitesimally small perturbations along their directions on columns of an $n \times N$ matrix $\delta X^p(0)$. Evolution of these perturbations over one period of (3-16) can be written in matrix form as (Hartman, 1982):

$$\delta X^p(T) = F^p_{0,T}\ \delta X^p(0) \tag{3-17}$$

where $F^p_{0,T}$ is the state transition (or Floquet) matrix of (3-16) over one period, which equals the product of Jacobians along the trajectory of $x^p(s)$:

$$F^p_{0,T} = F^p_{T-dt,T} \times \cdots \times F^p_{dt,dt+dt} \times F^p_{0,dt} \tag{3-18}$$

Each term on the right hand side of (3-18) is a Jacobian of (3-16) over one time step as denoted by subscripts, $F^p_{s,s+dt} = \left.\dfrac{\partial f\left(x^p(s), s+dt\right)}{\partial x}\right|_{x^p(s)}$. Since the Jacobian is not defined at the states with $\mathrm{mod}(s,T) = 0$, we set the Jacobian at this discontinuity point equal to the identity matrix, i.e.

$F^{p}_{kT-dt,kT} = I$ for all $k = 1,2,\cdots$.

Note that $F^{p}_{s,s+dt} = F_{\tau,\tau+dt}$, when $\mathrm{mod}(s,T) = \tau \neq 0$ and $x^{p}(s) = x^{a}(t)$ for $\mathrm{mod}(s,T) = 0$.

Therefore, under the definition of (3-16), we have $F^{p}_{0,T} = F_{t,t+T}$. Propagation of the perturbations in the original system is equivalent to propagating them in the auxiliary system over one period. After k iterations, i.e. k periods of (3-17), we have:

$$\delta X^{p}(kT) = \left(F_{t,t+T}\right)^{k} \delta X^{p}(0) \tag{3-19}$$

Let the complete real Schur decomposition of $F_{t,t+T}$ be written as follows:

$$F_{t,t+T}\ \zeta^{(n)} = \zeta^{(n)}\ \Lambda^{(n)} \tag{3-20}$$

where $\zeta^{(n)}$ is an $n \times n$ orthogonal matrix of Schur vectors. $\Lambda^{(n)}$ is an $n \times n$ upper quasi-triangular matrix with its diagonal elements being the eigenvalues of $F^{p}_{0,T}$ or two-by-two blocks of its complex conjugate eigen-pairs. Substituting for $F_{t,t+T}$ in (3-19) from (3-20) we have

$$\begin{aligned}\delta X^{p}(kT) &= \left[\zeta^{(n)}\ \Lambda^{(n)}\ \zeta^{(n)^{T}}\right]^{k} \delta X^{p}(0) \\ &= \zeta^{(n)}\ \Lambda^{(n)^{k}}\ \zeta^{(n)^{T}} \delta X^{p}(0)\end{aligned} \tag{3-21}$$

Therefore, as k grows all of the columns of $\delta X^{p}(kT)$ collapse on a single column of $\zeta^{(n)}$ that corresponds to the largest eigenvalue of $F_{t,t+T}$ and their magnitudes grow due to exponential growth of the leading eigenvalue in (3-21). In practice the initial perturbations have finite length

and the computational accuracy is lost when working with large numbers. Therefore, perturbations should be periodically rescaled and orthogonalized to prevent their collapse and computational overflow as in step 3 of the procedure.

If (3-16) has N unstable modes, the N columns of $\lim_{k\to\infty} \delta X^p(kT)$ converge after a few iterations of 2 and 3 to a basis for the unstable subspace of (3-16), which we call the N leading Floquet vectors (FVs) of the auxiliary periodic system. We take $\Xi^{(N)}_{t,t+T} = \lim_{k\to\infty} \delta X^p(kT)$ and use these locally unstable directions over the forecast period as the projection subspace in a reduced rank filter. Before proceeding to formulate the filter, we explain some geometrical properties of FVs in the following section.

3.5 Geometrical interpretation of Floquet vectors

Qualitatively speaking, state trajectory in a chaotic system is extremely sensitive to uncertainties in the state, model parameters, or forcing. For example, two trajectories with nearly identical initial conditions quickly separate and loose their similarity after a short time (Ruelle, 1989). In particular, because of the numerical inaccuracies and stochastic constraints that are present in the problem, such errors are inevitable and their growth leads to complete loss of predictability after a finite time. More specifically, it is not possible to make forecasts beyond a short horizon which is about two weeks in atmospheric applications under the most promising conditions (Lorenz, 1963).

Despite the fast initial growth of perturbations in a chaotic system, any arbitrary state within a

particular region of the state space known as the basin of attraction evolves after a finite transient period to a set that is referred to as the attractor of the system (Foale and Thompson, 1991). Due to the confinement of the chaotic state in the attractor, errors in these systems does not grow indefinitely and state estimation is in fact a problem of identifying the location of the truth within the attracting set. Therefore, understanding the geometrical properties of the attractor is important in developing proper algorithms for chaotic applications.

Global Lyapunov Exponents (GLEs) are a powerful tool for analyzing the attractor. It is known that growth rate of almost any infinitesimal perturbations that is propagated in a chaotic system approaches the first GLE and the perturbation itself aligns with the leading Lyapunov vector (LV). Similarly, if an ensemble of N random replicates of infinitesimal length are propagated in the system and frequently orthogonalized to prevent them from collapsing to the first LV, they will asymptotically span the subspace that is characterized by the first N leading LVs. Additionally, the volume of a hypercube with ensemble perturbations as its edges, will assume a growth rate equal to the sum of the first N GLEs (Nagashima and Baba, 1999).

Every chaotic system has a finite number of positive GLEs, while the sum of all of its exponents is zero if the system is Hamiltonian or negative if it is dissipative. The positive GLEs of the system show that over the whole attractor, in average how many mutually orthogonal perturbations experience growth and what are their growth factors. Although GLEs converge to a unique set, the LVs keep on changing as the perturbations travel along the attractor. The direction of LVs at a given point on the attractor, in essence summarizes all of the past amplifications and rotations of the modes of dynamics over the trajectory of that point.

The procedure for computing the GLEs and LVs is very similar to the procedure that was introduced in section 3.4. However, the auxiliary periodic system in (3-16) guarantees that the perturbations are only subject to the amplifications and rotations within the forecast window. Therefore, FVs can be used to analyze the structure of the attractor in the vicinity of the forecast trajectory, in the same way that the overall behavior of LVs is useful for understanding attractor's global properties.

In particular, consider the trajectories of a nominal state and a perturbed state over finite forecast window. If the perturbed state does not have any physical interpretation, meaning that it is not on the attractor, it will evolve towards the attractor so long as the magnitude of the perturbation is small such that the perturbed state is within the basin of attraction. Therefore, this perturbation followed a locally stable dynamics as it is propagated by (3-14). On the other hand, if the perturbed state is physically meaningful, it is already on the attractor and the chaotic nature of the system will drive it away from the trajectory of the nominal state, leading to a locally unstable behavior. Therefore, local stability of a perturbation or lack there of can reveal the meaningfulness of the perturbation from the point of view of the physics of the problem. The iterative propagation of a set of perturbations using (3-14) combined with their periodic orthogonalization and rescaling guarantee that the stable components of the perturbations vanish over a finite number of iterations and the perturbations align with the locally unstable directions, which at the same time correspond to the physically meaningful perturbations.

Before continuing to formulate the filter, we would like to discuss the relationship between FVs and the Bred vectors that are used for ensemble forecasting at the National Center for

Environmental Prediction. Bred vectors are computed via propagation of a set of arbitrary perturbations in the system over the forecast window from t to $t+T$, their orthogonalization (if needed), rescaling and subsequent propagation over the next forecast window from $t+T$ to $t+2T$. Thus, Bred vector procedure is essentially the procedure in section 3.4 with only one iteration. If dynamics of the system is such that the state transition matrix does not change over a few forecast periods, the corresponding breeding cycles become identical to multiple iterations of the FV procedure, meaning that Bred vectors converge to the FVs. Similar convergence happens if the stable directions of the state transition matrix over $[t, t+T]$ are strongly dissipative so that even a single iteration is sufficient to eliminate the stable components of the perturbations. Otherwise, the Bred vectors will in general be different from FVs.

3.6 Local Floquet vector Kalman Filter

Formulation of the Local Floquet vector Kalman Filter (LFKF) is very similar to SVKF in chapter 2. In particular, the update steps of the two filters are identical. However, in the propagation step of LFKF, instead of the Singular vectors the leading Floquet vectors are used as the basis for reducing the rank of the filter.

We assume that the state vector is already normalized by a chosen positive definite deterministic matrix as discussed in section 3.3 and use a simple Euclidean norm. The forecast and analysis equations are exactly as in (3-4). The Kalman gain is derived from a square root approximation to the analysis error covariance via the formulation of Andrews (1968). The square root approach in this formulation is similar to chapter 2 and avoids explicit calculation of large

analysis and forecast covariance matrices and also has an enhanced numerical precision. A proof of the equivalence of the square root analysis in Andrews (1968) as appears in Gelb (1974) to the classic Kalman analysis equation in (3-10) is given in appendix D.

A square root formulation requires that the square roots $\sqrt{R(t)}$ and $\sqrt{Q(t)}$ of the noise covariance matrices $R(t)$ and $Q(t)$ be easy to compute. Here we assume that $Q(t)$ is full rank and diagonal so $\sqrt{Q(t)}$ is an $n \times n$ diagonal matrix. We assume that $m << n$ and that $\sqrt{R(t)}$ may be easily computed from a singular value decomposition of $R(t)$. Both of these assumptions can be relaxed at the expense of complicating the algorithm.

The square root algorithm for computing the Kalman gain can be expressed as a recursion which is initialized at a specified time $t = 0$ and repeated at each subsequent measurement (or analysis) time. For simplicity of notation we assume that the time between measurements is fixed at T. We start by defining square roots $L^a(t) = \sqrt{P^a(t)}$ and $L^f(t) = \sqrt{P^f(t)}$ of the analysis and forecast covariance matrices, which have the same column spaces as $P^a(t)$ and $P^f(t)$. With these definitions, we can rewrite the square root versions of the classic update and propagation equations, with $t - T$ indicating the initial time or the most recent analysis time and t indicating the next analysis time:

Forecast from time t to $t + T$:

$$L^f(t+T) = \left[\tilde{L}^f(t+T) \,\middle|\, \sqrt{Q(t+T)} \right] \tag{3-22}$$

where | indicates concatenation of two dimensionally consistent matrices and

$$\widetilde{L}^f(t+T)=\left[F_{t,t+T}\ \Xi^{(N)}_{t,t+T}\right]\Xi^{(N)\ T}_{t,t+T}L^a(t) \tag{3-23}$$

Update at time $t+T$:

$$K(t+T)=L^a(t+T)L^a(t+T)^T H(t+T)^T R(t+T)^{-1} \tag{3-24}$$

where:

$$L^a(t+T)=L^f(t+T)-\Psi(t+T)H(t+T)L^f(t+T) \tag{3-25}$$

$$\Psi(t+T)=L^f(t+T)\left[H(t+T)L^f(t+T)\right]^T\sqrt{Z(t+T)}^{-T}\left[\sqrt{Z(t+T)}+\sqrt{R(t+T)}\right]^{-1} \tag{3-26}$$

$$Z(t+T)=\left[H(t+T)L^f(t+T)\right]\left[H(t+T)L^f(t+T)\right]^T+R(t+T) \tag{3-27}$$

Define $\widetilde{P}^f(t+T)=\widetilde{L}^f(t+T)\widetilde{L}^f(t+T)^T$ with $\widetilde{L}^f(t+T)$ according to (3-23). $\widetilde{P}^f(t+T)$ is the projection of the propagated analysis square root covariance $F_{t,t+T}L^a(t)$ onto the subspace of locally unstable perturbations (the column space of $\Xi^{(N)}_{t,t+T}$). The augmented term $\sqrt{Q(t+T)}$ in (3-22) accounts for the effect of dynamic model error and insures that (3-22) and (3-23) are equivalent to the classic covariance propagation equation in Kalman filter. The resulting expression for the reduced rank square root forecast covariance $L^f(t+T)$ is consistent with our requirement that the forecast uncertainties along all of the locally unstable directions are properly

represented in $L^f(t+T)$. The rest of the algorithm is compatible with classic Kalman filtering algorithms.

For computational efficiency the above expressions are modified to take advantage of the rank deficiency of several large matrices. This avoids the need to compute or store any matrices with more than $\max(m,N)$ columns (where it is presumed that $N << n$ and $m << n$). The resulting recursion is described by the following equations:

1. Initialization:

   - $f[\cdot]$, $H(t)$, $\sqrt{Q(t)}$, and $\sqrt{R(t)}$ specified for all $t > 0$

   - $x^a(0)$ and $L_0^a = \sqrt{P^a(0)}$ is specified (e.g. as a given diagonal matrix) or derived from a specified set of column vectors (e.g. random ensemble replicates). Number of columns p will generally be less than n.

At each time ($t = 0,T,2T,\cdots$):

2. Compute the forecast by (3-4):

$$x^f(t+T) = f\left[x^a(t), t+T \right]$$

3. Compute the locally unstable directions or the Floquet vectors, using the procedure described in section 3.4. We use (3-20) to write the ordered Schur decomposition of $F_{t,t+T}$ as $F_{t,t+T}\ \Xi^{(N)}_{t,t+T} = \Xi^{(N)}_{t,t+T}\ \Lambda^{(N)}$, where the columns of $\Xi^{(N)}_{t,t+T}$ are the leading FVs of the auxiliary system and $\Lambda^{(N)}$ is an $N \times N$ upper-quasi-triangular matrix whose diagonal 1×1 or 2×2 blocks correspond to the N leading eigenvalues or eigen-pairs of $F_{t,t+T}$.

This procedure iterates nonlinear forward integrations of the model over $[t, t+T]$. The matrix $F_{t,t+T}$ does not have to be calculated or stored. The matrices produced at time t are $F_{t,t+T}\Xi^{(N)}_{t,t+T}$ and $\Xi^{(N)}_{t,t+T}$.

4. Compute the matrix $\Gamma_{t,t+T}$:

If $t = 0$: $\Gamma_{0,T} = \Xi^{(N)}_{t,t+T}{}^{T} L^a_0$, $Dim[\Gamma_{0,T}] = N \times p$ (3-28)

p = number of vectors used to construct L^a_0

If $t > 0$: $\Gamma_{t,t+T} = \left[\left(\Xi^{(N)}_{t,t+T}\right)^T \tilde{L}^a(t) \mid \Phi(t) \right]$, $Dim[\Gamma_{t,t+T}] = N \times (N+n)$ (3-29)

$\tilde{L}^a(t), \Phi(t)$ from previous cycle

5. Compute $\tilde{\Gamma}_{t,t+T}$, a full rank but smaller version of $\Gamma_{t,t+T}$, such that $\Gamma_{t,t+T}\Gamma_{t,t+T}{}^{T} = \tilde{\Gamma}_{t,t+T}\tilde{\Gamma}_{t,t+T}{}^{T}$, $Dim[\tilde{\Gamma}_{t,t+T}] = N \times N$.

6. Compute $\tilde{L}^f(t+T)$, $Dim[\tilde{L}^f(t+T)] = n \times N$:

$$\tilde{L}^f(t+T) = \left[F_{t,t+T}\Xi^{(N)}_{t,t+T} \right] \tilde{\Gamma}_{t,t+T} \tag{3-30}$$

7. Compute $Z(t+T)$ in a revised form of (3-27), $Dim[Z(t+T)] = m \times m$:

$$Z(t+T) = \left[H(t+T)\tilde{L}^f(t+T) \right] \left[H(t+T)\tilde{L}^f(t+T) \right]^T +$$

$$\left[H(t+T)\sqrt{Q(t+T)}\right]\left[H(t+T)\sqrt{Q(t+T)}\right]^{T}+R(t+T) \tag{3-31}$$

8. Compute $\Psi(t+T)$ in a revised form of (3-26), $Dim[\Psi(t+T)]=n\times m$:

$$\Psi(t+T)=\left\{\tilde{L}^{f}(t+T)\left[H(t+T)\tilde{L}^{f}(t+T)\right]^{T}+\sqrt{Q(t+T)}\left[H(t+T)\sqrt{Q(t+T)}\right]^{T}\right\}\cdot$$
$$\sqrt{Z(t+T)}^{-T}\left[\sqrt{Z(t+T)}+\sqrt{R(t+T)}\right]^{-1} \tag{3-32}$$

9. Compute $\tilde{L}^{a}(t+T)$, $Dim[\tilde{L}^{a}(t+T)]=n\times N$:

$$\tilde{L}^{a}(t+T)=\tilde{L}^{f}(t+T)-\Psi(t+T)\left[H(t+T)\tilde{L}^{f}(t+T)\right] \tag{3-33}$$

10. Compute $\varphi(t+T)$, $Dim[\varphi(t+T)]=m\times n$:

$$\varphi(t+T)=\left[H(t+T)\sqrt{Q(t+T)}\right]$$
$$-\left[H(t+T)\Psi(t+T)\right]\left[H(t+T)\sqrt{Q(t+T)}\right] \tag{3-34}$$

11. Compute $K(t+T)$, $Dim[K(t+T)]=n\times m$:

$$K(t+T)=\tilde{L}^{a}(t+T)\left[H(t+T)\tilde{L}^{a}(t+T)\right]^{T}R(t+T)^{-1}$$
$$+\sqrt{Q(t+T)}\varphi(t+T)^{T}\ R(t+T)^{-1}$$

$$- \Psi(t+T)H(t+T)\sqrt{Q(t+T)}\varphi(t+T)^T \; R\left(t+T\right)^{-1} \tag{3-35}$$

12. Compute updated estimate (analysis):

$$x^a\left(t+T\right) = x^f\left(t+T\right) + K\left(t+T\right)\left[y\left(t+T\right) - H\left(t+T\right)x^f\left(t+T\right)\right] \tag{3-36}$$

13. Compute $\Phi(t+T)$ (for next cycle), $Dim\left[\Phi\left(t+T\right)\right] = N \times n$:

$$\Phi\left(t+T\right) = \left(\Xi^{(N)}_{t+T,t+2T}\right)^T \sqrt{Q\left(t+T\right)} - \left(\Xi^{(N)}_{t+T,t+2T}\right)^T \Psi\left(t+T\right)H\left(t+T\right)\sqrt{Q\left(t+T\right)} \tag{3-37}$$

14. Exit or return to Step 2.

As we mentioned earlier, for various reasons it is undesirable to include model error in many chaotic geophysical applications. Not only improper consideration of dynamic model error in these systems may lead to non-physical behavior and incorrect results, complete characterization of the dynamic model error is also a difficult task. It is common in geophysical chaotic systems to assume that the dynamic model error is zero. In absence of the dynamic model error, the update step changes as follows:

1. Initialization:

   - $f[\cdot]$, $H(t)$, and $\sqrt{R(t)}$ specified for all $t > 0$.
   - $x^a\left(0\right)$ and $L_0^a = \sqrt{P^a\left(0\right)}$ specified or derived.

At each time ($t = 0, T, 2T, \cdots$):

2. Compute forecast by (3-4):

$$x^f(t+T) = f\left[x^a(t), t+T\right]$$

3. Compute the locally unstable directions or the Floquet vectors, using the procedure described in section 3.4. We use (3-20) to write the ordered Schur decomposition of $F_{t,t+T}$ as $F_{t-T,t}\ \Xi^{(N)}_{t-T,t} = \Xi^{(N)}_{t-T,t}\ \Lambda^{(N)}$, where the columns of $\Xi^{(N)}_{t,t+T}$ are the leading FVs of the auxiliary system and $\Lambda^{(N)}$ is an $N \times N$ upper-quasi-triangular matrix whose diagonal 1×1 or 2×2 blocks correspond to the N leading eigenvalues or eigen-pairs of $F_{t,t+T}$.

   This procedure iterates nonlinear forward integrations of the model over $[t, t+T]$. The matrix $F_{t,t+T}$ does not have to be calculated or stored. The matrices produced at time t are $F_{t,t+T}\Xi^{(N)}_{t,t+T}$ and $\Xi^{(N)}_{t,t+T}$.

4. Compute the matrix $\Gamma_{t,t+T}$:

   If $t = 0$: $\Gamma_{0,T} = (\Xi^{(N)}_{0,T})^T L^a_0$, $Dim[\Gamma_{0,T}] = N \times p$ (3-38)

   p = number of vectors used to construct L^a_0

   If $t > 0$: $\Gamma_{t,t+T} = \left[\left(\Xi^{(N)}_{t,t+T}\right)^T L^a(t) \,\middle|\, \phi(t+T)\right]$, $Dim[\Gamma_{t,t+T}] = N \times (N+n)$ (3-39)

   $L^a(t)$ from previous cycle and $\phi(t+T)$ is a correction term explained below. This term, which is not included in the general recursion, accounts for growing errors that are missed in truncation of the locally stable directions in absence of dynamic model error:

$$\phi(t+T) = \left(\Xi_{t,t+T}^{(N)}\right)^T \left[I - \Omega(t)\,\Omega(t)^T \right] r(t) \tag{3-40}$$

$\Omega(t) =$ an orthogonal matrix with the same column space as $L^a(t)$

$r(t) =$ a scalar

5. Compute $\widetilde{\Gamma}_{t,t+T}$, a full rank but smaller version of $\Gamma_{t,t+T}$, such that

   $\Gamma_{t,t+T}\Gamma_{t,t+T}{}^T = \widetilde{\Gamma}_{t,t+T}\widetilde{\Gamma}_{t,t+T}{}^T$, $Dim[\widetilde{\Gamma}_{t,t+T}] = N \times N$.

6. Compute $\widetilde{L}^f(t+T)$, $Dim[\widetilde{L}^f(t+T)] = n \times N$:

$$\widetilde{L}^f(t+T) = \left[F_{t,t+T}\Xi_{t,t+T}^{(N)} \right] \widetilde{\Gamma}_{t,t+T} \tag{3-41}$$

7. Compute $Z(t+T)$, $Dim[Z(t+T)] = m \times m$:

$$Z(t+T) = \left[H(t+T)L^f(t+T) \right] \left[H(t+T)L^f(t+T) \right]^T + R(t+T)` \tag{3-42}$$

8. Compute $L^a(t+T)$, $Dim[L^a(t+T)] = n \times N$:

$$L^a(t+T) = L^f(t+T)\,\Pi^a(t+T) \tag{3-43}$$

where $Dim[\Pi^a(t+T)] = N \times N$ and:

$$\Pi^a(t+T) = I_{N\times N} - \left[H(t+T)L^f(t+T) \right]^T \sqrt{Z(t+T)}^{-T} \left[\sqrt{Z(t+T)} + \sqrt{R(t+T)} \right]^{-1}$$

$$\left[H(t+T)L^f(t+T) \right] \tag{3-44}$$

9. Compute $K(t+T)$, $Dim\,[K(t+T)] = n \times m$:

$$K(t+T) = L^a(t+T)\left[H(t+T)L^a(t+T) \right]^T R(t+T)^{-1} \tag{3-45}$$

10. Compute updated estimate (analysis):

$$x^a(t+T) = x^f(t+T) + K(t+T)\left[y(t+T) - H(t+T)x^f(t+T) \right] \tag{3-46}$$

11. Exit or return to Step 2.

The correction term that appears in (3-39) is needed to account for the fact that errors that were formerly stable but are becoming unstable can be missed if the model error covariance is zero. To see this it is useful to consider three successive update times $t-T$, t, and $t+T$. The update at time t is able to handle unstable directions between $t-T$ and t, and lie in the column space of $\Xi^{(N)}_{t-T,\,t}$. Now consider an error ε that was stable between $t-T$ and t but becomes unstable between t and $t+T$. This error lies in the column space of $\Xi^{(N)}_{t,\,t+T}$ at time t (because it is starting to grow) but it also lies in $\Xi^{(n-N)}_{t-T,\,t}$ (because it was previously stable and hence truncated from $\Xi^{(N)}_{t-T,\,t}$). Since it lies in the column space of $\Xi^{(n-N)}_{t-T,\,t}$ the error ε is orthogonal to the column spaces of $\Xi^{(N)}_{t-T,\,t}$, $L^f(t)$ and $L^a(t)$ (note that (3-41) and (3-43) imply that the column space of $L^a(t)$ lies in the column space of $L^f(t)$, which lies in the column space of $\Xi^{(N)}_{t-T,\,t}$).

Consequently, $L^a(t)$ has no projection along ε and the filter effectively assumes zero uncertainty in the ε direction.

Between t and $t+T$ the error ε is unstable rather than stable. However, the filter will not correct this error at $t+T$, even though it is known to be unstable and to lie in the column spaces of $\Xi^{(N)}_{t,\,t+T}$ and $L^f(t+T)$. This is because there is no projection of ε onto $L^a(t)$ and therefore no projection onto $\Gamma_{t,t+T}$ (see (3-39) for $\phi(t+T)=0$). If model error were included ε would project onto $L^f(t+T)$ at $t+T$ even though its uncertainty at t only consisted of dynamic model error. The correction term $\phi(t+T)$ is designed to compensate for the absence of dynamic model error so ε will project onto $\Gamma_{t,t+T}$ at $t+T$ if it is in the column space of $\Xi^{(N)}_{t,\,t+T}$.

To derive $\phi(t+T)$ define $\Omega(t)$ to be an orthogonal matrix that has the same column space as $L^a(t)$. Then the expression $\left[I_n-\Omega(t)\Omega(t)^T\right]r(t)$ defines a set of column vectors that lie in the null space of $L^a(t)$ and have magnitudes proportional to the specified scalar $r(t)$. This scalar weighting factor can be viewed as a representative standard deviation for uncertainties that are stable at *t* but are not resolved in the reduced rank filter.

When $\left[I_n-\Omega(t)\Omega(t)^T\right]r(t)$ is propagated forward to $t+T$ using the truncated $F_{t,t+T}$ the result is the augmentation of $\phi(t+T)$ from (3-40) in (3-39). Note that the column space of this correction term lies in the column space of $\Xi^{(N)}_{t,\,t+T}$ (errors unstable between t and $t+T$) but is

proportional to postulated uncertainties in the column space of $\Xi_{t-T,t}^{(n-N)}$ (errors stable between $t-T$ and t).

The scalar $r(t)$ should be selected to be large enough to insure that some uncertainty is assigned to stable errors that may become unstable but small enough to insure that the modified filter does not exaggerate the model's uncertainty. In the application discussed here it is reasonable to relate $r(t)$ to the level of measurement error uncertainty, which provides a rough upper bound for the uncertainty in unresolved stable errors as follows:

$$r(t) = \text{max singular value}\left[H^{+}(t)\sqrt{R(t)}\right] \tag{3-47}$$

where $H^{+}(t)$ is the $n \times m$ pseudo-inverse of $H(t)$. In other applications, a better $r(t)$ based on a stricter bound may be used.

3.7 Experiments with Lorenz 95 system

To test the filter, we have used a 144 dimensional Lorenz 95 system (Lorenz and Emanuel, 1998, Hansen, 1998). The governing equations are defined as follows:

$$\frac{dx_j}{dt} = \left(x_{j+1} - x_{j-2}\right)x_{j-1} - x_j + \theta \quad , \quad j = 1,\cdots,n$$
$$x_{-1} = x_{n-1} \quad , \quad x_0 = x_n \quad , \quad x_{n+1} = x_1 \tag{3-48}$$

where $n = 144$ and the variables make a cyclic chain. The first two quadratic terms only shift

the energy between state variables, while conserving the total energy, $\sum_n x_j^2$. The negative linear term damps the total energy and tends to bring the system to rest. This is countered by the forcing θ, which replenishes the energy and makes the system exhibit a wide range of dynamical properties; completely dissipative, quasi periodic or chaotic.

The mean and the standard deviation of x_j, are in the ranges of $[0, \theta]$ and $\left[0, \frac{\theta}{2}\right]$, respectively. Thus each state variable may be assumed to stay within $(-\theta, 2\theta)$ for 95% of the time, meaning that the magnitude of the natural variability of each state variable is about 3θ.

To find the forcing threshold for chaotic behavior we follow the analysis by Lorenz and Emanuel (1998). Given a steady solution as $x_j = \theta$, $j = 1, \cdots, n$, dynamics of perturbations δx_j , $j = 1, \cdots, n$ around this steady solution can be written as follows:

$$\frac{d}{dt}(\delta x_j) = \left(\delta x_{j+1} - \delta x_{j-2}\right)\theta - \delta x_j \tag{3-49}$$

Solving (3-49) for a solution with exponential form $\delta x_j = \sum_k p_k \, e^{ijk}$ gives:

$$\frac{dp_k}{dt} = \left[\left(e^{ik} - e^{-2ik}\right)\theta - 1\right] p_k \tag{3-50}$$

which becomes unstable only if $\mathrm{Re}\left[\left(e^{ik} - e^{-2ik}\right)\theta - 1\right] > 1$, i.e. $\left[\cos(k) - \cos(2k)\right] > \frac{1}{\theta}$. It is

easy to show that the expression on the left hand side reaches its maximum value of $\frac{9}{8}$ at $\cos(k) = \frac{1}{4}$, i.e. a wave with period of about 4.77. The closest wave with a integer period, that is a divisor of the state size, has a period of 6, meaning that $k = \frac{\pi}{3}$ and $\left[\cos(k) - \cos(2k)\right] = 1$. Therefore, the threshold forcing that leads to an unstable solution to (3-50) with 144 state variables is $\theta = 1$. Following previous work on Lorenz 95 system, we set $\theta = 8$ in our experiments, guaranteeing the chaotic behavior of the system in the sense that uncertainty in the state grows exponentially, while the resulting trajectory is bounded within a hyper-cube of 3θ along each side.

For numerical integration of (3-48), we use a fourth order Runge-Kutta scheme with $dt = 0.01$ (equivalent to 1.2 hrs in an atmospheric model), which we may occasionally reduce in case of numerical instability. We assume that at every 0.1 units of model time (12 hrs in an atmospheric model), noisy observations of 108 of the state variables are available. The standard deviation of the observation noise is assumed to be 0.10, corresponding to about 1% of the attractor radius.

Experiments are conducted over 16 units of model time (equivalent to 80 days in an atmospheric model), and the root mean square error (RMSE) time series is computed for different filters (LFKF, SVKF, and EnKF) as follows:

$$RMSE\left(x^t, N, t\right) = \sqrt{\frac{1}{n}\left\| x^a(t) - x^t(t) \right\|^2} \qquad (3\text{-}51)$$

where N is the rank of the filter, equal to the number of computed FVs (SVs) in LFKF (SVKF). In reduced rank EnKF when $N \le n$, the ensemble size is $N+1$. When $N > n$, the filter is full-ranked with $N+1$ ensemble members. SVKF implementation follows the formulation in chapter 2, that uses an iterative method for computing the singular vectors. A maximum of 5 iterations per singular vector (Floquet vector) are allowed in SVKF (LFKF). EnKF implementation is via a squared root scheme without Localization as appears in Evensen (2004). Our implementation of EnKF does not have the bias problem, which has been discussed in Sakov and Oke (2008), and Livings et al. (2008).

In the first set of experiments, we set $\sqrt{Q(t)} = 0.05\ I^{n\times n}$ and examine the performance of LFKF, SVKF and EnKF for a given N. Although Lorenz 95 system is chaotic, we have not experienced any structural instability due to the dynamic model error. The worst and best possible performances of a Kalman-based filter are benchmarked by an unconstrained integration of the model with no analysis (*Openloop*) and an EnKF with 1440 replicates (*Optimal*), respectively.

The time series of $RMSE\left(x^t, N, t\right)$ of different filters over a typical truth, for a number of chosen *N*'s are plotted on Figure 3-1, along with the Openloop and Optimal time series. Universally, RMSE of all of the filters is between the Openloop and the Optimal as expected, while all of the filters have a lower RMSE with a larger N. EnKF has the worst RMSE for a given rank of the filter, revealing its inefficiency due to the inherent randomness of the ensemble members. In particular, RMSE of the EnKF with $N = 15$ shows almost no improvement over the Openloop, while SVKF and LFKF with comparable rank are reducing the RMSE. When $N = 75$, EnKF

shows some improvement, but SVKF and LFKF have already converged to the Optimal. At last with $N = 135$, EnKF is able to reduce the RMSE to a level near the Optimal.

To guarantee that the results are general and do not depend on a special truth or selection of the observed states, the experiments are repeated for 40 different true trajectories, each with a different observation matrix. We measure the performance by the expected value of the asymptotic level of $RMSE\left(x^t, N, t\right)$:

$$Err(N) = \left\langle \lim_{t\to\infty} RMSE\left(x^t, N, t\right) \right\rangle_{x^t} \tag{3-52}$$

where $\left\langle \cdot \right\rangle_{x^t}$ denotes the expected value over different truths. In experiments, first we approximate $\lim_{t\to\infty} RMSE\left(x^t, N, t\right)$ by the mean value of $RMSE\left(x^t, N, t\right)$ after the initial transient period of 8 units of model time (80 assimilation cycles). Then we compute $Err(N)$ by averaging the asymptotic level of the analysis error over the 40 different truths. Figure 3-2 shows $Err(N)$ for SVKF, LFKF, and EnKF. $Err_{Openloop}$ and $Err_{Optimal}$ are also plotted to mark the worst and the best expected performance, respectively.

In agreement with Figure 3-1, $Err(N)$ of all three of the filters with a small *N* start at somewhere between $Err_{Openloop}$ and $Err_{Optimal}$, and improves towards $Err_{Optimal}$ as N grows. The performance of EnKF does not improve much for $N < 50$, followed by a rapid improvement for $50 < N < 70$, and convergence to the Optimal for $N > 70$. This is because the ensemble members in the EnKF pick the unstable directions randomly, meaning that an ensemble with size

smaller than the number of unstable directions may be missing the important modes with stronger instability. Thus, the overall performance of the EnKF starts to improve only after the number of replicates grows beyond the number of unstable directions.

The rate of improvement of SVKF and LFKF is remarkably faster and more uniform as N grows, because LFKF and SVKF follow a more systematic approach in picking the unstable directions based on their importance. The LFKF is out performed by SVKF, but closely follows its performance, even though LFKF follows a more convenient approach for building the rank reduction subspace than SVKF.

As a side note, after about 16 units of model time the performance of EnKF with $N = 500$ is almost identical to the assumed Optimal, i.e. EnKF with 1440 replicates. This validates our assumption that the EnKF with 1440 ensemble members (the assumed Optimal) performs equally well as the EnKF with infinite ensemble (the true Optimal).

In order to normalize the performance of different filters, we define the Asymptotic Optimality Index of a filter as the ratio of its error reduction with respect to the Openloop, to the maximum error reduction that is achieved by the Optimal filter:

$$\mathrm{AOI}(N) = \frac{\log\left[Err_{Openloop} \right] - \log\left[Err(N) \right]}{\log\left[Err_{Openloop} \right] - \log\left[Err_{Optimal} \right]} \quad , \quad 0 \le AOI(N) \le 1 \qquad (3\text{-}53)$$

An AOI close to unity means that the filter performs asymptotically near the Optimal, while an AOI near zero shows that the filter does not make any improvement over the Openloop, meaning

that the filtered trajectory is as poor of an estimate of the truth as the trajectory with no assimilations. Figure 3-3 shows the AOI of SVKF, LFKF, and EnKF versus $\frac{N}{n}$, the rank of the filter normalized by the state size. This plot is a normalized demonstration of Figure 3-2, showing that the LFKF performs nearly as well as the SVKF, while both of the filters are almost as good as the Optimal when $\frac{N}{n} > 0.3$ ($N > 50$). The EnKF converges to the Optimal when $\frac{N}{n} > 0.5$ ($N > 70$ as suggested in Figure 3-2).

In addition to $n = 144$, we repeated the above experiments with Lorenz 95 with different state sizes (18, 36, 72, 216, and 288, while the number of observed states was also scaled proportionally). We have found that Figure 3-3 does not change by the state size. This suggests that the number of unstable modes of Lorenz 95 is about $\frac{1}{3}$ of the state size, and both SVKF and LFKF are able to capture all of them with as small of a rank as possible.

To better understand the average computational cost of SVKF and LFKF for various N 's, we measured the CPU-time for each filter to complete the above experiments, and computed the average CPU-time per truth normalized by the CPU-time for a single forward integration of the model. The computational cost of the linear model and the adjoint model that are used in the SVKF, are in general different from the cost of the nonlinear model that is used in the LFKF and the EnKF. We have made the appropriate corrections to the CPU-time of SVKF, so that a single integration of the linear model and the adjoint model together, is equivalent to one integration of the nonlinear model. Therefore, this cost measure shows the computational cost of each filter in

terms of the equivalent number of non-linear model runs, as plotted against the rank of the filter in Figure 3-4. In reality, one iteration of the nonlinear model is cheaper than one iteration of the linear model and the adjoint model together.

As expected, EnKF shows a one-to-one linear growth of the computational cost with the rank of the filter. SVKF has an initial five-by-one increase rate due to the maximum allowed number of iterations being 5. However, slope for $N > 50$ starts to decrease, indicating that in average less than 5 iterations are needed for each vector to converge. LFKF has a higher cost for smaller N because the number of vectors that should be considered in the iterative procedure is larger than the number of desirable Floquet vectors N. This is true so long as N is smaller than the number of unstable modes, as verified by the crossing of the cost of SVKF and LFKF when N is about 50.

To see the tradeoff between the cost and the performance, the normalized CPU-times of different filters are plotted against the performance in Figure 3-5. The Optimal performance level is also shown for clarity. It can be seen that SVKF has the best efficiency. The competition between LFKF and EnKF depends on the required performance level. In particular, if a performance close to the Optimal is needed, LFKF is clearly more efficient than EnKF. However, if the computational resources are scarce and a moderate performance is acceptable, EnKF can be a good choice. It should be mentioned that these conclusions are model specific. In particular, the relative efficiency of the filters depends on the number of unstable directions and the number of required iterations for SVKF and LFKF to converge. It is expected that the LFKF outperforms the EnKF in the large geophysical systems that have a relatively small number of unstable

directions, because the efficiency of random ensemble members to capture the unstable modes will be drastically diminish.

To check whether the results will improve or not if we allow further iteration, we repeated the experiments allowing up to 100 iterations per vector. The results were almost identical to Figure 3-3 and not shown here. We conclude that limiting the number of iterations is a viable possibility for reducing the computational cost of LFKF and SVKF, without sacrificing the performance.

To test the LFKF when dynamic model error is zero we use the same experimental setup but with $Q(t) = 0$. Since a straightforward implementation of EnKF in absence of dynamic model error does not give satisfactory results due to rank deficiency LFKF is not tested against EnKF. Similar to the above experiments, a forward integration of the model without any update (Openloop) is assumed to represent the worst case scenario. For the best case scenario, the asymptotic RMSE level of the EnKF with a large ensemble size will not be a good measure because regardless of the ensemble size, EnKF will become rank deficient. However, if the ensemble size is large enough so that the EnKF does not diverge over the time frame of the experiments (16 units of model time), the corresponding limited time RMSE can still be used as the expected RMSE level of the Optimal filter. We observed that in most of the experiments, 1440 ensemble members were enough to prevent the divergence of the EnKF over 16 units of model time. Hence we use the corresponding RMSE level as the Optimal.

Figure 3-6 shows the RMSE of LFKF and SVKF for a typical truth. Similar to Figure 3-1, RMSE of SVKF and LFKF is between the bounds of the RMSE from the Openloop and the

Optimal. In general, the RMSE levels are lower than Figure 3-1 because there is no dynamic model error. Over this truth, the SVKF reduces the RMSE more rapidly than the LFKF. However, we have observed that over some other truths, LFKF has a more rapid response that SVKF. Therefore, in terms of transient behavior, neither LFKF nor SVKF are superior. In terms of the asymptotic level of RMSE, Figure 3-6 suggests that both filters perform equally well for large N. However, to confirm this observation we need to look at the average asymptotic RMSE level over multiple truths.

Figure 3-7 depicts $Err(N)$ for LFKF and SVKF, computed via (3-52). Similar to Figure 3-2, the performance of Openloop and the Optimal are also plotted for reference. In contrary to Figure 3-2, the improvement in the performance of both of the filters as N grows is no longer uniform. In particular, there is a sharp drop in $Err(N)$ of both of the filters. This is due to the absence of dynamic model error. In particular, when dynamic model error is present, the reduced rank approximation of the forecast error covariance is combined with the dynamic model error covariance. This will compensate for the underestimation of the forecast error in the reduced rank filters with a too small N along the important directions that cold not be considered in the filter.

Figure 3-7 clearly shows the impact of the geometry of the attractor on the performance of the filter. When $N > 50$, both of the filters perform at the same level because all of the unstable directions are considered. In contrast when $N < 20$, both of the filters perform poorly, suggesting that the first 20 unstable directions are essential for performance of the reduced rank filter. The unstable directions corresponding to $20 < N < 50$ are still necessary for convergence

of the reduced rank filter, but have less importance than the first 20. Additionally, every additional singular vector projects on all of the remaining unstable directions, while the number of unstable directions that are considered in LFKF directly grow with N. Therefore SVKF is able to project on more unstable directions than LFKF, with a given rank.

To complete the discussion, the normalized performance of SVKF and LFKF are plotted in Figure 3-8. Again we can see that both of the filters perform near the Optimal when $\frac{N}{n} > 0.3$ ($N > 50$), while SVKF outperforms LFKF for the same reason as above in the discussion of Figure 3-7.

3.8 Conclusion

Due to the large state size in geophysical applications, dynamics of the system is often projected on a lower dimensional subspace. The main difference among various reduced rank KF-based algorithms is in the choice of basis for this projection subspace. In this paper, we framed the reduced rank filtering problem from the perspective of stabilizing the local dynamics of the estimation error and followed a linear approximation of the error propagation. We showed that the locally unstable directions of the state transition matrix are needed to be captured for near optimal performance of any reduced rank filter.

We introduced an iterative procedure for computing a basis for the subspace of unstable directions that we called Floquet vectors because they were equivalent to the unstable directions of the Floquet matrix of an auxiliary periodic system, which we constructed over the forecast

trajectory. We discussed that the interpretation of Floquet vectors from the point of view of local geometry of the attractor of the system, parallels the interpretation of the Lyapunov vectors with regards to the global geometry of the attractor. We also explained the relationship between Floquet vectors and the Bred vectors.

We built a reduced rank filter using the Floquet vectors and examined its performance against SVKF and EnKF on a chaotic Lorenz 95 system with dynamic model error. We showed that for a given rank of the filter, LFKF performs very closely to SVKF, while both of the filters outperform EnKF due to its inefficiency in capturing the maximum number of unstable directions with a given ensemble size.

In terms of the computational cost, the iterative process for computing the Floquet vectors requires about 5 iterations per vector for Lorenz 95. This makes LFKF inferior to EnKF for small problems. However, in large systems of interest in geophysical systems, a successful implementation of EnKF requires too many replicates that may not be possible. In such problems, LFKF can be an appealing algorithm due to its rigorous approach to stabilize the error dynamics.

Additionally, when the rank of the filter was too small, the procedure would not converge because the number of computed Floquet vectors was much smaller than the number of unstable directions. Therefore, more Floquet vectors than the rank of the filter had to be computed, seeming to add to the computational cost of the filter when the selected rank is too small. However, the suggested rank for a successful implementation of LFKF is at least equal to the average number of unstable directions. In other words, similar to any reduced rank filter,

implementation of the LFKF with a rank that is much smaller than the number of unstable directions will be far from optimal and is not recommended. Therefore, the computational cost of LFKF with a very small rank is not important for practical purposes.

When dynamic model error is zero, we proposed a solution for possible rank deficiency of LFKF, by formulating a provision for the filter to consider the stable directions that due to the chaotic dynamics become unstable, following an approach similar to the SVKF. We showed that LFKF performs near optimal under when dynamic model error is zero, as long as all of the unstable directions are considered.

Although the preliminary results of LFKF are very promising and the algorithm is in principle scalable to large systems, an actual implementation of LFKF in a large chaotic system will be very informative and is the natural step to follow this work. Additionally, through out this paper, we maintained that the model is structurally stable. We leave in depth analysis of the suitability of LFKF for systems that are subject to structural instabilities to future work.

3.9 References

Andrews, A., 1968: A square root formulation of the Kalman covariance equations. *AIAA Journal*, **6**, pp 1165-1166.

Bishop, C. H., B. J. Etherton, and S. J. Majumdar, 2001: Adaptive Sampling with the Ensemble Transform Kalman Filter. Part I: Theoretical Aspects. *Mon. Wea. Rev.*, **129**, pp 420-436.

Buehner, M., and P. Malanotte-Rizzoli, 2003: Reduced-rank Kalman filter applied to an

idealized model of the wind-driven ocean circulation, *J. Geophys. Res.*, **108**, p 3192

Buizza, R., and T. N. Palmer, 1995: The singular vector structure of the atmospheric general circulation. *J. Atmos. Sci.* **52**, 9, pp 1434-1456.

Cane, M., A. Kaplan, R. N. Miller, B. Tang, E. C. Hackert, and A. J. Busalacchi, 1996: Mapping tropical Pacific sea level: Data assimilation via a reduced state space Kalman filter. *J. Geophys. Res.*, **101**, pp 22 599 –22 617.

Ehrendorfer M., and J. J. Tribbia, 1997: Optimal prediction of forecast error covariance through singular vectors. *J. Atmos. Sci.* **54**, pp 286-313.

Evensen, G., 1994: Sequential data assimilation with a nonlinear quasi-geostrophic model using Monte-Carlo methods to forecast error statistics. *J. Geophys. Res.,* **99**, pp 10 143–10 162.

Evensen, G., 2004: Sampling strategies and square root analysis schemes for the EnKF. *Ocean Dynamics*, **54**, pp 539-560.

Farrell, B. F., and P. J. Ioannou, 1996: Generalized stability theory. Part 1: Autonomous operators. *J. Atmos. Sci.*, **53**, pp 2025-2040.

Farrell, B. F., and P. J. Ioannou, 2001: State estimation using a reduced order Kalman filter, *J. Atmos. Sci.*, **58**, pp 3666-3680.

Foale, S., and J. M. T. Thompson, 1991: Geometrical concepts and computational techniques of nonlinear dynamics. *Comp. Methods Appl. Mech. Eng.*, **89**, pp 381-394.

Fukumori, I., and P. Malanotte-Rizzoli, 1995: An approximate Kalman filter for ocean data assimilation: An example with an idealized Gulf stream model, *J. Geophys. Res.*, **100**, pp 6777-6793

Gaspari, G. and S. E. Cohn, 1999: Construction of correlation functions in two and three dimensions. *Quart. J. Roy. Meteor. Soc.*, **125**, pp 723-757.

Gelb, A., Ed., 1974: *Applied Optimal Estimation*. The MIT Press, p 306.

Golub, H. G., and C. F. Van Loan, 1996: Matrix computations, *The Johns Hopkins University Press.*, Baltimore, USA, pp 313-326.

Hansen, J. A., 1998: Adaptive observations in spatially extended, nonlinear dynamical systems, PhD thesis, Oxford University, pp 207.

Hartman, P., 1982: Ordinary Differential Equations, 2nd edition, *Birkhauser*, Boston, USA. pp 45-65.

Houtekamer, P. L., and H. L. Mitchell, 2001: A sequential ensemble Kalman filter for atmospheric data assimilation. *Mon. Wea. Rev*., **129**, pp 123-137.

Ide, K., and M. Ghil, 1997a: Extended Kalman filtering for vortex systems. Part I: Methodology and point vortices. *Dyn. Atmos. Oceans*, **27**, pp 301-332

Ide, K., and M. Ghil, 1997b: Extended Kalman filtering for vortex systems. Part II: Rankine vortices and observing-system design. *Dyn. Atmos. Oceans*, **27**, pp 333–350

Jaeger, L., and H. Kantz, 1997: Homoclinic tangencies and non-normal Jacobians - Effects of noise in nonhyperbolic chaotic systems. *Physica D*, **105**, pp 79-96.

Kalnay, E., 2003: Atmospheric modeling, data assimilation and predictability, *Cambridge University Press*, Cambridge, UK, pp 220-248.

Kraut, S., and C. Grebogi, 2004: Escaping from nonhyperbolic chaotic attractors. *Phys. Rev. Lett.*, **92**, number 23, 234101.

Lorenz, E. N., 1963: Deterministic non-periodic flow. *J. Atmos. Sci.*, **20**, p 130.

Lorenz, E., and K. Emanuel, 1998: Optimal sites for supplementary weather observations: Simulation with a small model, *J. Atmos. Sci.*, **55**, pp 399-414.

Miller, R., Ghil, M., Gauthiez, F., 1994: Advanced data assimilation in strongly nonlinear dynamical systems. *J. Atmos. Sci.*, **51**, pp 1037-1056

Miller, R. N., E. F. Carter, and S. T. Blue, 1999: Data assimilation into nonlinear stochastic models, *Tellus*, **51A**, pp 167-194

Molteni, F., R. Buizza, T. N. Palmer, and T. Petroliagis, 1996: The new ECMWF ensemble prediction system: Methodology and Validation. *Quart. J. Roy. Meteor. Soc.* **122**, pp 73-119.

Mukougawa, H., M. Kimoto, and S. Yoden, 1991: A relationship between local error growth and quasi-stationary states: Case study in the Lorenz system. *J. Atmos. Sci.* **48**, pp 1231-1237.

Nagashima, H. and Y. Baba, 1999: Introduction to Chaos, Physics and Mathematics of chaotic

phenomena. *IOP Publishing Ltd*, Bristol, UK. pp 13-40.

Palmer, T. N., R. Gelaro, J. Barkmeijer, and R. Buizza,1998: Singular vectors, metrics and adaptive observations. *J. Atmos. Sci.*, **55**, pp 633-653.

Paul, D., 2007: Asymptotics of sample eigenstructure for a large dimensional spiked covariance model. *Statistica Sinica*, **17**, pp 1617-1642.

Pham, D. T., J. Verron, and M. C. Roubaud, 1998: A singular evolutive extended Kalman filter for data assimilation in oceanography. *J. Marine Sys.*, **16**, pp 323-340.

Risken, H., 1996: *The Fokker-Planck Equation - Methods of Solution and Applications.* Springer, New York, USA.

Ristic, B., S. Arulampalam, and N. Gordon, 2004: *Beyond the Kalman Filter - Particle Filters for Tracking Applications.* Artech House, Boston, USA.

Robert, C., K. T. Alligood, E. Ott, and J. A. Yorke, 2000: Explosions of chaotic sets. *Physica D*, **144**, pp 44-61.

Ruelle, D., 1989: Deterministic Chaos: The Science and the Fiction. *Proc. R. Soc. Lon. Series A, Math. and Phys. Sci.*, **427**, **No. 1873**, pp 241-248.

Schroer, C. G., E. Ott, and J. A. Yorke, 1998: Effect of noise on nonhyperbolic chaotic attractors. *Phys. Rev. Lett.*, **81**, pp 1397-1400.

Sun, C., Z. Hao, M. Ghil, and J. D. Neelin, 2002: Data assimilation for a coupled ocean-

atmosphere model. Part I: Sequential state estimation. *Mon. Wea. Rev.*, **130**, pp 1073-1099.

Toth, Z., and E. Kalnay, 1993: Ensemble forecasting at NMP: the generation of perturbations. *Bull. Amer. Meteor. Soc.* **74**, pp 2317-2330.

Toth, Z., and E. Kalnay, 1997: Ensemble forecasting at NCEP: the Breading method. *Mon. Wea. Rev.* **125**, pp 3297-3319.

Verron, J., L. Gourdeau, D. T. Pham, R. Murtugudde, and A. J. Busalacchi, 1999: An extended Kalman filter to assimilate satellite altimeter data into a nonlinear numerical model of the tropical Pacific Ocean: Methods and validation, *J. Geophys. Res.*, **104**, pp 5441-5458

Yakubovich, V. A. and V. M. Starzhinskii, 1975: Linear differential equations with periodic coefficients, *John Wiley & Son Inc.*, New York, USA, pp 70-91.

Zang, Xiaoyun and P. Malanotte-Rizzoli, 2003: A comparison of assimilation results from the ensemble Kalman filter and the reduced-rank extended Kalman filter, *Nonlinear Processes in Geophysics*, **10**, 477-491.

3.10 Figures

Figure 3-1: RMSE time series for a typical truth, 144D chaotic Lorenz 95 with dynamic model error

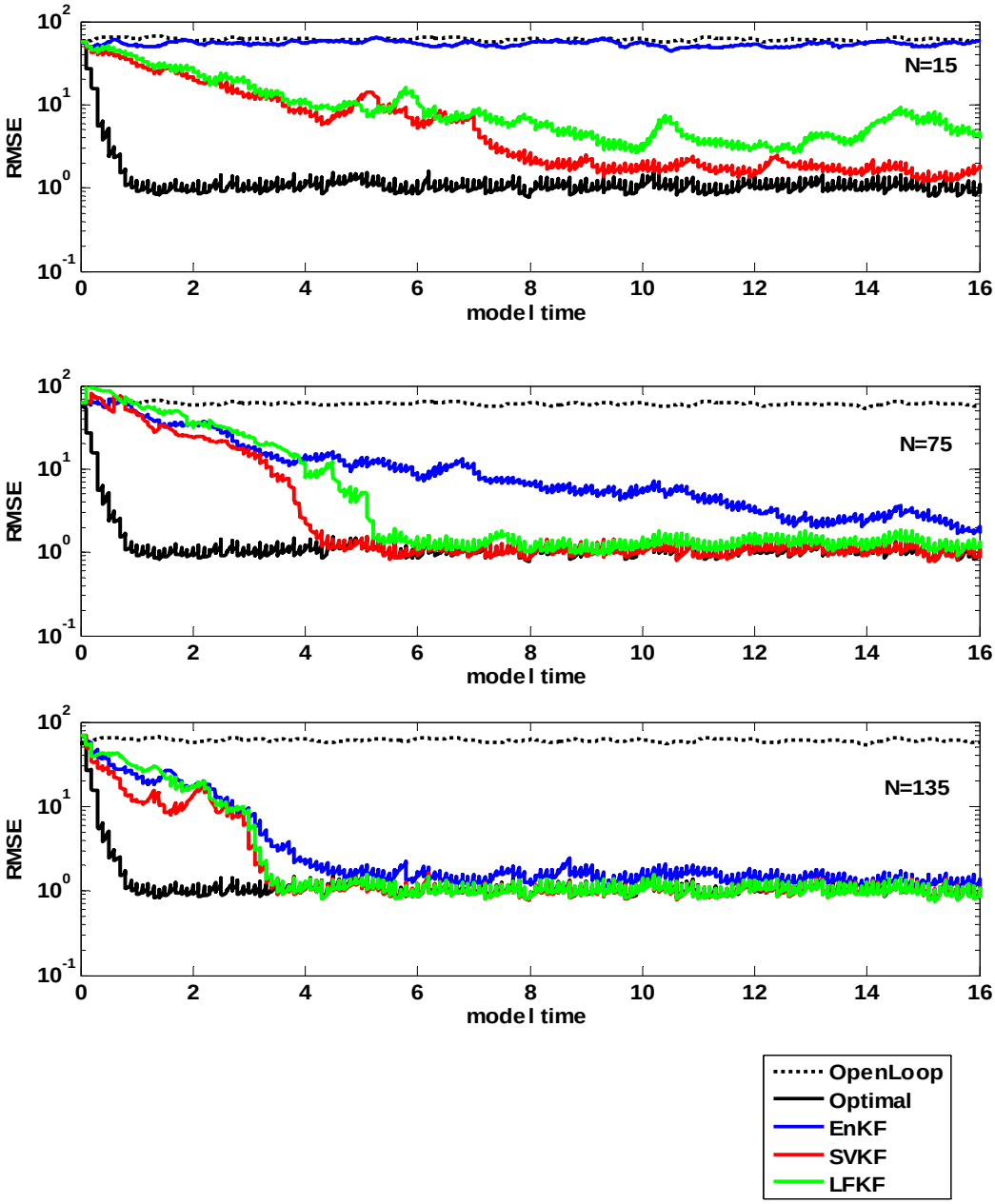

Figure 3-2: Performance vs. Rank of the filter, 144D chaotic Lorenz 95 with dynamic model error

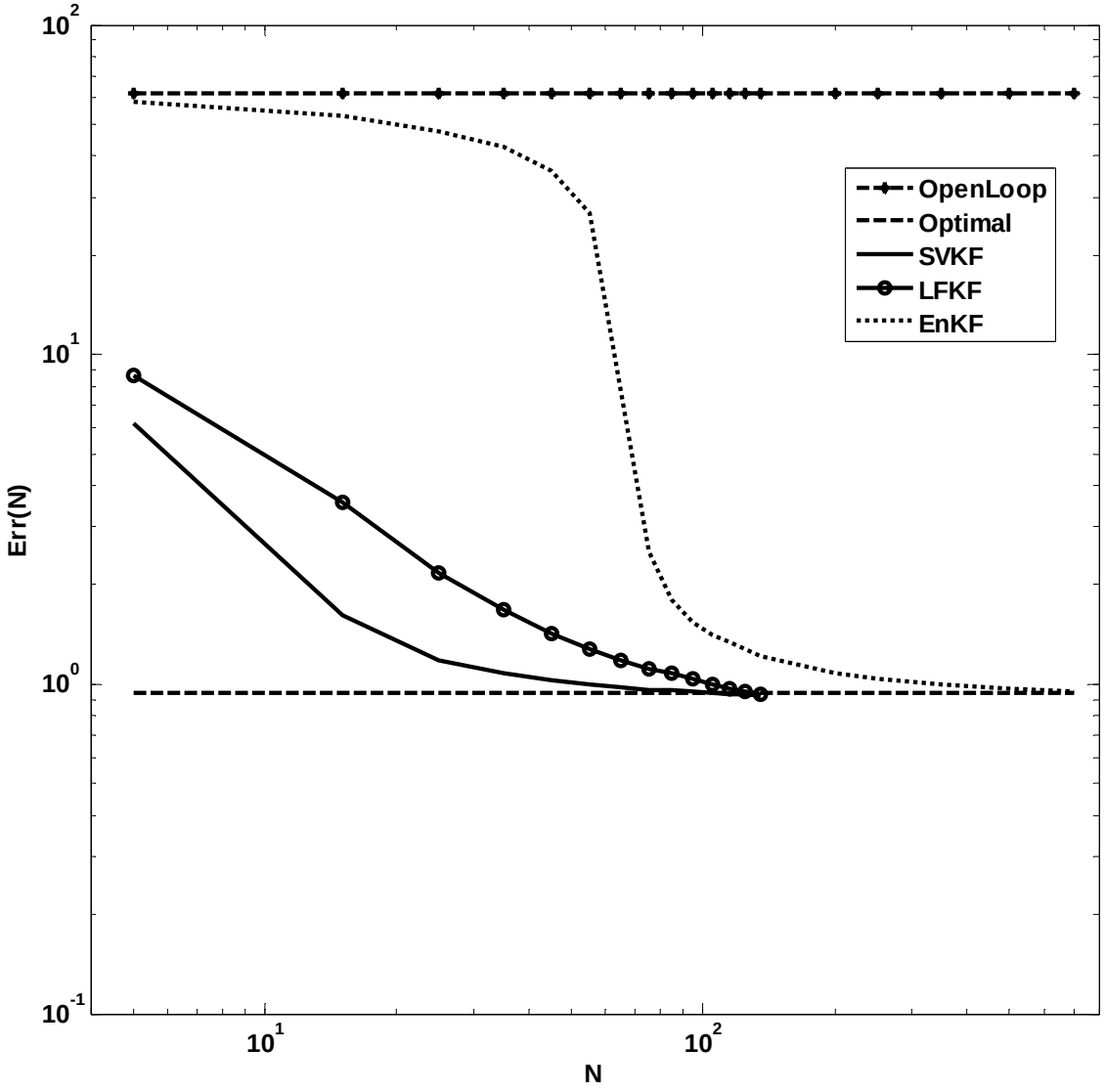

Figure 3-3: Normalized Optimality, 144D chaotic Lorenz 95 with dynamic model error

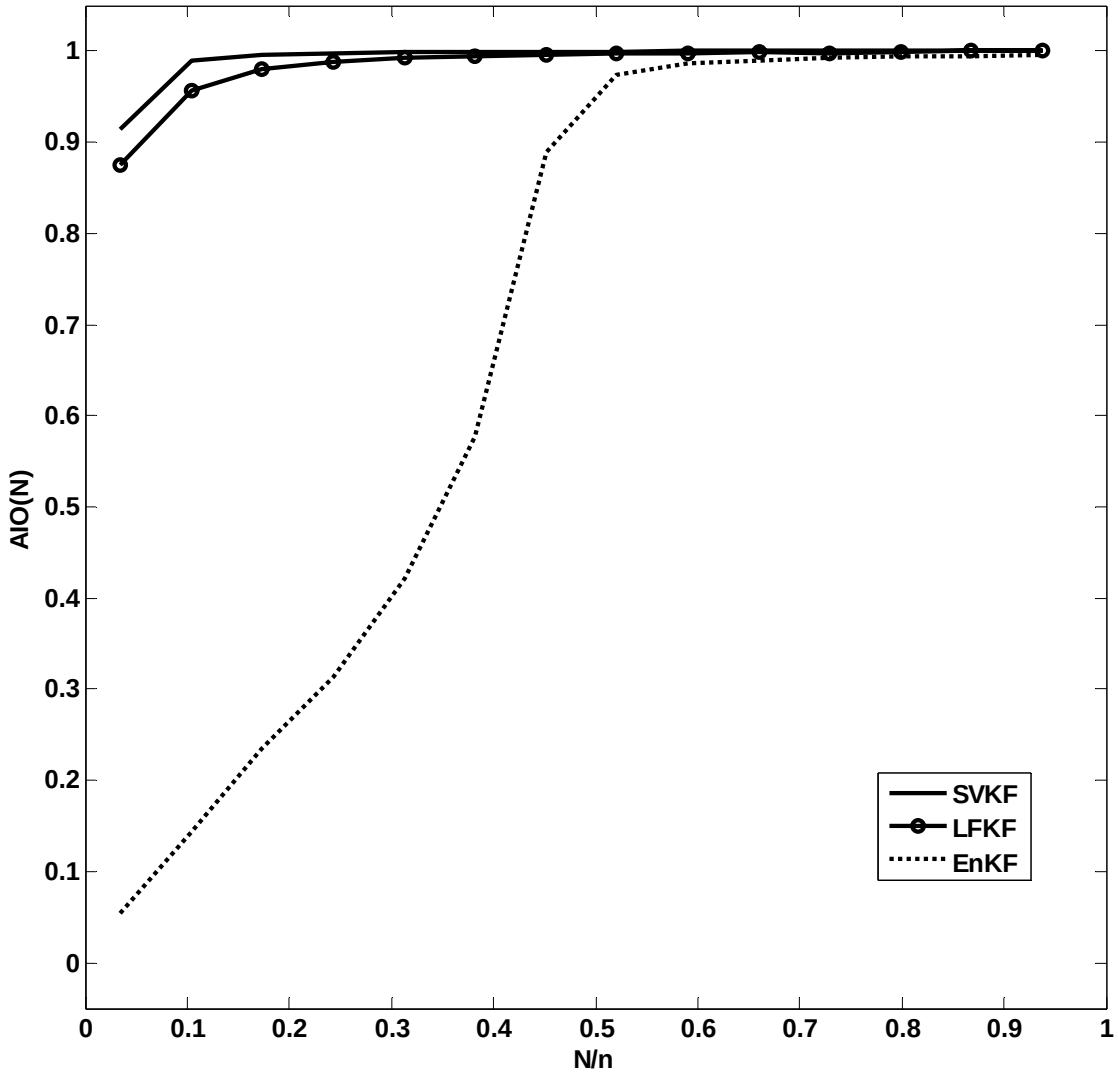

Figure 3-4: Computational cost vs. Rank of the filter, 144D chaotic Lorenz 95 with dynamic model error

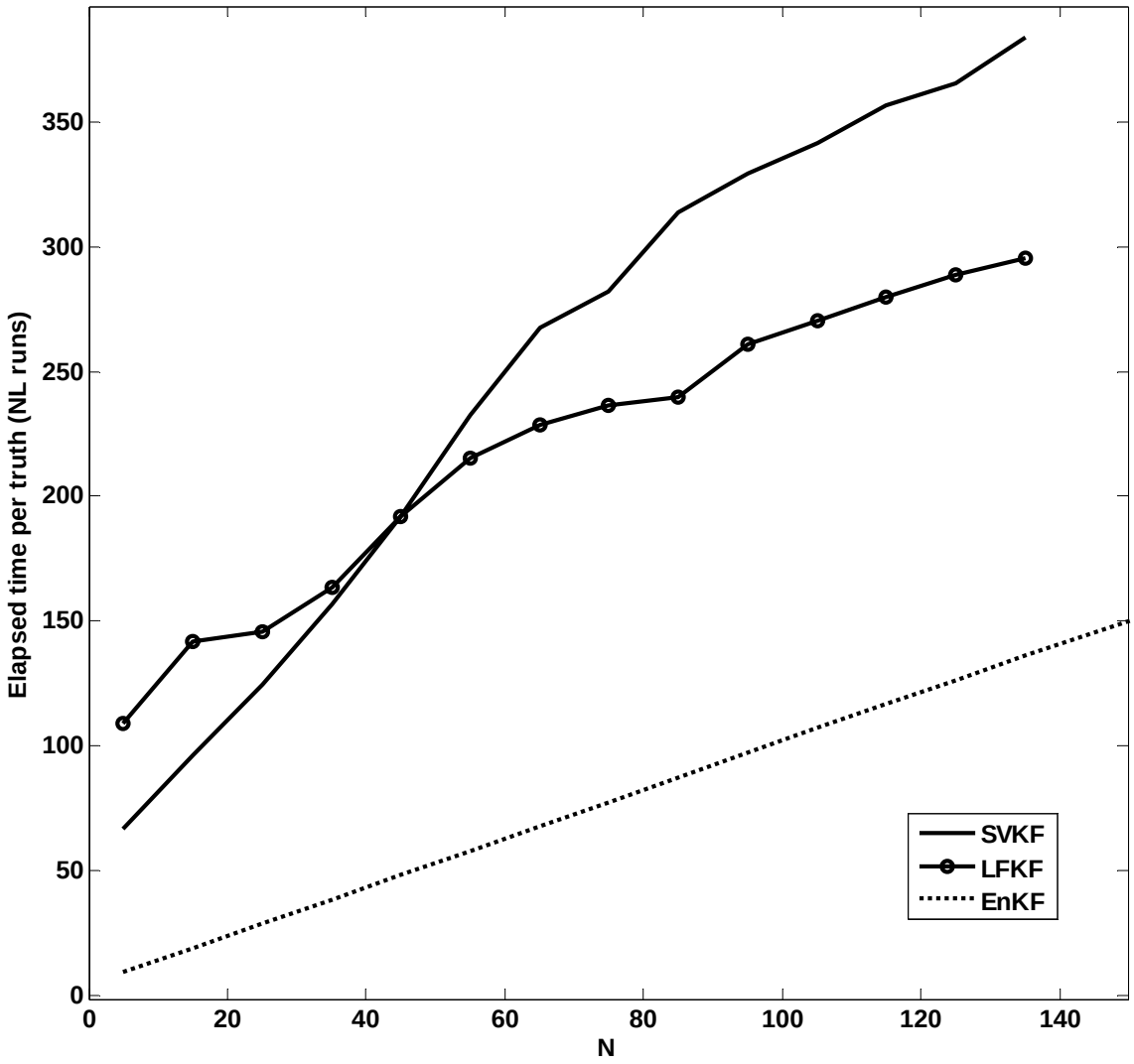

Figure 3-5: Computational cost vs. Performance, 144D chaotic Lorenz 95 with dynamic model error

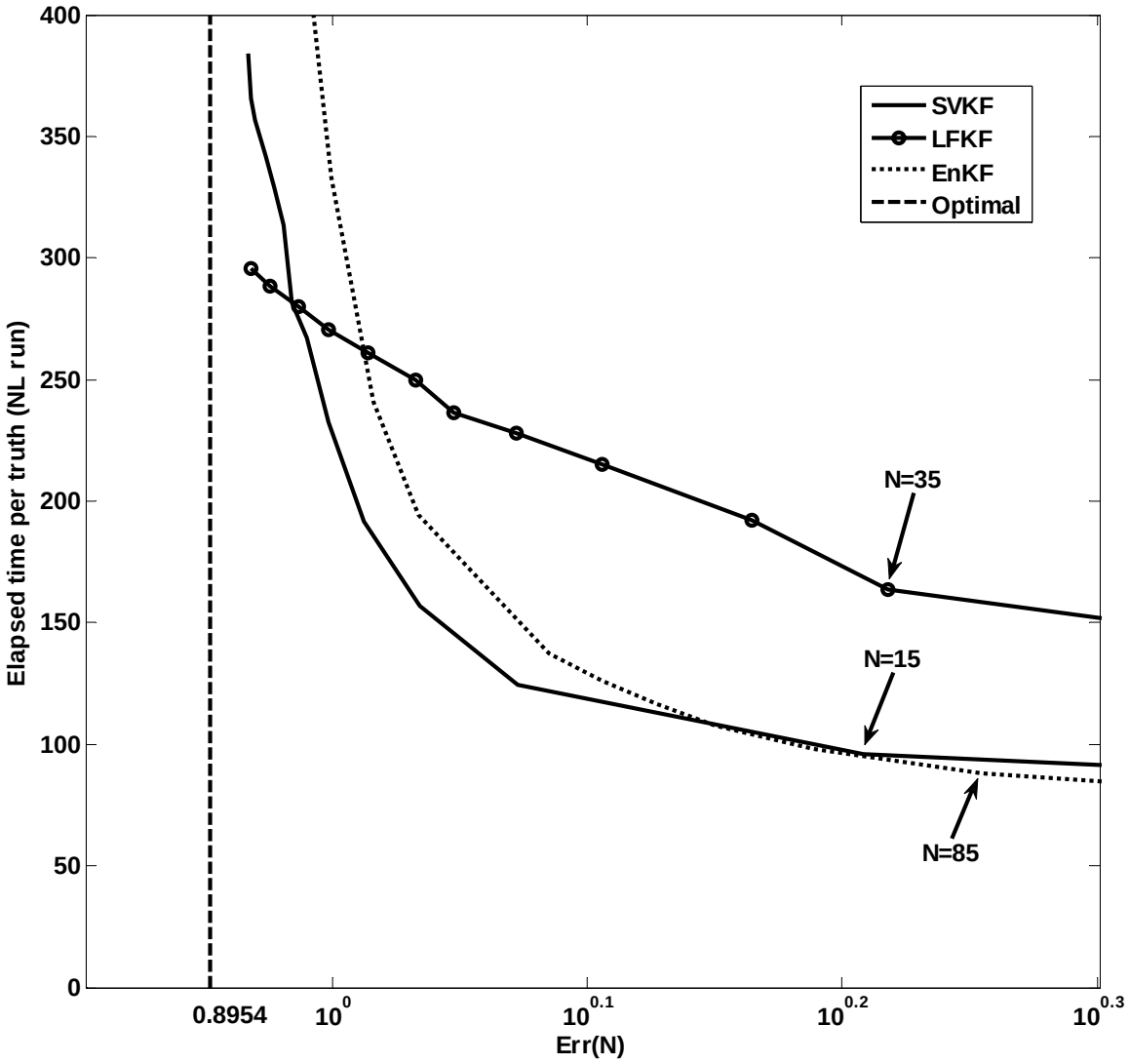

Figure 3-6: RMSE time series for a typical truth, 144D chaotic Lorenz 95, no dynamic model error

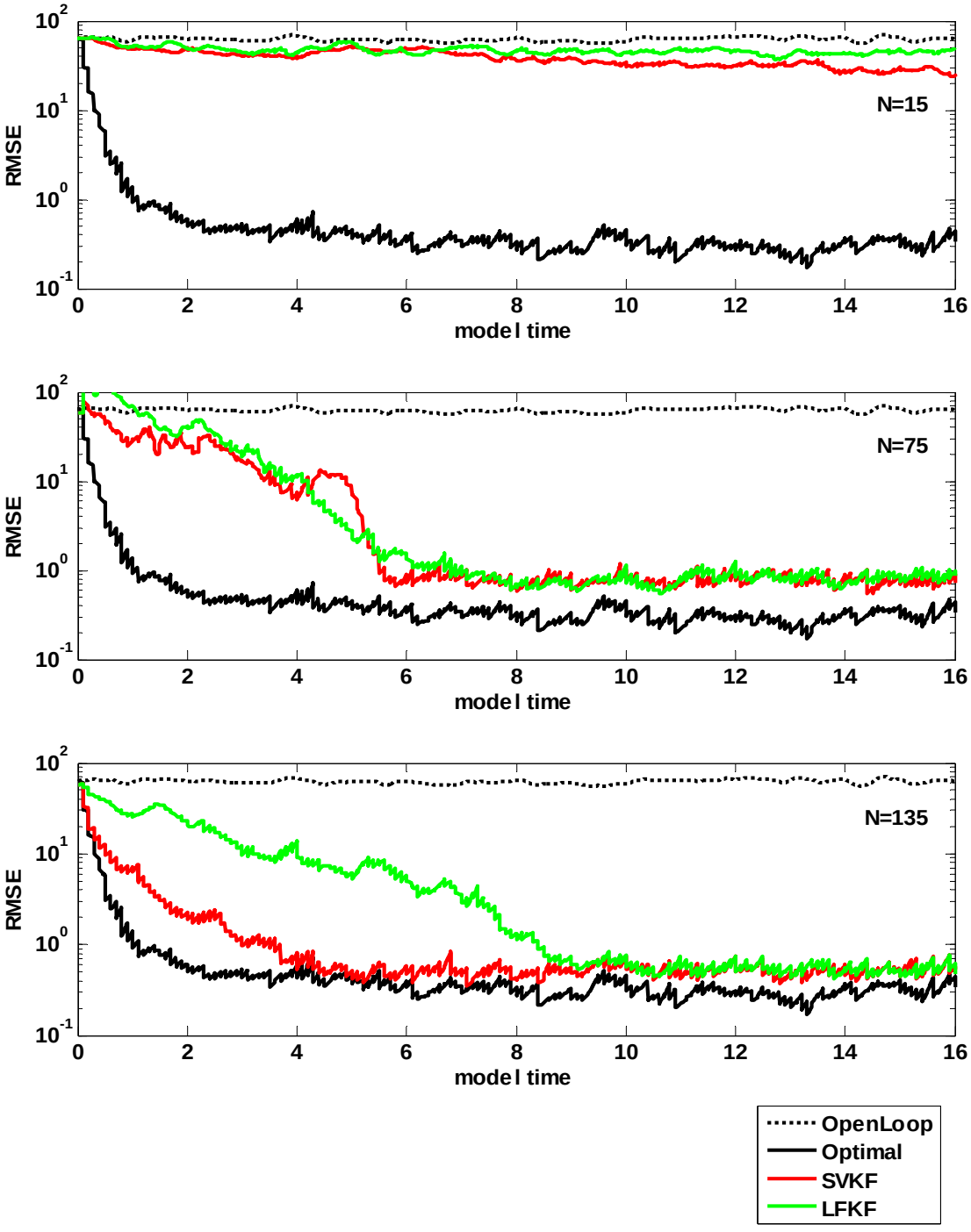

Figure 3-7: Performance vs. Rank of the filter, 144D chaotic Lorenz 95, no dynamic model error

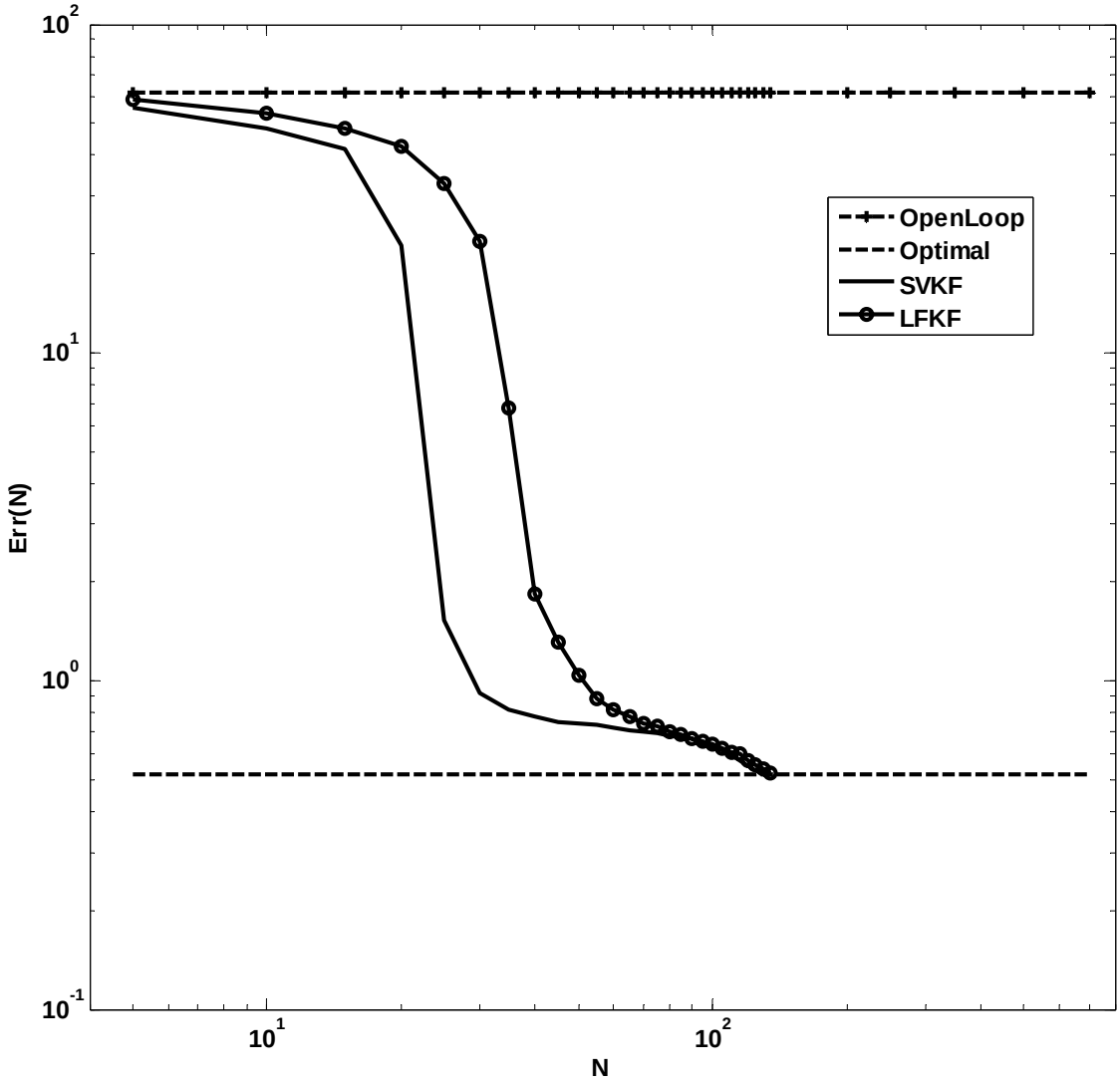

Figure 3-8: Normalized Optimality, 144D chaotic Lorenz 95, no dynamic model error

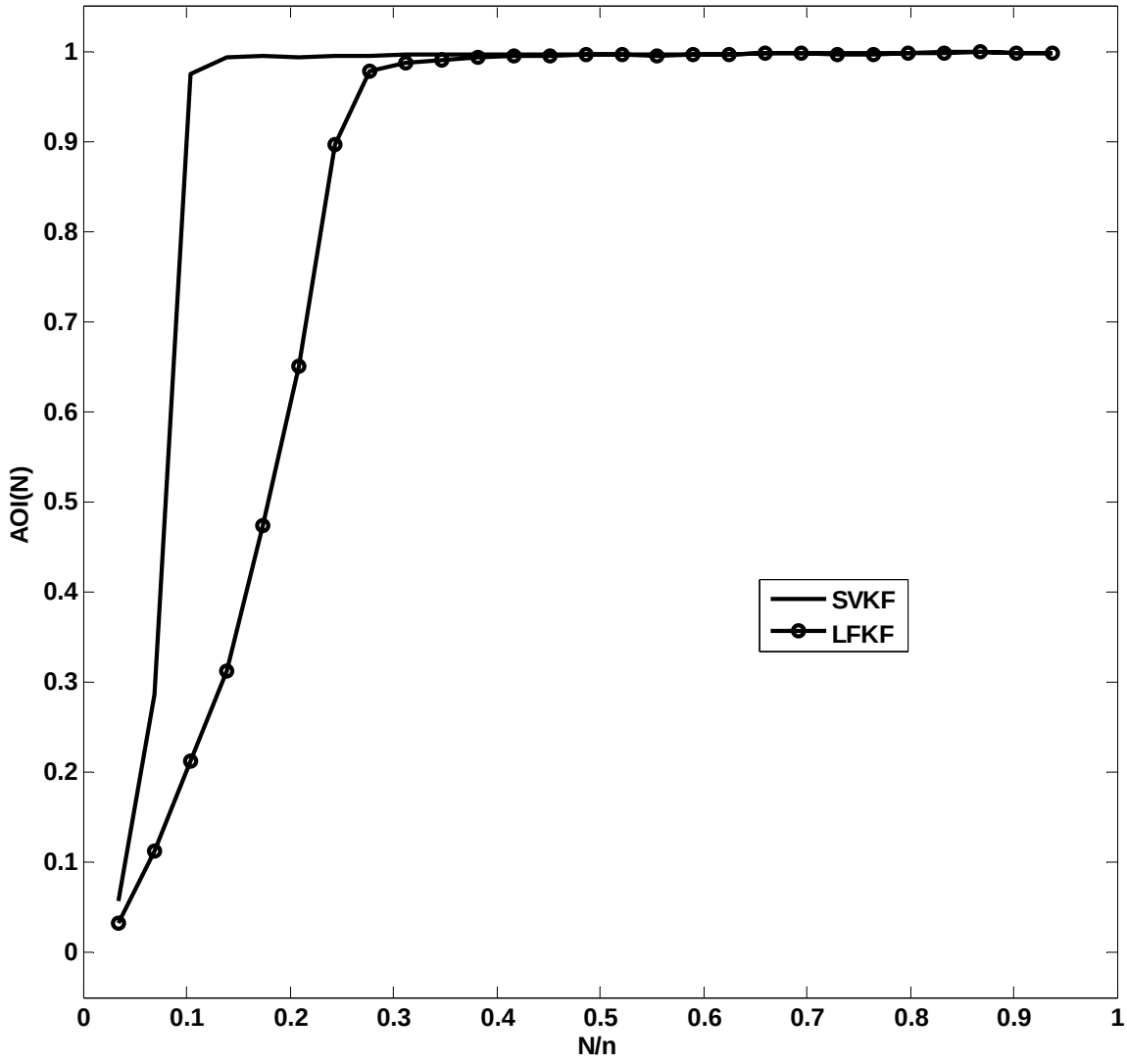

4 Filtering in Chaotic Geophysical Systems: Implementation in an Idealized Quasi-geostrophic Ocean Model

4.1 Introduction

Results in chapters 2 and 3 suggest that Singular Vector Kalman Filter and Local Floquet vector Kalman are two promising algorithms for filtering in chaotic geophysical applications. In this chapter, an idealized wind-driven reduced-gravity quasi-geostrophic ocean circulation model is used to investigate some of the issues that arise in implementation of these filters in large systems. The dynamic model error is assumed to be zero. This allows an efficient revision of the covariance update equation that is suitable for assimilating a very large vector of observations. The experiments suggest that the proper selection of the observation operator is crucial for the performance of the filters. A metric for observability is suggested that can be helpful for verifying effectiveness of an observation operator as well as for designing an adaptive observation network. Results show that when the system is observable, both of the filters can reduce the estimation error down to the level of observation noise.

4.2 Background

Data assimilation as a method for estimating variables and/or parameters of a system has received considerable attention in a wide array of geophysical applications. The estimation problem is posed in a probabilistic framework as the minimization of the expected error in the estimated values of variables of interest (analysis) with respect to their true values (truth), by combining the predicted values (forecast) by a model of the underlying dynamical system and noisy measurements of the truth (observation). The optimum analysis is computed according to the Bayes rule, using the joint probability distribution of the forecast error and the observation noise. We focus on filtering, where the observations are assimilated sequentially as they arrive via a recursive formulation.

When both the dynamical model (for propagating the state) and the observation operator (for relating the observations to the truth) are linear, and the uncertainties are Gaussian random variables, the optimum estimate is computed by the Kalman filter as a linear combination of the observation and the forecast, with the weights specified according to the covariance matrices of the observation noise and the forecast error. In presence of nonlinearities, the uncertainty distributions do not remain Gaussian and higher moments are needed to characterize them. This involves nonlinear operations on the probability distribution functions, and in general does not have any analytical solutions. A Monte Carlo based Particle Filter was proposed to approximate the optimal estimate by evaluating the statistics of a set of replicates (Arulampalam, 2002). However the number of replicates that are needed for convergence in these methods grows with the number of state variables, rendering them impractical for large systems such as in

geophysical applications with $O(10^5)$ state variables.

When the nonlinearities in the dynamical system or the observation operator are not too strong, they can be linearized around the best estimate of the state and used in a Kalman filter to compute a suboptimal solution, a technique known as the Extended Kalman Filter (EKF) (Miller et al., 1994; Miller et al., 1999; Picard, 1991). Unfortunately, even when the linearization is valid, the EKF is too costly in large systems. In fact, full specification of the forecast error covariance entails computing the state transition matrix of the system over the forecast window (also known as the tangent linear model (TLM) in geophysical sciences). This requires developing a code for the TLM, which is difficult in complex systems, or conducting as many integrations of the nonlinear model as the size of the state, which is not computationally feasible.

Reduced rank methods have been developed to resolve just the dominant structures of the forecast error covariance (Fukumori and Malanotte-Rizzoli, 1995; Cane et al., 1996; Buehner and Malanotte-Rizzoli, 2003; Buehner et al., 2003 Farrell and Ioannou, 2001; Heemink et al., 2001; Lermusiaux and Robinson, 1999; Pham et al., 1998; Ubaldi, 2005 and 2006; Evensen, 2003 and 2004). The success of these methods depends on the dynamical properties of the underlying system and the validity of the rank-reduction assumptions. In linear or weakly nonlinear systems with quasi-stationary dynamics, the dominant structures of uncertainty do not undergo strong changes over time and can be identified by the long term evolution of the system. These dominant structures, also known as the Empirical Orthogonal Functions (EOFs) of the system capture most of the uncertainty structures in quasi-stationary systems (Toumazou, 2001; Buehner and Malanotte-Rizzoli, 2003, henceforth BM). Thus, they can be used for

reduced rank representation of the forecast error covariance in a filter, as in the Reduced Rank extended Kalman Filter of BM who showed that a few leading EOFs were able to resolve most of the forecast uncertainty in a periodic quasi-geostrophic ocean circulation model, and successfully implemented the RRKF on the periodic ocean model. BM reported that the RRKF did not perform well on a chaotic version of the model. This can be explained by dynamical properties of chaotic systems.

When the underlying system is chaotic, as in many oceanic and atmospheric applications, the dominant uncertainty structures change considerably over time (Nagashima and Baba, 1999). Therefore, attempting to reduce the rank of the system by means of a set of stationary structures such as the EOFs is inappropriate. The results of BM in chaotic ocean model are in agreement with other experiments on chaotic systems, emphasizing the importance of resolving the time-varying structures of forecast uncertainty (Zichmann, 2000; Nese, 1989; Hokougawa, 1991; Gyarmati, 2003; Trevisan, 1993 and 1995).

Ensemble-based methods such as the Ensemble Kalman Filter (EnKF) use an ensemble of replicates to propagate the structures of uncertainties over the forecast window (Evensen 1994, 1997, 2003, and 2004). Specifically, it is assumed that the ensemble members that are computed at the update step represent the uncertainty structures in the analysis estimate. These analysis ensemble members are propagated by the nonlinear dynamics, yielding a set of propagated ensemble members, which are assumed to represent the uncertainty structures in the forecast estimate. Since the ensemble members are propagated by the nonlinear forward model, they aggregate the time-varying structures of the dynamical model over the forecast window, hence

the appeal of ensemble based filters for chaotic systems (Zang and Malanotte-Rizzoli, 2003, henceforth ZM). However, performance of ensemble filters greatly depends on the ensemble size, which becomes a burden in large oceanic and atmospheric applications. In particular, the affordable number of replicates in these applications is much smaller than the dimension of the state space, meaning that almost always the covariance of the ensemble members has a low rank. In other words, the forecast covariance does not have any projections on many directions that are in the null-space of the ensemble covariance. This can be problematic in many applications.

From a geometrical point of view, the filters ability to reduce the estimation error along any directions depends solely on the relative magnitude of the observation uncertainty and the forecast uncertainty based on the approximated forecast covariance. But the forecast uncertainty along any directions in the null-space is zero. Thus, the filter assumes the forecast to be perfect in the null-space and corrects it only in the subspace of ensemble members. This does not cause any problems as long as the ensemble subspace includes all of the directions that require correction in the forecast In particular, if ensemble members can resolve the dominant structures of uncertainty at all times, then the filter will perform well. In oceanic and atmospheric applications, the number of these dominant structures is much smaller than the size of the state (Kalnay, 2003; Yano, 1992). However, since the ensemble members are inherently random, EnKF is inefficient in capturing them, meaning that the number of replicates that are needed for convergence of the filter is much more than the number of dominant structures.

Another issue in implementation of EnKF in chaotic oceanic and atmospheric applications is the representation of the dynamic model error, which is typically included by adding random

perturbations to the state equation. Unfortunately, such perturbations can induce non-physical anomalies or imbalances. This is a serious problem for example in the numerical weather prediction, where small perturbations in model states can generate spurious inertial or gravity waves (Barwell and Bromley, 1988, Daley, 1991, Gauthier and Thépaut, 2001, Fillion, 2002, Neef et al., 2006). It is a much less serious problem in oceanographic applications as the hydrostatic approximation used in most Ocean General Circulation models, and in particular QG models , filter out gravity waves, In effect, the model error perturbation drives forecast vectors off the attractor into regions of the state space where they follow non-physical trajectories. For this reason, most ensemble filters used in meteorological data assimilation applications do not include dynamic model error, also known as the perfect model scenario assuming that the only sources of uncertainty in the forecast are the initial condition and the noisy observations,.

Unfortunately, when the EnKF is formulated without dynamic model error, the ensemble members tend to loose their independence over a few assimilation cycles, and become rank deficient. In other words, the rank of the ensemble covariance, i.e. the number of independent ensemble perturbations decline and the filter eventually looses its ability to capture all of the dominant directions of uncertainty. To resolve the rank deficiency of the EnKF, a number of empirical methods such as Variance Inflation and Localization have been suggested, which increase the rank of the ensemble covariance at the expense of altering its correlation structures (Houtekamer and Mitchell, 2001; Hamill et al., 2001; Anderson and Anderson, 1999). Here, we briefly discuss the Localization which is more common.

In Localization, the ensemble covariance matrix is multiplied element-by-element by a matrix of

weights that are computed using a Localization function, enforcing our a priori knowledge about the physically meaningful correlation structures. For example, it is commonly assumed that the states which are distant in the physical domain are not strongly correlated (Pereira and Berre, 2006; ZM). The resulting correlation function eliminates the spurious correlations and essentially increases the rank of the ensemble covariance matrix. As the result, the filter considers some non-zero but suboptimal uncertainty along the null-space directions, which would otherwise be missed. Although the EnKF with Localization seems to be a viable option in many applications, its performance will deteriorate severely with a bad choice of Localization function.

In chapters 2 and 3, we introduced two Kalman-based algorithms, the SV-based Kalman Filter (SVKF) and the Local Floquet vector Kalman Filter (LFKF), that were based on identifying the transient dominant structures of uncertainty in a chaotic system. Specifically, SVKF resolves propagation of uncertainties along the directions they are growing (leading singular vectors of the TLM), and LFKF resolves propagation of uncertainties along the locally unstable directions (leading Floquet vectors of the TLM). The preliminary results from implementation of the filters in the Lorenz95 system were promising for both the cases with and without dynamic model error.

This work constitutes a logical extension not only of the work in chapters 2 and 3 but also of the work by ZM, as it implements the SVKF and LFKF in the same quasi-geostrophic model of the wind-driven ocean circulation, which exhibits chaotic dynamics in the low viscosity regime. ZM's goal was to compare the effectiveness of assimilations carried out using the RRKF and the

EnKF. They found that in the chaotic regime the EnKF greatly outperforms the RRKF (which is equivalent to Optimal Interpolation) and that 32 ensemble members are sufficient to describe the non-stationary, inhomogeneous and anisotropic structure of the forecast error covariance. As both SVKF and LFKF are based on directly identifying the transient dominant structures of uncertainty in a chaotic system, they do not need a Localization function as the E KF of ZM.

The paper is organized as follows. In section 4.3 we exploit the absence of dynamic model error to revise the covariance update equation to a form that is more efficient than the formulations in chapters 2 and 3. In Section 3 we briefly describe the model, its parameters and properties. In section 4.5 we discuss the experiment setup and results. Finally, in section 4.6 we present our conclusions.

4.3 Filter formulation

In this section, we present a version of the analysis step in SVKF and LFKF that is suitable when $m >> N$ and the dynamic model error is assumed to be zero, a common situation in oceanic and atmospheric applications with remotely sensed data where a large vector of observations has to be assimilated. First we review the general formulation of the filters from chapters 2 and 3.

We choose the potential vorticity as the n-dimensional state vector $q(t)$, and measure the distance in the state space by the Euclidean norm in the space of potential vorticity:

$$\left\| q(t) \right\| = \sqrt{q^T(t) q(t)} \qquad (4\text{-}1)$$

We use the superscripts t, f, and a to differentiate the true (unknown), forecast (prior) and analysis (posterior) states. These various states can be viewed geometrically as points in the n-dimensional state space. Differences between states (errors, perturbations, etc.) can be viewed as n-dimensional vectors with characteristic magnitudes and directions. We suppose the true states evolve from time s to time t according to the following state equation:

$$q^t(t) = \varphi\left[q^t(s), t \right] \tag{4-2}$$

where $\varphi\left[q, t \right]$ represent the nonlinear operator for propagating the state by the model as explained in Section 4.4. We assume the initial condition $q^t(t_0)$ at $s = t_0$ is a random vector with a known mean $\overline{q^t(t_0)}$ and covariance matrix $P^t(t_0)$.

We consider a simple linear observation operator and denote the m-dimensional vector of observations by $Y(t)$, which whenever available can be written as a linear function of the true state:

$$Y(t) = H(t)\, q^t(t) + \upsilon(t) \tag{4-3}$$

with $H(t)$ being the $m \times n$ observation matrix. The measurement error $\upsilon(t)$ is assumed to be uncorrelated with $q^t(t_0)$, and have a zero mean and known covariance $R(t)$.

The equations for the analysis and the forecast states follow

$$q^f(t+T) = \varphi\left(q^a(t), t+T \right)$$
$$q^a(t) = q^f(t) + K(t)\left[Y(t) - H(t)\, q^f(t) \right] \tag{4-4}$$

It is understood that the analysis state is computed whenever a new observation is available. The filter is assumed to be initialized with $q^a(t_0) = \overline{q^t(t_0)}$.

$K(t)$ is a Kalman-based $n \times m$ gain matrix:

$$K(t) = L^a(t)\left[H(t)L^a(t) \right]^T R(t)^{-1} \tag{4-5}$$

where $L^a(t)$ is a square-root of the analysis error covariance, $P^a(t) = L^a(t)L^a(t)^T$. Note that in practice we do not have to compute the Kalman gain explicitly. Instead, we can just compute the product $L^a(t)\left\{ \left[H(t)L^a(t) \right]^T \left[R(t)^{-1} \left[Y(t) - H(t)q^f(t) \right] \right] \right\}$ by three matrix-vector multiplications, starting with the innermost bracket.

Let $L^f(t)$ denote the square-root of the forecast error covariance, $P^f(t) = L^f(t)L^f(t)^T$. When the dynamic model error is zero, $L^a(t)$ and $L^f(t)$ in a filter of rank N are $n \times N$ matrixes that are related as follows:

$$L^a(t) = L^f(t)\,\Delta(t) \tag{4-6}$$

where

$$\Delta(t) = I - \left[H(t)L^f(t) \right]^T \sqrt{Z(t)}^{-T} \left[\sqrt{Z(t)} + \sqrt{R(t)}\, W_m(t) \right]^{-1} \left[H(t)L^f(t) \right] \tag{4-7}$$

$$Z(t) = \left[H(t)L^f(t) \right] \left[H(t)L^f(t) \right]^T + R(t) \tag{4-8}$$

and $W_m(t)$ is an arbitrary $m \times m$ orthogonal matrix.

Although $\Delta(t)$ is only $N \times N$, (4-7) requires inversion of large $m \times m$ matrices $\sqrt{Z(t)}$ and $\sqrt{Z(t)} + \sqrt{R(t)}\, W_m(t)$, which can be avoided as follows. For convenience, we drop the time notation. It is understood that all of the variables are at time t.

First we perform a change of variables in the observation space to make the observation noise white. Let $\hat{H} = \sqrt{R}^{-1} H$ so that $H = \sqrt{R}\, \hat{H}$. We can rewrite the equation for Z as

$$\begin{aligned} Z &= \left(\sqrt{R}\hat{H}L^f \right) \left(\sqrt{R}\hat{H}L^f \right)^T + R \\ &= \sqrt{R} \left(\hat{H}L^f \right) \left(\hat{H}L^f \right)^T \sqrt{R}^T + \sqrt{R}\sqrt{R}^T \\ &= \sqrt{R} \left[\left(\hat{H}L^f \right) \left(\hat{H}L^f \right)^T + I^{m \times m} \right] \sqrt{R}^T \end{aligned} \tag{4-9}$$

Let

$$\hat{Z} = \left(\hat{H}L^f \right) \left(\hat{H}L^f \right)^T + I^{m \times m} \tag{4-10}$$

and define its square-root $\sqrt{\hat{Z}}$ such that $\hat{Z} = \sqrt{\hat{Z}}\sqrt{\hat{Z}}^T$. It easily follows that $\sqrt{Z} = \sqrt{R}\sqrt{\hat{Z}}$.

Let the SVD of the $m \times N$ matrix $\hat{H}\tilde{L}^f$ be written as

$$\hat{H}\tilde{L}^f = U_m \Sigma_m V_m{}^T \tag{4-11}$$

where columns of the $m \times N$ matrix U_m form the orthogonal basis for an N-dimensional subspace within an m-dimensional space, Σ_m is $N \times N$ and diagonal, and V_m is $N \times N$ and orthogonal.

Now we solve (4-7) in the N-dimensional space that is spanned by the columns of U_m. If $U_m{}^{\perp}$ denote the $m \times (m - N)$ complement of U_m, $\left[U_m \middle| U_m{}^{\perp} \right]$ is an $m \times m$ orthogonal matrix, and we have

$$U_m U_m{}^T + U_m{}^{\perp} U_m{}^{\perp T} = I^{m \times m} \tag{4-12}$$

Substituting from (4-11) and (4-12) in (4-10) we have

$$\begin{aligned} \hat{Z} &= \left(U_m \Sigma_m V_m{}^T \right)\left(U_m \Sigma_m V_m{}^T \right)^T + U_m U_m{}^T + U_m{}^{\perp} U_m{}^{\perp T} \\ &= U_m \, \Sigma_m^2 \, U_m{}^T + U_m U_m{}^T + U_m{}^{\perp} U_m{}^{\perp T} \\ &= U_m \left(\Sigma_m^2 + I^{N \times N} \right) U_m{}^T + U_m{}^{\perp} U_m{}^{\perp T} \end{aligned} \tag{4-13}$$

Therefore, $\sqrt{\hat{Z}}$ may be written as

$$\sqrt{\hat{Z}} = \left[U_m \sqrt{\Sigma_m^2 + I^{N\times N}} \;\middle|\; U_m{}^{\perp} \right] = \left[U_m \;\middle|\; U_m{}^{\perp} \right] \begin{bmatrix} \sqrt{\Sigma_m^2 + I^{N\times N}} & 0 \\ 0 & I^{(m-N)\times(m-N)} \end{bmatrix} \tag{4-14}$$

Substituting for H and $\sqrt{Z}$ in (4-7) we have

$$\begin{aligned}
\Delta &= I - \left[\sqrt{R}\hat{H}\ L^f \right]^T \left(\sqrt{R}\sqrt{\hat{Z}} \right)^{-T} \left[\sqrt{R}\sqrt{\hat{Z}} + \sqrt{R}\ W_m \right]^{-1} \left(\sqrt{R}\hat{H}\ L^f \right) \\
&= I - \left[\left(\hat{H}L^f \right)^T \sqrt{R}^T \right] \left(\sqrt{\hat{Z}}^{-1} \sqrt{R}^{-1} \right)^T \left[\sqrt{R} \left(\sqrt{\hat{Z}} + W_m \right) \right]^{-1} \left(\sqrt{R}\ \hat{H}L^f \right) \\
&= I - \left[\left(\hat{H}L^f \right)^T \sqrt{R}^T \right] \left(\sqrt{R}^{-T} \sqrt{\hat{Z}}^{-T} \right) \left[\left(\sqrt{\hat{Z}} + W_m \right)^{-1} \sqrt{R}^{-1} \right] \left(\sqrt{R}\ \hat{H}L^f \right) \\
&= I - \left(\hat{H}L^f \right)^T \left(\sqrt{R}^T\ \sqrt{R}^{-T} \right) \sqrt{\hat{Z}}^{-T} \left(\sqrt{\hat{Z}} + W_m \right)^{-1} \left(\sqrt{R}^{-1} \sqrt{R} \right)\ \hat{H}L^f \\
&= I - \left(\hat{H}L^f \right)^T \quad I \quad \sqrt{\hat{Z}}^{-T} \left(\sqrt{\hat{Z}} + W_m \right)^{-1} \quad I \quad \hat{H}L^f \\
&= I - \left(\hat{H}L^f \right)^T \sqrt{\hat{Z}}^{-T} \left(\sqrt{\hat{Z}} + W_m \right)^{-1} \hat{H}L^f
\end{aligned} \tag{4-15}$$

Further substituting in (4-15) for $\hat{H}L^f$ and $\sqrt{\hat{Z}}$ from (4-11) and (4-14), and choosing $W_m = \left[U_m \middle| U_m{}^{\perp} \right]$ we have

$$\Delta = I - \left(U_m \Sigma_m {V_m}^T \right)^T \left(\left[U_m \middle| {U_m}^\perp \right] \begin{bmatrix} \sqrt{\Sigma_m^2 + I^{N\times N}} & 0 \\ 0 & I^{(m-N)\times(m-N)} \end{bmatrix} \right)^{-T}$$

$$\left(\left[U_m \middle| {U_m}^\perp \right] \begin{bmatrix} \sqrt{\Sigma_m^2 + I^{N\times N}} & 0 \\ 0 & I^{(m-N)\times(m-N)} \end{bmatrix} + \left[U_m \middle| {U_m}^\perp \right] \right)^{-1} \left(U_m \Sigma_m {V_m}^T \right)$$

$$= I - V_m \Sigma_m {U_m}^T \left(\begin{bmatrix} \sqrt{\Sigma_m^2 + I^{N\times N}} & 0 \\ 0 & I^{(m-N)\times(m-N)} \end{bmatrix} \left[U_m \middle| {U_m}^\perp \right]^T \right)^{-1}$$

$$\left(\left[U_m \middle| {U_m}^\perp \right] \begin{bmatrix} \sqrt{\Sigma_m^2 + I^{N\times N}} + I^{N\times N} & 0 \\ 0 & I^{(m-N)\times(m-N)} + I^{(m-N)\times(m-N)} \end{bmatrix} \right)^{-1} U_m \Sigma_m {V_m}^T$$

$$= I - V_m \Sigma_m {U_m}^T \left(\left[U_m \middle| {U_m}^\perp \right] \begin{bmatrix} \sqrt{\Sigma_m^2 + I^{N\times N}} & 0 \\ 0 & I^{(m-N)\times(m-N)} \end{bmatrix}^{-1} \right)$$

$$\left(\begin{bmatrix} \sqrt{\Sigma_m^2 + I^{N\times N}} + I^{N\times N} & 0 \\ 0 & 2I^{(m-N)\times(m-N)} \end{bmatrix}^{-1} \left[U_m \middle| {U_m}^\perp \right]^T \right) U_m \Sigma_m {V_m}^T$$

$$= I - V_m \Sigma_m {U_m}^T \left[U_m \middle| {U_m}^\perp \right] \begin{bmatrix} \sqrt{\Sigma_m^2 + I^{N\times N}}^{-1} & 0 \\ 0 & I^{(m-N)\times(m-N)} \end{bmatrix}$$

$$\begin{bmatrix} \left(\sqrt{\Sigma_m^2 + I^{N\times N}} + I^{N\times N} \right)^{-1} & 0 \\ 0 & 0.5I^{(m-N)\times(m-N)} \end{bmatrix} \begin{bmatrix} {U_m}^T \\ {U_m}^{\perp T} \end{bmatrix} U_m \Sigma_m {V_m}^T$$

$$= I - V_m \Sigma_m \left[I^{N\times N} \middle| 0^{N\times(m-N)} \right]$$

$$\begin{bmatrix} \sqrt{\Sigma_m^2 + I^{N\times N}}^{-1} \left(\sqrt{\Sigma_m^2 + I^{N\times N}} + I^{N\times N} \right)^{-1} & 0 \\ 0 & 0.5I^{(m-N)\times(m-N)} \end{bmatrix} \begin{bmatrix} I^{N\times N} \\ 0^{(m-N)\times N} \end{bmatrix} \Sigma_m {V_m}^T$$

$$= I - V_m \Sigma_m \left[\sqrt{\Sigma_m^2 + I^{N\times N}}^{-1} \left(\sqrt{\Sigma_m^2 + I^{N\times N}} + I^{N\times N} \right)^{-1} \middle| 0^{N\times(m-N)} \right] \begin{bmatrix} I^{N\times N} \\ 0^{(m-N)\times N} \end{bmatrix} \Sigma_m {V_m}^T$$

$$= I - V_m \left[\Sigma_m \sqrt{\Sigma_m^2 + I^{N\times N}}^{-1} \left(\sqrt{\Sigma_m^2 + I^{N\times N}} + I^{N\times N} \right)^{-1} \Sigma_m \right] V_m{}^T \tag{4-16}$$

Since all of the matrices in the bracket are diagonal we have:

$$\Delta = I - V_m \left[\Sigma_m^2 \sqrt{\Sigma_m^2 + I^{N\times N}}^{-1} \left(\sqrt{\Sigma_m^2 + I^{N\times N}} + I^{N\times N} \right)^{-1} \right] V_m{}^T \tag{4-17}$$

Therefore to compute Δ, we only need V_m and Σ_m, which are computed from eigen-decomposition of the $N \times N$ matrix $\left(\hat{H}L^f\right)^T \left(\hat{H}L^f\right) = \left(HL^f\right)^T R^{-1} \left(HL^f\right)$, i.e.

$$\left(HL^f\right)^T R^{-1} \left(HL^f\right) = V_m \Sigma_m^2 V_m^T \tag{4-18}$$

while the matrix in the bracket of (4-17) is diagonal and its nonzero elements can be computed by solving N scalar equations.

In the forecast step, consider the forecast window $[t-T, t]$. Since the dynamic model error is assumed to be zero, we need to repopulate the variance in the null-space of the analysis error covariance after each update step, following the approach in chapters 2 and 3. The square-root of the forecast error covariance, $L^f(t)$ is computed as follows:

$$L^f(t) = \left[F_{t-T,t} \;\; \Xi_{t-T,t}^{(N)} \right] D_{t-T,t} \tag{4-19}$$

where $D_{t-T,t}$ is an $N \times N$ matrix equivalent of the $N \times (N+n)$ matrix

$$\widetilde{D}_{t-T,t} = \left[\Xi_{t-T,t}^{(N)\ T} L^a(t-T) \middle| \left(\Xi_{t-T,t}^{(N)\ T} - \left(\Xi_{t-T,t}^{(N)\ T} O(t-T) \right) O(t-T)^T \right) r(t-T) \right] \tag{4-20}$$

such that $D_{t-T,t} D_{t-T,t}{}^T = \widetilde{D}_{t-T,t} \widetilde{D}_{t-T,t}{}^T$. $O(t-T)$ is an $n \times N$ orthogonal matrix with the same column space as $L^a(t-T)$ and $r(t-T)$ is chosen to be

$$r(t-T) = \max \text{singular value} \left[\left[H(t-T)^T H(t-T) \right]^{-1} H(t-T)^T \sqrt{R(t-T)} \right] \tag{4-21}$$

$F_{t-T,t}$ is the state transition matrix over the forecast trajectory $q^f(t) = \varphi\left[q^a(t-T), t \right]$, defined as

$$F_{t-T,t} = F_{t-dt,t} \times \cdots \times F_{t-T+dt,t-T+2dt} \times F_{t-T,t-T+dt} \tag{4-22}$$

and each term on the right hand side, $F_{\tau,\tau+dt} = \left. \dfrac{\partial \varphi\left[q(\tau), \tau + dt \right]}{\partial q} \right|_{q(\tau)}$ is an $n \times n$ Jacobian matrix (or propagator) evaluated at $q(\tau)$, the best estimate of the state, which is the forecast except just after an update, when it is the analysis.

$\Xi_{t-T,t}^{(N)}$ is a basis for the rank reduction subspace. In the LFKF, columns of $\Xi_{t-T,t}^{(N)}$ are the N leading Schur vectors of $F_{t-T,t}$ and we have

$$F_{t-T,t}\ \Xi_{t-T,t}^{(N)} = \Xi_{t-T,t}^{(N)}\ \Gamma^{(N)} \tag{4-23}$$

where $\Gamma^{(N)}$ is an $N \times N$ upper-quasi-triangular matrix whose diagonal 1×1 or 2×2 blocks correspond to the N leading eigenvalues or eigen-pairs of $F_{t-T,t}$.

In SVKF, columns of $\Xi^{(N)}_{t-T,t}$ are the N leading right Singular vectors of $F_{t-T,t}$ and we have

$$F_{t-T,t}\ \Xi^{(N)}_{t-T,t} = U^{(N)}_{t-T,t}\ \Sigma^{(N)} \tag{4-24}$$

where $\Sigma^{(N)}$ is an $N \times N$ diagonal matrix with its diagonal elements being the N leading Singular values of $F_{t-T,t}$, and $U^{(N)}_{t-T,t}$ is the $n \times N$ matrix of the corresponding N leading left Singular vectors.

4.4 Quasi-geostrophic ocean model

The wind-driven quasi-geostrophic ocean circulation with various boundary conditions, wind stress patterns, or viscosity parameterizations, has been previously studied by many investigators (Holland, 1978; McCalpin and Haidvogel, 1996; Meacham and Berloff, 1997; Berloff and Meacham, 1998; Meacham, 2000; Mahadevan et al., 2001; Primeau, 2002). In this section, we briefly review the model and its parameters for chaotic dynamics, following the work in BM and ZM.

The model has a single layer with a constant thickness of $H = 500$ (m) that rests on top of a motionless and infinitely deep bottom layer, and is forces at the surface by the wind stress. The model configuration is an idealized rectangular basin with zonal width of 2048 (Km) and meridional width of 4096 (Km), with no-slip boundaries. The zonal width of the basin

$L = 2048$ (Km) is used to define the dimensionless spatial coordinates x and y such that $0 < x < 1$ and $0 < y < 2$. The domain is discretized into a uniform grid of 129×257 with square mesh elements with resolution of 16 (Km).

The state variable is the potential vorticity q over the whole domain. The evolution of q is coupled with the stream function ψ and is written in non-dimensional form as follows:

$$\frac{\partial q}{\partial t} + \delta_I^2 J(\psi, q) + \frac{\partial \psi}{\partial x} = \delta_M^3 \nabla^4 \psi + \omega(y) \tag{4-25}$$

$$q = \left(\nabla^2 - \lambda^2\right)\psi \tag{4-26}$$

where $J(\psi, q) = \frac{\partial \psi}{\partial x}\frac{\partial q}{\partial y} - \frac{\partial \psi}{\partial y}\frac{\partial q}{\partial x}$. $\delta_M = \left(\frac{\nu}{\beta L^3}\right)^{\frac{1}{3}}$ and $\delta_I = \left(\frac{f\,W}{HL^2\beta^2}\right)^{\frac{1}{2}}$ are respectively, the dimensionless Munk and Inertial boundary layer scales. The model uses the β plane approximation with $f_0 = 10^{-4}$ ($\sec^{-1}$) the planetary vorticity for a mid-latitude basin and $\beta = 2\times10^{-11}$ ($\mathrm{m^{-1}s^{-1}}$) its latitudinal gradient.

The model exhibits a rich variety of dynamical regimes as the uniform eddy viscosity υ is changed, and becomes chaotic when $\upsilon = 100$ ($\mathrm{m^2s^{-1}}$). $\lambda = \frac{L}{L_D}$ is the non-dimensional inverse of the internal (Rossby) deformation radius L_D, which is chosen to be 48 (Km) for the chaotic regime corresponding to an ocean circulation rich in meso-scale, strongly non-linear eddies.

The vertical Ekman velocity w_E is written $w_E = W\omega(y)$, where W is its dimensional scale and

$\omega(y)$ is a non-dimensional function describing its spatial pattern. By choosing $W = \frac{\tau_0}{L\rho_0 f}$ with $\tau_0 = 0.05\ (\mathrm{Kg\,m^{-1}s^{-2}})$ and $\rho_0 = 1000\ (\mathrm{Kg\,m^{-3}})$, and $\omega(y) = -\sin(\pi y)$, the wind forcing corresponds to applying a shear stress of $\tau = -\frac{\tau_0}{\pi}\cos(\pi y)$, uniform in x and sinusoidal in y.

t is the non-dimensional model time and its unit corresponds to about 0.9 days. The vorticity equation (4-25) is spatially discretized by a second order finite difference scheme and advanced in time using a second order Runge-Kutta method with a time step of 0.1 (about 2 hours). The Jacobian $J(\psi, q)$ is discretized following Arakawa (1966). The stream function is computed by inverting the elliptic relation (4-26) following the method in Mahadevan et al. (2001).

The domain is spun up from rest for 2500-4500 days. The wind stress during the spin-up is slightly perturbed by adding a small noise that is just enough to break the symmetry of the flow. Beyond the spin-up and in all of the experiments, the wind stress is steady and symmetric as explained earlier.

4.5 Experiments setup and results

The performance of any reduced rank filter depends on the ability of the projection subspace in resolving the correct uncertainty of the forecast with respect to the truth. In both SVKF and LFKF, it is assumed that the analysis error at the beginning of the forecast trajectory is small such that the forecast and the true trajectories are close enough. This would guarantee that the computed dominant directions of uncertainty capture a significant portion of the forecast error.

Otherwise, if the analysis error is so large that this fundamental assumption is violated, the computed uncertainty structures at the time of update are wrong, leading to further departure of the analysis estimate from the truth until the forecast skill is completely lost. To have a good analysis estimate at the beginning of the first forecast period, we start the filter with the analysis step.

The choice of the observation operator is another important factor in the performance of the filter. Regardless of the rank of the filter, the ability of the update step to produce a good estimate depends on the quality and relevance of the observations. We leave an in-depth analysis of the observability of the chaotic system to future work. It suffices our purpose to choose an observation vector that has good spatial distribution over the states that are most variable.

In the ocean system under investigation, the patter of the wind stress combined with the Coriolis effect leads to formation of turbulent high energy from the western boundary to about the center of the basin. This can be seen in Figure 4-1, where we have depicted the relative variability of the potential vorticity over the model domain, based on the standard deviation of a sample of the state vectors drawn from a long integration of the model. Due to the distribution of the most variable states in the western part of the domain, it is natural to expect that the filter will perform well only if enough observations are made in this area. We have conducted experiments with three different observation networks of sizes 235, 119 and 30, as shown in Figure 4-1, Figure 4-5, and Figure 4-8, respectively.

The quality and time interval between observations is constrained by the capability of the

observation devices. As in BM< and ZM for the chaotic regime, we assume that observations are collected at every 10 units of model time (9 days). The observation noise is assumed to be stationary and uncorrelated in space, with a standard deviation that is equal to 10% of the natural variability of each observed state. The initial estimate which undergoes the starting update step is assumed to be an arbitrary state on the attractor, and its error covariance is computed based on a large sample of states over the whole attractor.

As we discussed in chapters 2 and 3, identifying all of the growing/unstable directions over the forecast period is important for successful filtering in chaotic applications, while neglecting any of these directions will adversely impact the performance of the filter. In order to estimate the number of growing directions, we analyzed the singular-value structure of the TLM of the system over 9 days (i.e. the forecast horizon in the experiments). All of the singular values that are greater than one indicate growing directions and need to be retained in the filter. Since the number of growing directions varies in different parts of the attractor, we conducted our analysis over 500 different TLMs. Figure 4-2 depicts the spectrum of the first 140 singular values of these TLMs. The number of growing directions in our sample varies between 45 and 75, thus any successful filter cannot have a rank which is smaller than 75.

To measure the performance of the filters, we compute the root mean square error (RMSE) time-series of the estimated state with respect to the truth:

$$RMSE(q,N,t)=\sqrt{\frac{1}{n}\left\| q(t)-q^{t}(t)\right\|^{2}} \qquad (4\text{-}26)$$

where $q(t)$ is the best estimate of the filter, which can be the analysis or the forecast estimate. We have implemented LFKF and SVKF with various ranks of the projection subspace on a single truth over 1600 units of model time (about 4 years).

Figure 4-3 and Figure 4-4 respectively show the RMSE of LFKF and SVKF with various ranks when 235 states as shown in Figure 4-1 were observed. To see the improvement as the result of filtering, we have also shown an Openloop RMSE time-series computed by propagation of the initial condition without assimilating any observations. It can be seen that the performance of the filter improves as the rank of the filter is increased. In particular, when the rank of the filter is 100 or more, both the LFKF and SVKF are able to reduce the estimation error to the levels below the observation noise. The SVKF seems to be more sensitive to the missing growing directions than the LFKF. SVKF with too small a rank completely looses track of the truth, following by further error in the growing directions. In contrary, the LFKF seem to be more robust if the rank of the filter is not sufficient.

In the second set of experiments, we reduce the number of observations to 119 states as shown in Figure 4-5. When the filters were initialized arbitrarily, neither SVKF not LFKF could reduce the estimation error (results not shown). This could be due to the missing growing/unstable directions or the lack of observability. To isolate the effect of subspace accuracy from the observability issue, we initialized the filters with an initial state that was close to the truth. Figure 4-6 and Figure 4-7 show the RMSE time series of the LFKF and the SVKF, respectively. Both of the filters are able to maintain the quality of the estimate when the filters have rank of 100 or more, meaning that the 119 observations are sufficient to track the truth as long as the

rank of the filter is larger than the number of growing/unstable directions. The LFKF again seems to be more robust when some of the unstable directions are temporarily missed. In contrast, the SVKF needs to include all of the growing directions.

It should be mentioned that these results are based on a single true trajectory. It is quite possible that for another truth, the SVKF would work as well as the LFKF with a small rank. What these results suggest is that the LFKF is more robust than the SVKF.

We also conducted a third set of experiments, with 30 observations as shown in Figure 4-8, following the work of BM and ZM. 30 observation sites were sufficient for the EnKF to converge. We initialized the filters with a good initial condition so that the computed growing/unstable directions are accurate. The RMSE time series of the LFKF and the SVKF are shown in Figure 4-9 and Figure 4-10, respectively. Regardless of the rank of the filter, neither the LFKF nor the SVKF could maintain the quality of the estimation error. However, we saw that when 119 states were observed the filters of ranks 100 or more could retain the estimation error. Therefore, the reason for the poor performance of the filters is that 30 observations are not enough for SVKF and LFKF to track the truth. A further possibility for this divergence is that the distribution of the observation sites may not capture all the most unstable modes, and that an optimal array design for the chaotic and turbulent region of the circulation is needed.

4.6 Conclusions

In this paper, a chaotic wind-driven quasi-geostrophic ocean circulation model was used to investigate the implementation issues of the SVKF and the LFKF in a more realistic geophysical

system. Following the previous work of BM and ZM, it was assumed that the dynamic model error was zero. A new formulation of the analysis step was provided that was mostly suitable when the size of the observation vector is larger than the rank of the filter.

Experiments were conducted with various observation networks. When the observation network was large enough and had good spatial distribution over the more turbulent areas, both the SVKF and the LFKF had remarkable performance, as long as the rank of the filters were larger than the number of growing/unstable directions. The performances of the filters were lost with smaller ranks, amid more robustness of LFKF. This is in agreement with expected pattern based on the preliminary experiments on the Lorenz 95 system in chapters 2 and 3.

When only 30 states were observed, neither of the filters could produce acceptable estimates, regardless of the rank of the filter. With an intermediate observation size of 119, the SVKF and the LFKF could produce good estimates only if they were initialized by good estimates so that the computed growing/unstable directions were accurate.

These results are based on experiments over a single true trajectory. For other true trajectories, we expect similar pattern of performance improvement; i.e. very small estimation error when the rank of the filter is larger than the number of growing/unstable directions (75 based on the spectrums in Figure 4-2).

The observability of the system is a major issue. Our results show that a poor observation network will lead to poor performance of the filters which otherwise would produce excellent estimates. It may be possible to track other true trajectories with fewer observations, but our results show that such results will not be robust and reliable. Our results can serve as a starting

point for a more thorough investigation of observability in such chaotic systems.

4.7 References

Anderson, J. L., B. Wyman, S. Zhang, and T. Hoar, 2005: Assimilation of surface pressure observations using an ensemble filter in an idealized global atmospheric prediction system. *J. Atmos. Sci.*, **62**, pp 2925-2938.

Arakawa, A., 1966: Computational design for long-term integration of the equations of fluid motions, *J. Comput. Phys.*, **1**, pp 119-143.

Berloff, P. S., and S. P. Meacham, 1998: The dynamics of a simple baroclinic model of the wind-driven circulation. *J. Phys. Oceanogr.*, **28**, pp 361–388.

Buehner, M., and P. Malanotte-Rizzoli, 2003: Reduced-rank Kalman filter applied to an idealized model of the wind-driven ocean circulation, *J. Geophys. Res.*, **108**, p 3192

Buehner, M., P. Malanotte-Rizzoli, A. J. Busalacchi and T. Inui, 2003: Estimation of the Tropical Atlantic circulation from altimetry data using a Reduced Rank Kalman Filter. *Interhemispheric water exchanges in the Atlantic Ocean, Elsevier Oceanographic Series,* **68**, pp 49-92.

Cane, M., A. Kaplan, R. N. Miller, B. Tang, E. C. Hackert, and A. J. Busalacchi, 1996: Mapping tropical Pacific sea level: Data assimilation via a reduced state space Kalman filter. *J. Geophys.*

Res., **101**, pp 22 599 –22 617.

Daley, R., 1991: *Atmospheric Data Analysis*. Cambridge University Press, UK, p 457.

Evensen, G., 1994: Sequential data assimilation with a nonlinear quasi-geostrophic model using Monte-Carlo methods to forecast error statistics. *J. Geophys. Res.,* **99(C5)**, pp 10 143-10 162.

Evensen, G., 1997: Advanced data assimilation for strongly nonlinear dynamics. *Mon. wea. Rev.*, **125**, pp 1342-1354.

Evensen, G., 2003: The ensemble Kalman filter: theoretical formulation and practical implementation. *Ocean Dyn.*, **53**, pp 343-367.

Evensen, G., 2004: Sampling strategies and square root analysis schemes for the EnKF. *Ocean Dynamics*, **54**, pp 539-560.

Farrell, B. F., and P. J. Ioannou, 2001: State estimation using a reduced order Kalman filter, *J. Atmos. Sci.*, **58**, pp 3666-3680.

Fillion, L., 2002: Variational Assimilation of precipitation data and gravity wave excitation. *Mon. Wea. Rev.*, **130**, pp 357-371.

Fukumori, I., and P. Malanotte-Rizzoli, 1995: An approximate Kalman filter for ocean data assimilation: An example with an idealized Gulf Stream model. *J. Geophys. Res.*, **100**, pp 6777-6793.

Gelb, A., Ed., 1974: *Applied Optimal Estimation*. The MIT Press, Cambridge, USA.

Hamill, T. M., J. S. Whitaker, and C. Snyder, 2001: Distance-dependent filtering of background error covariance estimates in an ensemble Kalman filter. *Mon. Wea. Rev.*, **129**, pp 2776-2790.

Holland, W. R., 1978: The role of meso-scale eddies in the general circulation of the ocean: Numerical experiments using a wind-driven quasi-geostrophic model. *J. Phys. Oceanogr.*, **8**, pp 363-392.

Houtekamer, P. L., and H. L. Mitchell, 2001: A sequential ensemble Kalman filter for atmospheric data assimilation. *Mon. Wea. Rev*., **129**, pp 123-137.

Kalnay, E., 2003: *Atmospheric modeling, data assimilation and predictability*. Cambridge University Press, UK, pp 220-248.

Mahadevan, A., J. Lu, S. P. Meacham, and P. Malanotte-Rizzoli, 2001: The predictability of large-scale wind-driven flows. *Nonlin. Proc. Geophys.*, **8**, pp 449-465.

McCalpin, J. D., and D. B. Haidvogel, 1996: Phenomenology of the low-frequency variability in a reduced gravity, quasi-geostrophic double-gyre model. *J. Phys. Oceanogr.*, **26**, pp 739-752.

Meacham, S. P., 2000: Low-frequency variability in the wind-driven circulation. *J. Phys. Oceanogr.*, **30**, pp 269-293.

Meacham, S. P., and P. Berloff, 1997: Barotropic wind-driven circulation in a small basin. *J. Mar. Res.*, **55**, pp 523-563.

Nagashima, H. and Y. Baba, 1999: Introduction to Chaos, Physics and Mathematics of chaotic

phenomena. *IOP Publishing Ltd*, Bristol, UK. pp 13-40.

Neef, L. J., S. M. Polavarapu, T. G. Shepherd, 2006: Four-dimensional data assimilation and balanced dynamics. *J. Atmos. Sci.*, **63**, pp 1840-1858.

Ott, E., B. R. Hunt, I. Szunyogh, A. V. Zimin, E. J. Kostelich, M. Corazza, E. Kalnay, D. J. Patil, and J. Yorke, 2006: A local ensemble Kalman filter for atmospheric data assimilation. *Submitted to Mon. Wea. Rev., Revised May 24, 2006.*

Primeau, F., 2002: Multiple equilibria and low-frequency variability of wind-driven ocean currents. *J. Phys. Oceanogr.*, **32**, pp 2236-2256.

Verron, J., L. Gourdeau, D. T. Pham, R. Murtugudde, and A. J. Busalacchi, 1999: An extended Kalman filter to assimilate satellite altimeter data into a nonlinear numerical model of the tropical Pacific Ocean: Method and validation, *J. Geophys. Res.*, **104**, pp 5441-5458.

Zang, Xiaoyun and P. Malanotte-Rizzoli, 2003: A comparison of assimilation results from the ensemble Kalman filter and the reduced-rank extended Kalman filter, *Nonlinear Processes in Geophysics*, **10**, 477-491.

4.8 Figures

Figure 4-1: Network of 235 observed states. Background is the relative variability of the potential vorticity over the model domain.

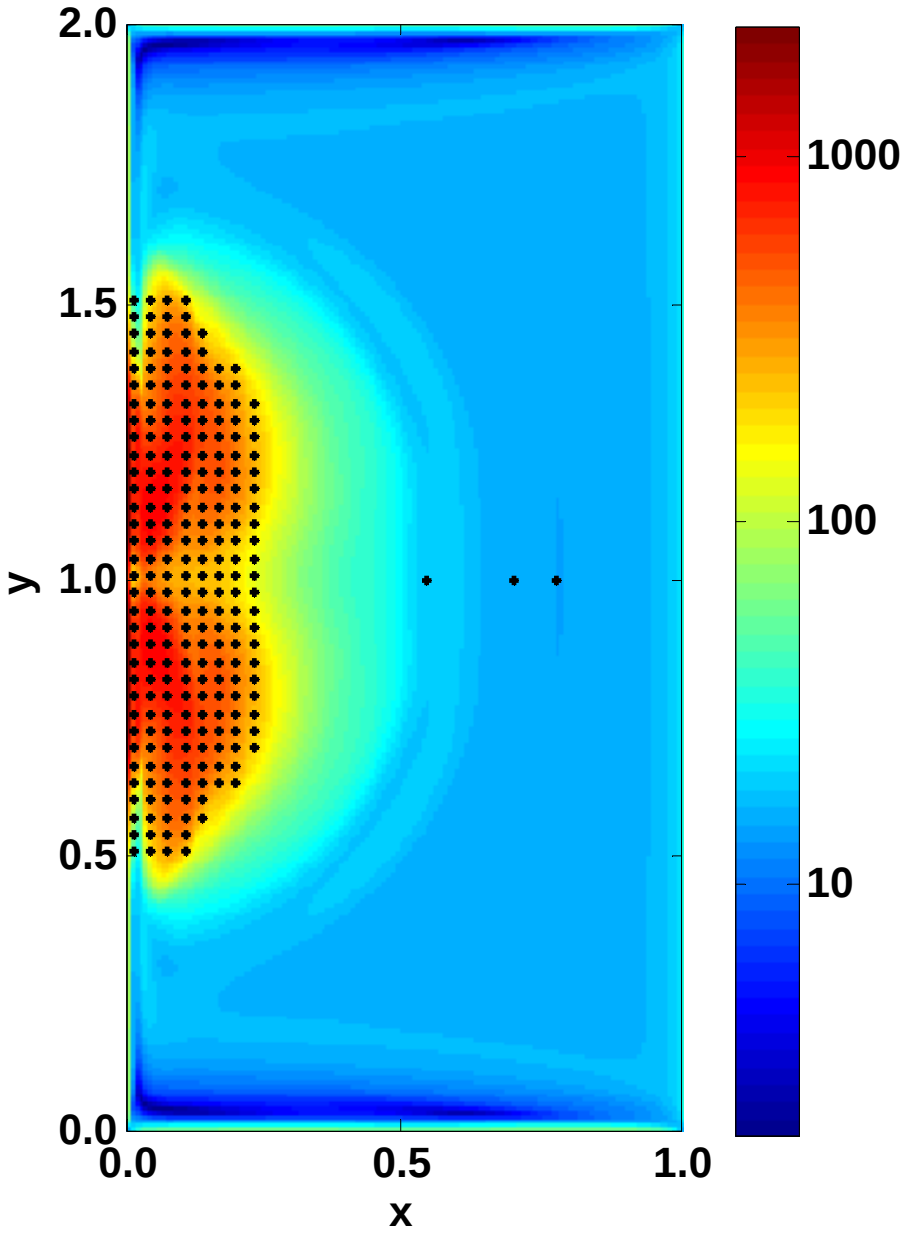

Figure 4-2: Singular Value spectrum of 500 randomly selected Tangent Linear Models. Each linear model s computed over 10 units of model time.

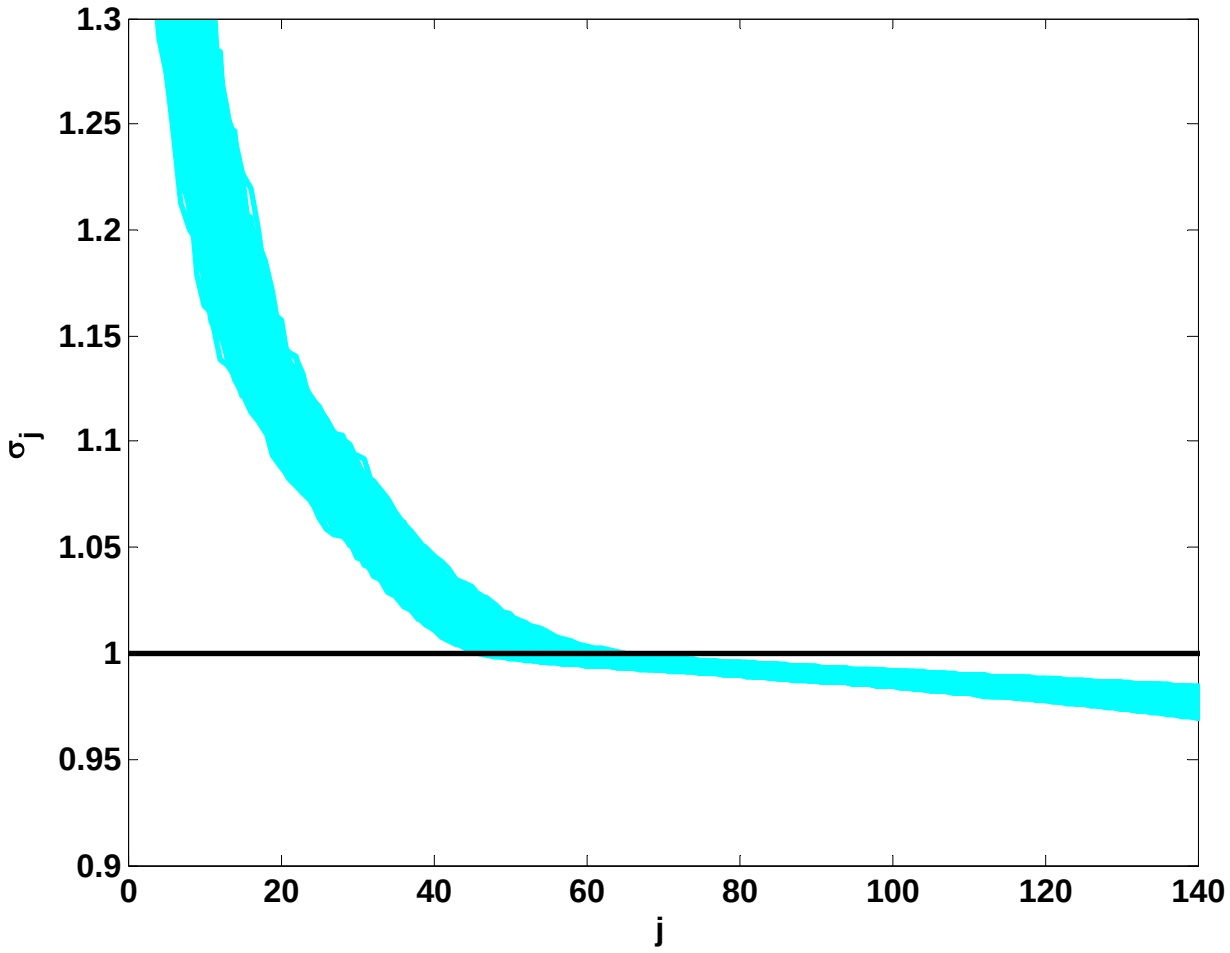

Figure 4-3: RMSE of LFKF with various ranks, quasi-geostrophic ocean model with 235 observations.

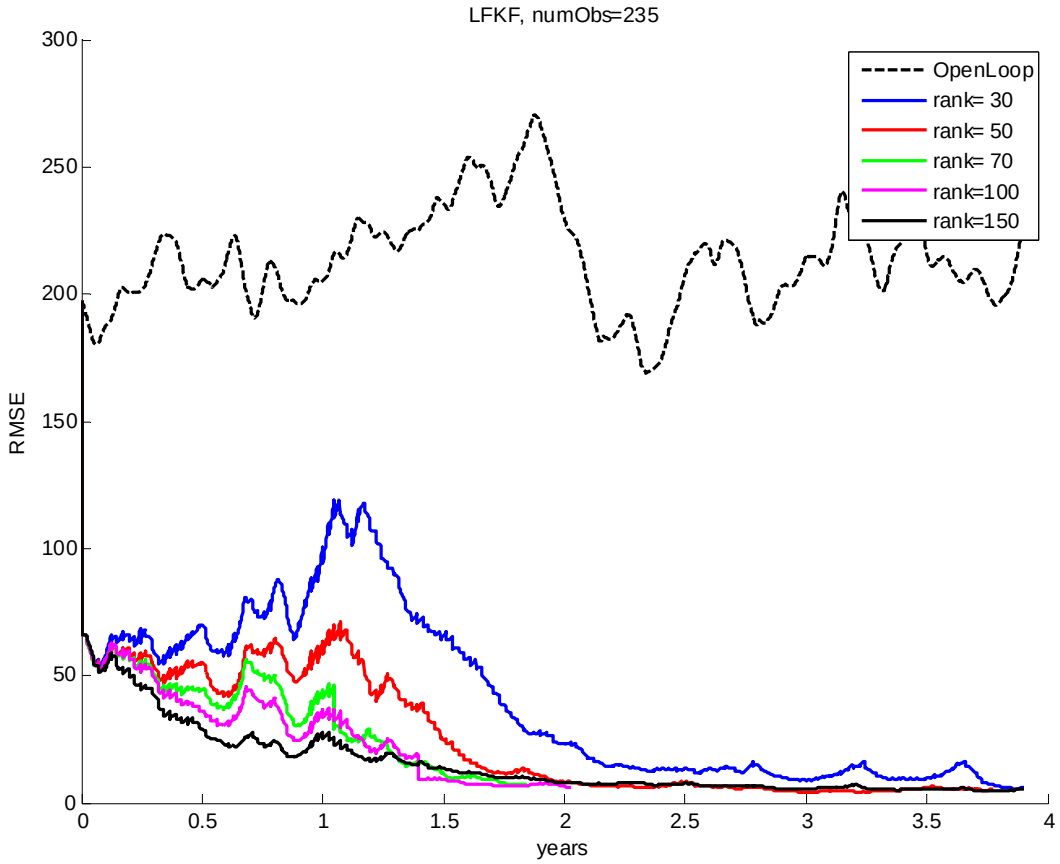

Figure 4-4: RMSE of SVKF with various ranks, quasi-geostrophic ocean model with 235 observations.

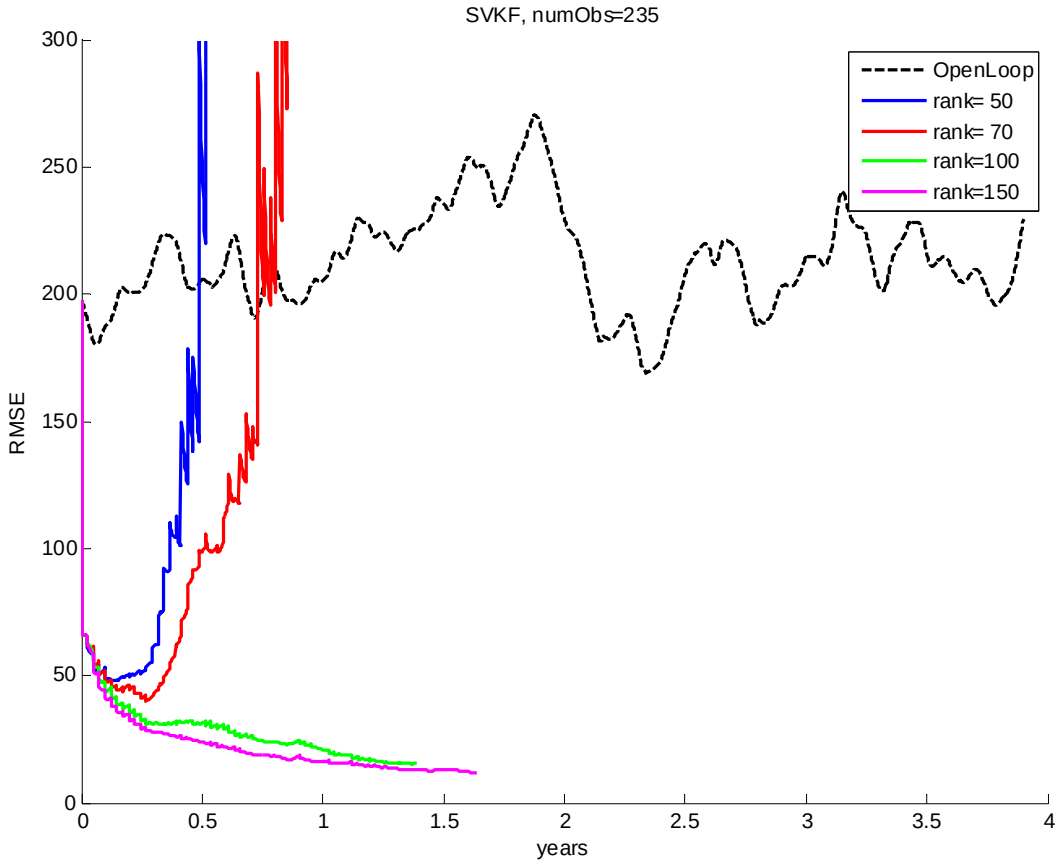

Figure 4-5: Network of 119 observed states. Background is the relative variability of the potential vorticity over the model domain.

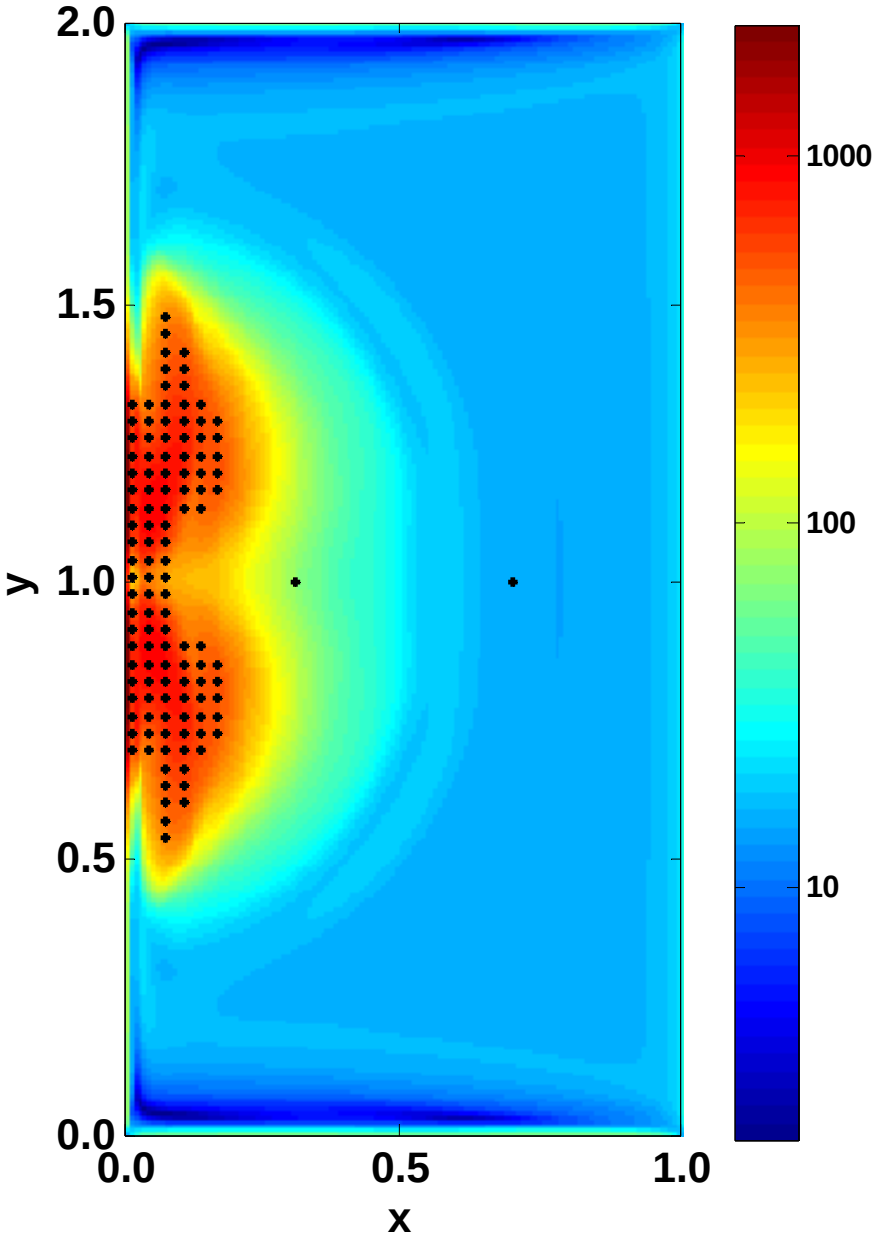

Figure 4-6: RMSE of LFKF with various ranks, quasi-geostrophic ocean model with 119 observations.

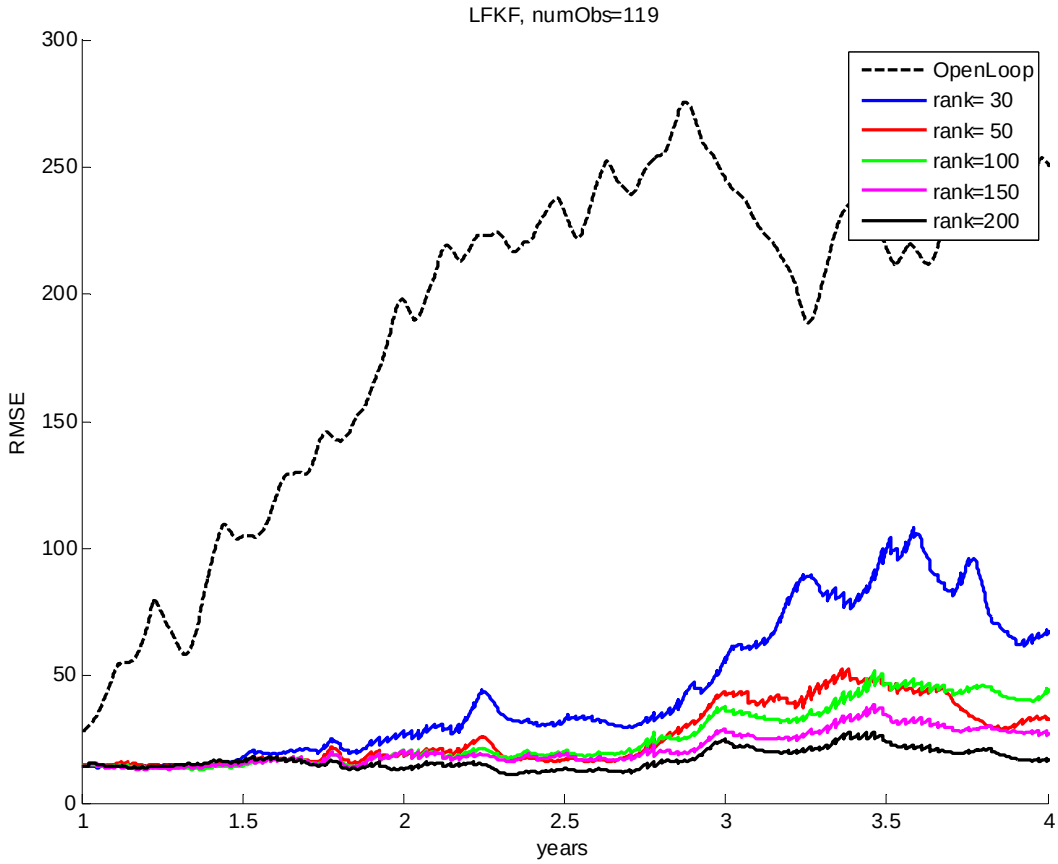

Figure 4-7: RMSE of SVKF with various ranks, quasi-geostrophic ocean model with 119 observations.

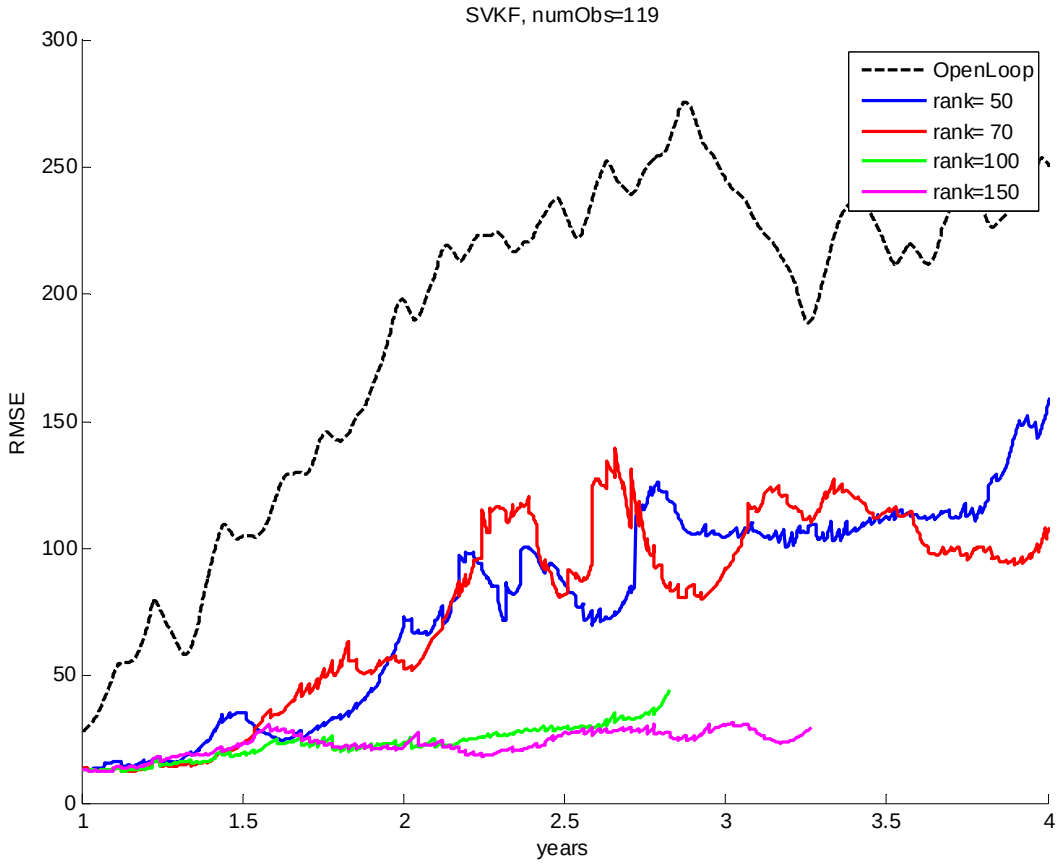

Figure 4-8: Network of 119 observed states. Background is the relative variability of the potential vorticity over the model domain.

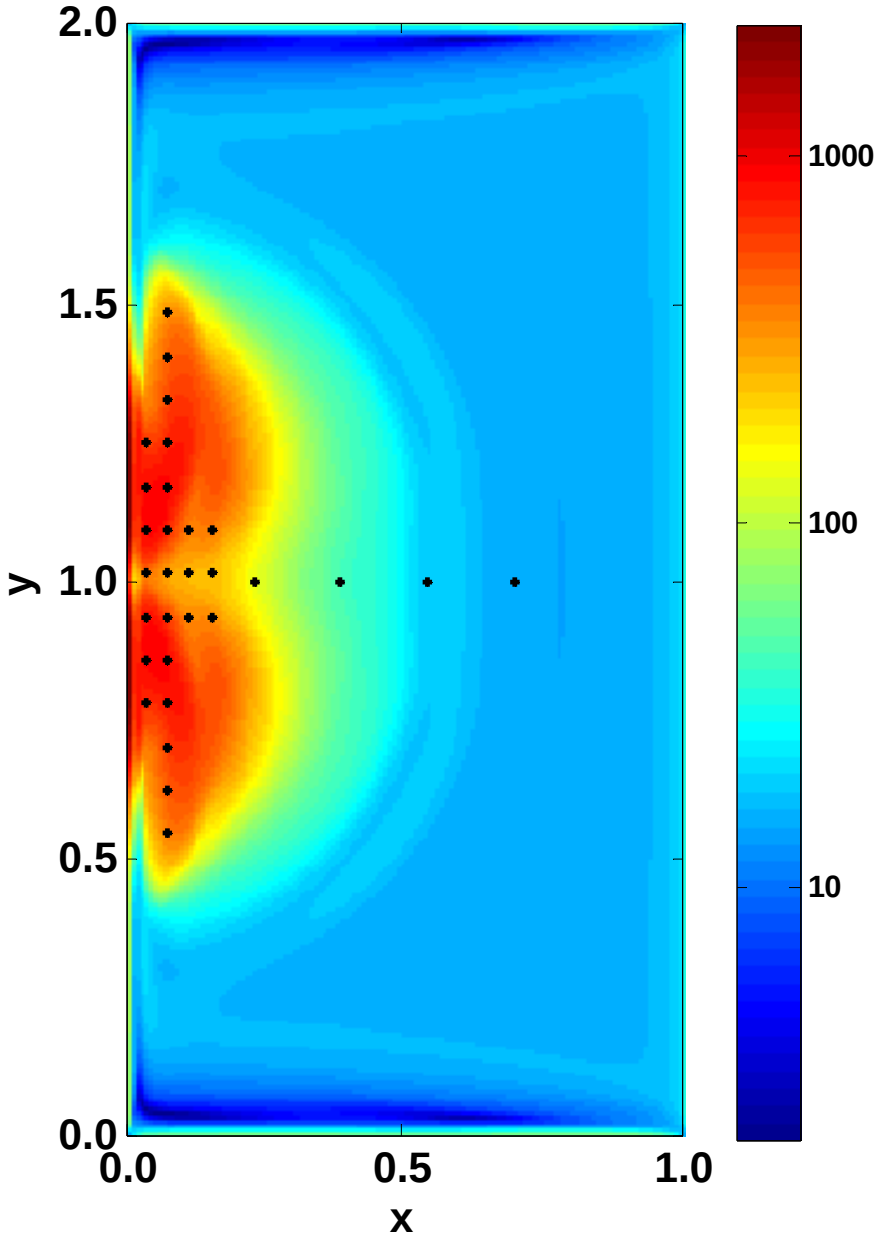

Figure 4-9: RMSE of LFKF with various ranks, quasi-geostrophic ocean model with 30 observations.

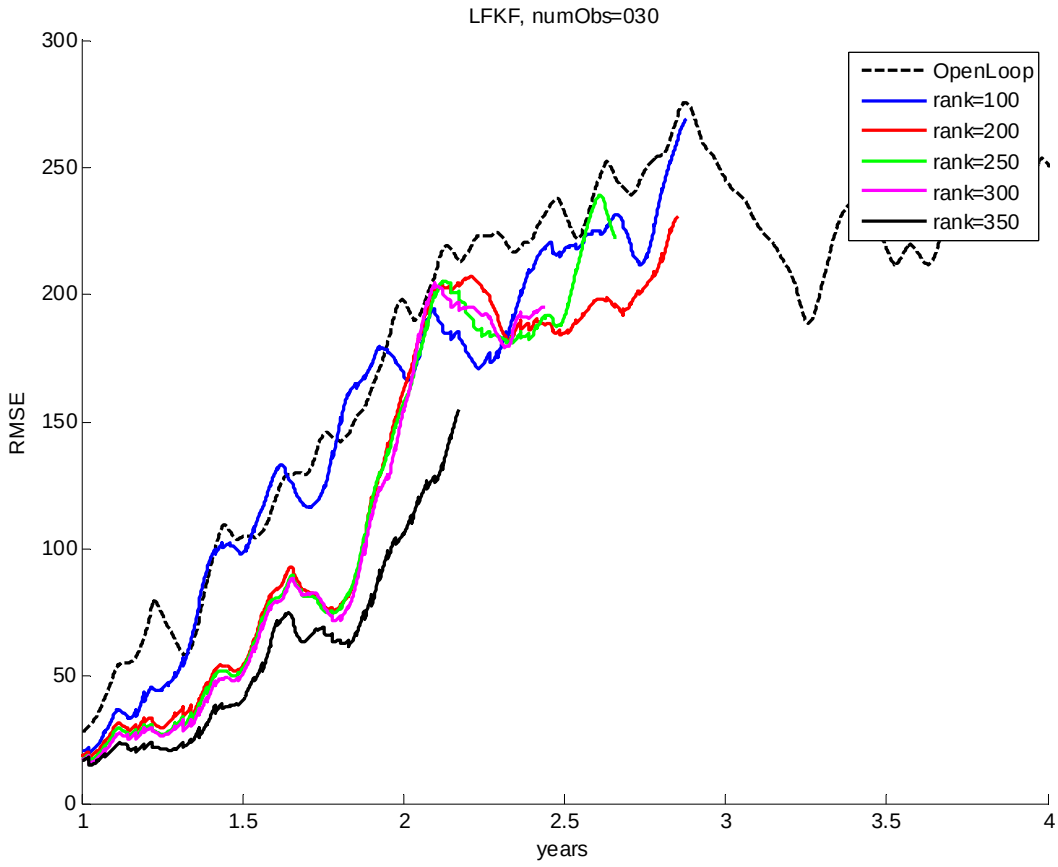

Figure 4-10: RMSE of SVKF with various ranks, quasi-geostrophic ocean model with 30 observations.

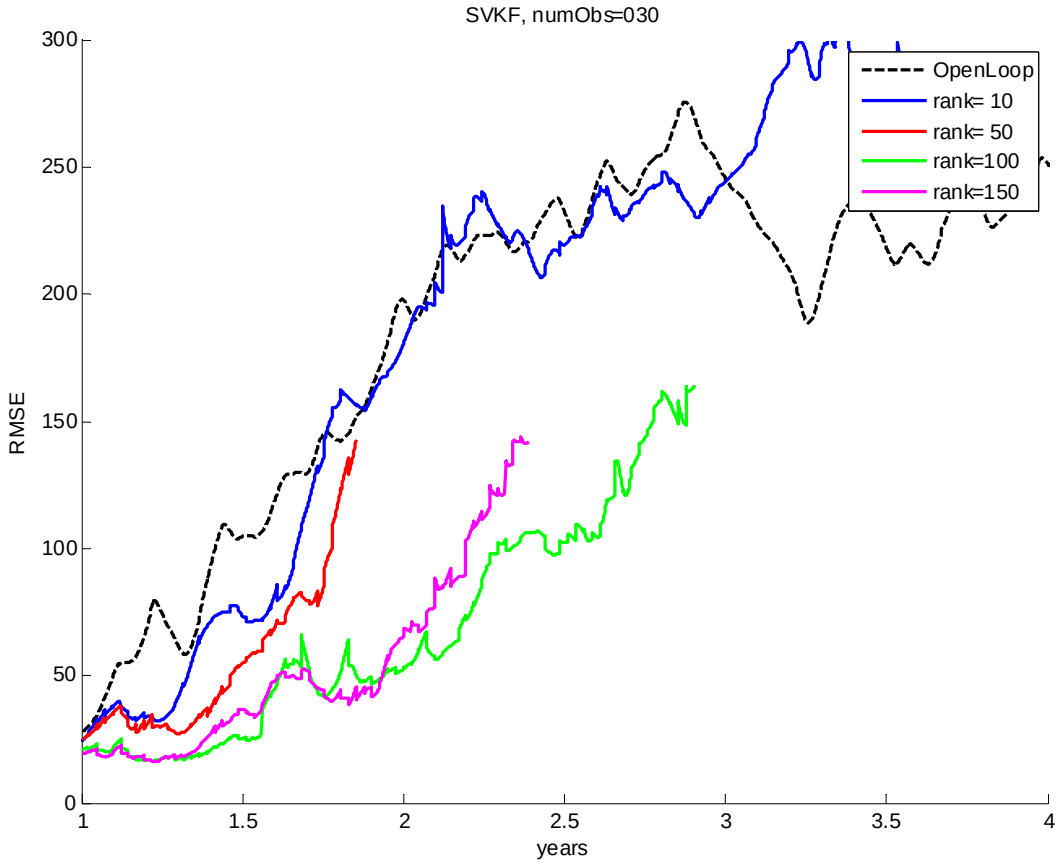

5 Concluding Remarks

This thesis addresses the problem of filtering in chaotic and large geophysical systems. In chaotic systems, uncertainties experience growth or instability only along a subset of directions. This is promising for geophysical applications with enormous state size, because the order of the problem may be remarkably reduced by solving it on the subspace of these important directions for an approximate suboptimal solution. In filtering, the best estimate of the state (analysis) is found recursively by correcting the prediction of the model (forecast) as the measurements of the system (observations) become available. If the filter uses a linear Kalman-based update, the extent of the correction to the forecast is mainly controlled by the error covariance of the forecast. Therefore, a reduced rank filter can be successful if only if the important information in the forecast error covariance is conserved. In this work, two different methods were introduced to reduce the rank of the forecast error covariance without compromising any important information about the forecast uncertainty.

In Chapter 2, the problem was approached from the perspective of growth potential of the uncertainty over the forecast window. Under the assumption that the dynamics of the error can be approximated by a linear model, the growing directions were identifies as the leading singular vectors (SVs) of the corresponding state transition matrix, and computed via iterative integrations of the linear forward and adjoint models of the system. The Singular Vector Kalman Filter (SVKF) was formulated in a square root form by projecting the forecast error covariance on the subspace of these SVs. Experiments with a chaotic Lorenz 95 system with additive dynamic model error showed that once all of the growing SVs were resolved, SVKF performed

very close to the Optimal linear filter, defined as an Ensemble Kalman Filter (EnKF) with a very large ensemble size.

In chapter 3, the problem was approached from the perspective of stability of the error dynamics over the forecast window. Under the assumption of linearity of the error propagation, the unstable directions of error dynamics were identified as the unstable eigenvectors of the state transition matrix. It was shown that the subspace of these unstable directions was spanned by the leading Floquet vectors (FVs) of an auxiliary periodic system that was built over the trajectory of the forecast. The FVs were computed via iterations of the nonlinear forward model and used for the basis of the projection subspace in the Local Floquet Kalman Filter (LFKF), formulated in a square root form parallel to the SVKF. The LFKF, unlike SVKF did not require the adjoint of the system. LFKF was tested on the chaotic Lorenz 95 system. The results showed that LFKF performed better than EnKF but it was slightly inferior to SVKF. However, when the rank of the filter was greater than the number of growing or unstable directions, both the LFKF and the SVKF performed almost the same as the Optimal. Since computation of FVs does not require any linear model or its adjoint, LFKF is more suitable than SVKF in applications where the adjoint model is not available or is difficult to build.

Since the additive dynamic model error may lead to complications in chaotic geophysical systems such as the atmosphere, it is common in these applications to assume that there is no dynamic model error, also known as the perfect model scenario. Elimination of the dynamic model error has important consequences in ensemble filtering algorithms that are very popular in nonlinear systems. In particular, it is commonly observed that when dynamic model error is

zero, ensemble members loose their independence, leading to underestimation of the forecast uncertainty. Current techniques to resolve this problem are ad hoc and involve enforcing the forecast error covariance to have a predefined structure. Consequently, the important time-dependent uncertainty information that is essential for performance of the filter may be lost.

Both the SVKF and the LFKF were examined when dynamic model error was zero. It was shown that both of the filters could potentially loose the uncertainty information along the directions that had been previously unimportant but suddenly needed to be considered in the reduced rank filter, a situation common in chaotic systems. Since resolving the uncertainty along these newly important directions is essential for performance of the filter, the algorithms had to be slightly modified to allow proper characterization of the forecast uncertainty. After this provision, both of the filters were tested on the chaotic Lorenz 95 system without dynamic model error. Results show that both of the filters perform near optimal when their rank is large enough to capture all of the important directions. However, when the rank of the filters were too small, their performance deteriorated more drastically than the experiments with the additive noise, because presence of dynamic model error could partially compensate for underestimation of forecast uncertainty along the discarded directions that are still important but are not essential, i.e. have small growth or instability factor.

If a system is self-adjoint in the sense that its linear and adjoint models are the same, its SVs and FVs are the same. However, this is not true in most of the chaotic systems, meaning that the SVKF and the LFKF use different subspaces to project the forecast error covariance. To resolve this conflict, it was shown that once all of the growing SVs were included, all of the unstable

FVs were guaranteed to be stabilized by the SVKF, confirming the excellent performance of both of the filters.

The computational cost of the filters we re also measured and normalized by a single nonlinear integration of the model, under the assumption that each iteration with the linear forward and adjoint models was as expensive as an iteration with the nonlinear model. The experiments showed that 5 iterations were enough to compute the SVs and FVs with a good precision. Analysis of the trade-off between the performance and the computational cost showed that SVKF is the superior algorithm, while LFKF is a suitable substitute in applications where the adjoint model is not available or does not converge.

In Chapter 4, SVKF and LFKF were implemented in an idealized chaotic wind-driven quasi-geostrophic ocean circulation system with over 30,000 variables. We introduced an alterative formulation of the covariance update step when dynamic model error is zero, particularly suitable when a large vector of observations were to be assimilated such as in remote sensing applications. The experiments showed that both of the filters were able to produce excellent estimates when the observation operator was selected properly, even if they were initialized at a completely random initial estimate.

We briefly discussed the observability issue. Our results show that a poor choice of observed states would lead to complete loss of performance of a filtering algorithm. This emphasizes the role of the observation operator and calls for in-depth analysis of the observability issue in chaotic dynamics.

6 Appendices

6.1 Appendix A: Effect of dynamic model error in chaotic systems

Under the hyperbolicity of the attractor, dynamics can be decomposed into directions which experience either contraction or growth. However, when the intersection of stable and unstable manifolds is tangent to the attractor, it is called the homoclinic tangency (HT) and the attractor is not hyperbolic anymore (Jaeger and Kantz, 1997). HTs are the point on the attractor with strongest nonlinearity, where linearization-based algorithms fail. HTs are uniquely determined as the pre-images or images of the primary homoclinic tangency (PHT), which is the HT that is closest to the boundary of the basin of attraction (Kraut and Grebogi, 2004).

HTs are also extremely important in analysis of the structural stability of chaotic systems in response to perturbations. In particular, consider the unperturbed trajectory of an initial condition inside the basin of attraction that quickly falls on the attractor. Trajectory of the very same initial condition with perturbations may get far from the attractor and even leave the basin of attraction. This effect is called explosion of the chaotic trajectory and is more likely to happen in the vicinity of HTs (Jaeger and Kantz, 1997, Schroer et al., 1998, Robert et al., 2000). This has important implications in data assimilation in chaotic systems. In geophysical applications, occurrence of these structural instabilities due to perturbations is also known as gravity wave

excitation by unbalanced dynamics (Daley, 1991; Fillion, 2002; Neef et al., 2006).

Although the HTs are harder to find in large and highly dissipative chaotic systems such as the Lorenz 95 that we have used in our experiments, their impact can be illustrated on small chaotic systems such as Henon map (Henon, 1976), whose dynamics is written as:

$$\begin{bmatrix} x_{t+1} \\ y_{t+1} \end{bmatrix} = \begin{bmatrix} a - x_t^2 + b \cdot y_t \\ x_t \end{bmatrix} + \omega_t \qquad \text{(A1)}$$

where (x_t, y_t) are the state variables, (a, b) are the parameters, and ω_t is a perturbation vector. Figure 6-1 shows the attractor and its basin of attraction in absence of perturbations, i.e. $\omega_t = 0$. A_0 is an ensemble of 1000 replicates that are generated randomly within the basin of attraction around a point on the attractor. Without perturbations, all of these replicates converge to the attractor within a few time-steps, as labeled by A_1, A_2, ... However, if randomly generated Gaussian perturbations are added to the state at each step, trajectories that start from the same initial conditions follow completely different trajectories. In our simple experiment, 18 ensemble members (%1.8 of the replicates) escaped the basin of attraction within 10 time-steps, when they were subject to perturbations with standard deviation of 0.01 (about 0.002 of the attractor size). Additionally, as expected the escaping ensemble members concentrated in the neighborhood of the PHT and its pre-images.

In the data assimilation algorithms, there are three places, where perturbations are added to the state, namely initialization of the ensemble members, dynamic model error in the propagation step, and observation noise in the analysis step. Avoiding the instabilities in the initialization

time is the easiest of the three and there are various methods to ensure that ensemble members are on the attractor or in its basin of attraction. However, avoiding instabilities due to dynamic model error or in the analysis step is more complicated. A few methods are developed for preventing these unbalanced dynamics and structural instabilities, amid an active research on this topic (Gauthier and Thépaut, 2001, Wee and Kuo, 2004).

6.2 Appendix B: Iterative method for computing singular vectors

Detailed procedure for computing the leading singular vectors of $F_{t,t+T}$ defined in (2-7) is discussed in this appendix. Following the notation in (2-8), and noting that the adjoint of the real $F_{t,t+T}$ is its transpose, we have:

$$\begin{aligned} F_{t,t+T} &= U_{t,t+T}\Sigma_{t,t+T}{V_{t,t+T}}^T \\ {F_{t,t+T}}^T &= V_{t,t+T}\Sigma_{t,t+T}{U_{t,t+T}}^T \end{aligned} \tag{B-1}$$

Therefore,

$$\begin{aligned} {F_{t,t+T}}^T F_{t,t+T} &= \left(V_{t,t+T}\Sigma_{t,t+T}{U_{t,t+T}}^T \right)\left(U_{t,t+T}\Sigma_{t,t+T}{V_{t,t+T}}^T \right) \\ &= V_{t,t+T}\Sigma_{t,t+T}^2{V_{t,t+T}}^T \end{aligned} \tag{B-2}$$

which is the eigen-decomposition of the Hermitian matrix ${F_{t,t+T}}^T F_{t,t+T}$. Therefore, the leading

singular vectors of $F_{t,t+T}$ in $V_{t,t+T}^{N}$ are the same as the leading eigenvectors of ${F_{t,t+T}}^{T}F_{t,t+T}$ and may be computed by an iterative Lanczos algorithm.

In the Lanczos method, the N leading eigenvectors of ${F_{t,t+T}}^{T}F_{t,t+T}$ are computed by iterating (B-3) and (B-4):

$$V_{t,t+T}^{(k)} = \text{Gram Schmidt}\left[\widetilde{V}_{t,t+T}^{(k)}\right] \tag{B-3}$$

$$\widetilde{V}_{t,t+T}^{(k+1)} = \left({F_{t,t+T}}^{T}F_{t,t+T}\right)V_{t,t+T}^{(k)} \qquad , k = 0,1,2,\cdots \tag{B-4}$$

initialized by $V_{t,t+T}^{(0)}$ whose columns are N arbitrary but mutually independent perturbations, $v_{t,t+T}^{i\,(0)}$ for $i = 1,\cdots,N$. The iteration in k continue until the column space of $V_{t,t+T}^{(k)}$ converge to an invariance N dimensional subspace (Saad, 1992). In practice, (B-4) is done in two steps. First, $V_{t,t+T}^{(k)}$ is multiplied by $F_{t,t+T}$

$$\widetilde{U}_{t,t+T}^{(k)} = F_{t,t+T}V_{t,t+T}^{(k)} \tag{B-5}$$

Then the resulting $\widetilde{U}_{t,t+T}^{(k)}$ is multiplied by ${F_{t,t+T}}^{T}$:

$$\widetilde{V}_{t,t+T}^{(k+1)} = {F_{t,t+T}}^{T}\widetilde{U}_{t,t+T}^{(k)} \tag{B-6}$$

When the fastest growing directions of a nonlinear system are needed and the linearity

assumption is valid, (B-5) can be conducted by propagating individual ${v_{t,t+T}^{i}}^{(k)}$'s using the nonlinear model as follows:

$$\tilde{u}_{t,t+T}^{i\ (k)} = \frac{1}{\delta}\left\{ f\left[x(t) + \delta \cdot {v_{t,t+T}^{i}}^{(k)}, t+T \right] - f\left[x(t), t+T \right] \right\} \qquad ,i = 1,\cdots,N \qquad \text{(B-7)}$$

where $\tilde{u}_{t,t+T}^{i\ (k)}$'s are columns of $\tilde{U}_{t,t+T}^{(k)}$. Similarly, (B-6) can be done using the adjoint model along the forecast trajectory over $[t, t+T]$. This is very similar to the method for computing SVs at the European Center for Medium-range Weather Forecasts, without using the Hessian of the variational cost function . After the convergence, columns of ${\tilde{U}_{t,t+T}}^{(k)}$ and ${V_{t,t+T}}^{(k)}$ are along the needed leading singular vectors in $U_{t,t+T}^{N}$ and $V_{t,t+T}^{N}$, respectively. Additionally, magnitude of $\tilde{u}_{t,t+T}^{i\ (k)}$'s are the corresponding singular values, which are diagonal elements of $\Sigma_{t,t+T}^{N}$.

6.3 Appendix C: Verification of the Kalman gain computed via the recursion in Section 2.3

In this appendix, it is shown that the Kalman gain computed in (2-30) is equivalent to (2-19). If we denote

$$\Theta(t+T) = \sqrt{Q(t+T)} - \Psi(t+T)\left[H(t+T)\sqrt{Q(t+T)} \right] \qquad \text{(C-1)}$$

therefore $\Xi(t+T) = H(t+T)\,\Theta(t+T)$, and (2-30) can be rewritten as

$$
\begin{aligned}
K(t+T) &= \widetilde{L}^a(t+T)\left[H(t+T)\widetilde{L}^a(t+T)\right]^T R(t+T)^{-1} \\
&\quad + \sqrt{Q(t+T)}\,\Theta(t+T)^T H(t+T)^T R(t+T)^{-1} \\
&\quad - \Psi(t+T)\left\{\left[H(t+T)\sqrt{Q(t+T)}\right]\Theta(t+T)^T H(t+T)^T\right\} R(t+T)^{-1} \\
&= \left[\widetilde{L}^a(t+T)\widetilde{L}^a(t+T)^T\right] H(t+T)^T R(t+T)^{-1} \\
&\quad + \left[\sqrt{Q(t+T)}\,\Theta(t+T)^T\right] H(t+T)^T R(t+T)^{-1} \\
&\quad - \left[\Psi(t+T)\,H(t+T)\sqrt{Q(t+T)}\,\Theta(t+T)^T\right] H(t+T)^T R(t+T)^{-1} \\
&= \left[\begin{array}{l}\widetilde{L}^a(t+T)\widetilde{L}^a(t+T)^T + \sqrt{Q(t+T)}\,\Theta(t+T)^T \\ \quad - \Psi(t+T)\,H(t+T)\sqrt{Q(t+T)}\,\Theta(t+T)^T\end{array}\right] H(t+T)^T R(t+T)^{-1} \\
&= \left[\begin{array}{l}\widetilde{L}^a(t+T)\widetilde{L}^a(t+T)^T + \\ \left(\sqrt{Q(t+T)} - \Psi(t+T)\,H(t+T)\sqrt{Q(t+T)}\right)\Theta(t+T)^T\end{array}\right] H(t+T)^T R(t+T)^{-1} \\
&= \left[\widetilde{L}^a(t+T)\widetilde{L}^a(t+T)^T + \Theta(t+T)\Theta(t+T)^T\right] H(t+T)^T R(t+T)^{-1} \\
&= \left[\widetilde{L}^a(t+T)\middle|\Theta(t+T)\right]\left[\widetilde{L}^a(t+T)\middle|\Theta(t+T)\right]^T H(t+T)^T R(t+T)^{-1} \qquad \text{(C-2)}
\end{aligned}
$$

To prove that (2-30) is equivalent to (2-19), we only need to show that $L^a(t+T)$ in (2-20) is

equivalent to $\left[\widetilde{L}^a(t+T)\middle|\Theta(t+T)\right]$ in (C-2). We have:

$$\begin{aligned}\widetilde{L}^a(t+T) &= \widetilde{L}^f(t+T) - \Psi(t+T)H(t+T)\widetilde{L}^f(t+T)\\ &= \left[I - \Psi(t+T)H(t+T)\right]\widetilde{L}^f(t+T)\\ \Theta(t+T) &= \sqrt{Q(t+T)} - \Psi(t+T)H(t+T)\sqrt{Q(t+T)}\\ &= \left[I - \Psi(t+T)H(t+T)\right]\sqrt{Q(t+T)}\end{aligned} \tag{C-3}$$

Therefore,

$$\left[\widetilde{L}^a(t+T)\middle|\Theta(t+T)\right] = \left[I - \Psi(t+T)H(t+T)\right]\left[\widetilde{L}^f(t+T)\middle|\sqrt{Q(t+T)}\right] \tag{C-4}$$

If $\widetilde{L}^f(t+T)$ in (2-25) is a valid computation of (2-18), we can use (2-17) and it follows that

$$\begin{aligned}\left[\widetilde{L}^a(t+T)\middle|\Theta(t+T)\right] &= \left[I - \Psi(t+T)H(t+T)\right]L^f(t+T)\\ &= L^f(t+T) - \Psi(t+T)H(t+T)L^f(t+T)\\ &= L^a(t+T)\end{aligned} \tag{B5}$$

Therefore, we are left to show that $\widetilde{L}^f(t+T)$ in (2-25) is a valid computation of (2-18).

$\Phi(t)$ in (2-24) is computed at the previous cycle using (2-32), which after (C-1) can be written as

$$\Phi(t+T) = \left(V^N_{t+T,t+2T}\right)^T \Theta(t+T) \tag{B6}$$

Using (C-6) and substituting for $\Phi(t)$ in (2-24) we have:

$$\Gamma_{t,t+T} = \left[\left(V^N_{t,t+T}\right)^T \tilde{L}^a(t) \,\middle|\, \left(V^N_{t,t+T}\right)^T \Theta(t) \right] = \left(V^N_{t,t+T}\right)^T L^a(t) \tag{B7}$$

which combined with (2-25) is equivalent to (2-18). This completes the proof.

6.4 Appendix D: Verification of the square root analysis scheme

In this appendix, it is shown that computing the analysis error covariance by its square root $L^a(t)$ in (2-20)-(2-22) is equivalent to the more conventional formulation in (2-14). We drop the time notation for convenience.

First, rewrite (2-14) as follows:

$$\begin{aligned} L^a L^{aT} &= L^f L^{fT} - L^f L^{fT} H^T \left(HP^f H^T + R \right)^{-1} HL^f L^{fT} \\ &= L^f \left[I - L^{fT} H^T \left(HP^f H^T + R \right)^{-1} HL^f \right] L^{fT} \end{aligned} \tag{D-1}$$

Using (2-22) we have:

$$\left(HP^f H^T + R\right)^{-1} = \left(\sqrt{Z}\,\sqrt{Z}^T\right)^{-1} = \sqrt{Z}^{-T}\sqrt{Z}^{-1}$$

$$= \Omega + \Omega^T - \left(\Omega + \Omega^T - \sqrt{Z}^{-T}\sqrt{Z}^{-1}\right)$$

$$= \Omega + \Omega^T - \Omega\left(\Omega^{-1} + \Omega^{-T} - \Omega^{-1}\sqrt{Z}^{-T}\sqrt{Z}^{-1}\,\Omega^{-T}\right)\Omega^T$$

$$= \Omega + \Omega^T - \Omega\begin{pmatrix}\sqrt{Z}\sqrt{Z}^T - \sqrt{Z}\sqrt{Z}^T + \Omega^{-1}\sqrt{Z}^{-T}\sqrt{Z}^T + \\ \sqrt{Z}\sqrt{Z}^{-1}\Omega^{-T} - \Omega^{-1}\sqrt{Z}^{-T}\sqrt{Z}^{-1}\Omega^{-T}\end{pmatrix}\Omega^T$$

$$= \Omega + \Omega^T - \Omega\left[\sqrt{Z}\sqrt{Z}^T - \begin{pmatrix}\sqrt{Z}\sqrt{Z}^T - \Omega^{-1}\sqrt{Z}^{-T}\sqrt{Z}^T - \sqrt{Z}\sqrt{Z}^{-1}\Omega^{-T} + \\ \Omega^{-1}\sqrt{Z}^{-T}\sqrt{Z}^{-1}\Omega^{-T}\end{pmatrix}\right]\Omega^T$$

$$= \Omega + \Omega^T - \Omega\left[\sqrt{Z}\sqrt{Z}^T - \left(\Omega^{-1}\sqrt{Z}^{-T} - Z\right)\left(\Omega^{-1}\sqrt{Z}^{-T} - \sqrt{Z}\right)^T\right]\Omega^T \qquad \text{(D-2)}$$

for any Ω that is full-rank $m \times m$.

We choose $\Omega = \left(\sqrt{Z}\sqrt{Z}^T + \sqrt{R}\Theta\sqrt{Z}^T\right)^{-1}$ with Θ being an arbitrary $m \times m$ orthogonal matrix,

$\Theta\Theta^T = I$. It follows that $\Omega^{-1}\sqrt{Z}^{-T} - \sqrt{Z} = \sqrt{R}\Theta$. Further substitution in (D-2) gives:

$$\left(HP^f H^T + R\right)^{-1} = \Omega + \Omega^T - \Omega\left(\sqrt{Z}\,\sqrt{Z}^T - \sqrt{R}\Theta\Theta^T\sqrt{R}^T\right)\Omega^T$$

$$= \Omega + \Omega^T - \Omega\left(\sqrt{Z}\sqrt{Z}^T - R\right)\Omega^T$$

$$= \Omega + \Omega^T - \Omega \left(H \; L^f \; L^{f^T} \; H^T \right) \Omega^T \tag{D-3}$$

Now we substitute (D-3) in the term in the brackets in (D-1):

$$I - L^{f^T} H^T \left(HP^f H^T + R \right)^{-1} HL^f = I - L^{f^T} H^T \left[\Omega + \Omega^T - \Omega \left(HL^f L^{f^T} H^T \right) \Omega^T \right] HL^f$$

$$= I - L^{f^T} H^T \; \Omega \; HL^f - L^{f^T} H^T \; \Omega^T \; HL^f + L^{f^T} H^T \; \Omega \left(HL^f L^{f^T} H^T \right) \Omega^T \; HL^f$$

$$= \left(I - L^{f^T} H^T \; \Omega \; HL^f \right) \left(I - L^{f^T} H^T \; \Omega \; HL^f \right)^T \tag{D-4}$$

Thus (D-1) can be written in square root form as

$$L^a = L^f \sqrt{I - L^{f^T} H^T \left(HP^f H^T + R \right)^{-1} HL^f} = L^f \left(I - L^{f^T} H^T \; \Omega \; HL^f \right)$$

$$= \left(I - L^f L^{f^T} H^T \; \Omega \; H \right) L^f \tag{D-5}$$

All we need to show is that (D-5) is equivalent to (2-20) with (2-21). It is easy to see that $\Psi(t)$ in (2-21) is equivalent to

$$\Psi = L^f \left(HL^f \right)^T \sqrt{Z}^{-T} \left(\sqrt{Z} + \sqrt{R} \right)^{-1} = L^f L^{f^T} H^T \left(\sqrt{Z} \sqrt{Z}^T + \sqrt{R} \sqrt{Z}^T \right)^{-1} = L^f L^{f^T} H^T \; \Omega \tag{D-6}$$

Substituting (D-6) in (2-20) gives (D-5).

6.5 Appendix E: Proof of the theorem on stability of the singular vector Kalman filter

This appendix poses a theorem on projection of the unstable eigenvectors of a given matrix on a subspace that is spanned by its leading left (final) singular vectors. This theorem means that the gain matrix in an SVD-based low rank filter will use an approximate covariance matrix that has projection on all of the unstable modes of the system and hence stabilizes the system.

Theorem: Given a square matrix with p unstable eigenvalues, no unstable right eigenvectors are orthogonal to the subspace that is spanned by its p leading left (final) singular vectors.

Proof: Let A be a square matrix of size n with p unstable eigenvalues. Denote the ordered singular value decomposition (SVD) of A by:

$$A = U \cdot \Sigma \cdot V^T \tag{E-1}$$

where $\Sigma = diag(\sigma_1, \cdots, \sigma_n)$ with $\sigma_1 \geq \cdots \geq \sigma_n$ are the singular values of A in decreasing order, and $U = \left[\cdots \middle| u_i \middle| \cdots \right]$ and $V = \left[\cdots \middle| v_i \middle| \cdots \right]$ are two orthogonal $n \times n$ matrices with respectively, left and right singular vectors of A as their columns. Additionally, let the ordered eigen-decomposition of A be as follows:

$$A = W \, \Lambda \, W^{-1} \tag{E-2}$$

where $\Lambda = diag(\lambda_1, \cdots, \lambda_n)$ with $|\lambda_1| \geq \cdots \geq |\lambda_p| \geq 1 \geq |\lambda_{p+1}| \geq \cdots \geq |\lambda_n|$ are the eigenvalues of A in decreasing order, and their corresponding right eigenvectors, w_i are the columns of W.

(E-1) can be rewritten as follows:

$$\begin{aligned} A &= \sum_{i=1}^{n} \sigma_i \, u_i \, v_i^T \\ &= \sum_{i=1}^{p} \sigma_i \, u_i \, v_i^T + \sum_{i=p+1}^{n} \sigma_i \, u_i \, v_i^T \\ &= A_{1:p} + A_{p+1:n} \end{aligned} \qquad \text{(E-3)}$$

Where $A_{1:p}$ and $A_{p+1:n}$ are respectively, the SVD-based $n \times n$ reduced rank approximation of A and its compliment. We need to show that none of w_k's for $k = 1, \cdots, p$ is orthogonal to u_i for $i = 1, \cdots, p$.

Consider w_k with $|\lambda_k| \geq 1$. If w_k is not orthogonal to all v_i's, for $i = 1, \cdots, p$, it will have some projection on u_i for $i = 1, \cdots, p$, and hence is not orthogonal to all u_i's for $i = 1, \cdots, p$.

We need to show that if w_k is orthogonal to all v_i's, for $i = 1, \cdots, p$, then it cannot be orthogonal to all u_i's for $i = 1, \cdots, p$.

If w_k is orthogonal to all v_i's, for $i = 1, \cdots, p$, then $w_k \in$ subspace $(v_{p+1}, \cdots, v_n)$ and $A_{1:p} \, w_k = 0$. Therefore,

$$A_{p+1:n} \, w_k = A_{p+1:n} \, w_k + A_{1:p} \, w_k = A \, w_k = \lambda_k \, w_k \qquad \text{(E-4)}$$

meaning that λ_k is an eigenvalue of $A_{p+1:n}$. Since magnitude of any eigenvalue of a given matrix is bounded from above and below by its largest and smallest singular values, respectively, it follows that:

$$1 < |\lambda_k| \le \sigma_{p+1} \le \sigma_p \le \left|\hat{\lambda}_j\right| \quad \text{, for } j = 1, \cdots, p \tag{E-5}$$

where $\hat{\lambda}_j$ is an eigenvalue of $A_{1:p}$. Therefore, $A_{1:p}$ itself has p unstable modes. If w_k is also orthogonal to all u_i's for $i = 1, \cdots, p$, then A has to have $p+1$ unstable modes that contradicts our assumption. This completes the proof.

6.6 Appendix F: Review of the Floquet theorem

In this section, a brief review of the Floquet theorem is presented. The complete proof can be found in Yakubovich and Starzhinskii (1975).

6.6.1 Definitions

Consider the following linear differential equation:

$$\delta \dot{z}(s) = \Phi(s)\, \delta z(s) \tag{F-1}$$

where $\delta z(s)$ is a column vector of length *n* and $\Phi(s)$ is the $n \times n$ matrix function. We assume $\Phi(s)$ is piecewise continuous and integrable. In that case (F-1) has a continuous solution that is

unique. Without loss of generality, we can write (F-1) in temporally discreet from as:

$$\delta z(s+1) = A(s)\,\delta z(s) \tag{F-2}$$

Let $\delta z_j(s)\,(j = 1, \cdots, m)$ be m arbitrary solutions to (F-1) with m initial conditions $\delta z_j(0)$. Then the $n \times m$ matrix $\delta Z(s) = \left[\, \delta z_1(s) \,\middle|\, \cdots \,\middle|\, \delta z_m(s) \,\right]$ solves the following matrix differential equation:

$$\delta Z(s+1) = A(s)\,\delta Z(s) \tag{F-3}$$

with initial condition $\delta Z(0)$.

If $n = m$ and $\delta Z(0) = I_n$, $\delta Z(s)$ is called the *matrizant* of the system (henceforth denoted as $\Omega(s)$). From Lioville-Jacobi formula,

$$\det \Omega(s) = \det \Omega(0) \prod_{\tau=0}^{s-1} \left[\det A(\tau) \right] = \prod_{\tau=0}^{s-1} \left[\det A(\tau) \right]. \tag{F-4}$$

Therefore, $\Omega(s)$ will remain invertible as long as $A(s)$ is full-rank. In that case, columns of the matrizant matrix will remain linearly independent and can be used as a basis for any solutions to (F-3). In particular, any $n \times m$ solution $\delta Z_1(s)$ to (F-3) with initial condition $\delta Z_1(0)$ may be expressed as:

$$
\begin{aligned}
\delta Z_1(s) &= A(s-1)\,\delta Z_1(s-1) \\
&= \left[\Omega(s)\,\Omega^{-1}(s-1)\right]\delta Z_1(s-1) \\
&= \left[\Omega(s)\,\Omega^{-1}(s-1)\right]\left[\Omega(s-1)\,\Omega^{-1}(s-2)\right]\delta Z_1(s-2) \\
&= \left[\Omega(s)\,\Omega^{-1}(s-1)\right]\left[\Omega(s-1)\,\Omega^{-1}(s-2)\right]\cdots\left[\Omega(1)\,\Omega^{-1}(0)\right]\delta Z_1(0) \\
&= \Omega(s)\,\delta Z_1(0)
\end{aligned}
\tag{F-5}
$$

If elements of $A(s)$ are T -periodic functions such that $A(s+T) = A(s)$,

$$
\begin{cases}
\Omega(s+T+1) = A(s+T)\Omega(s+T) = A(s)\,\Omega(s+T) \\
\Omega(s+1) = A(s)\,\Omega(s)
\end{cases}
\tag{F-6}
$$

Thus, both sides of (F-6) solve (F-2) with the initial condition $\Omega(0) = I_n$. Hence, from uniqueness of the solution to (F-2), (F-6) holds:

$$
\Omega(s+T) = \Omega(s)\,\Omega(T) \tag{F-7}
$$

The reverse is also true, i.e. from (F-7), it follows that (F-2) is periodic:

$$
\begin{aligned}
A(s+T) &= \Omega(s+T+1)\,\Omega(s+T)^{-1} \\
&= \left[\Omega(s+1)\,\Omega(T)\right]\left[\Omega(T)^{-1}\Omega(s)^{-1}\right] \\
&= A(s)
\end{aligned}
\tag{F-8}
$$

Therefore, the matrizant of (F-3) satisfies (F-6), if and only if $A(s+T) = A(s)$.

If $A(s)$ is *T*-periodic, $\Omega(T)$, the matrizant matrix evaluated at $s = T$, is called the *monodromy*

matrix of (F-2) and its eigenvalues are referred to as the *multipliers* of the system. The set of all of the multipliers is called the *spectrum* of the system. In the remainder of this appendix, we focus on T -periodic case of (F-2).

6.6.2 Floquet-Lyapunov Theorem

Let $B^{n\times n}$ denote the T -th root of $\Omega(T)$, defined as $\Omega(T) = B^{\{T\}}$, where $B^{\{T\}}$ means that B is raised to the power T (not to be confused by "transpose"). Therefore, B is a constant matrix.

Define $Q(s) = \Omega(s)\, B^{\{s\}^{-1}}$. It follows that $Q(s)$ is T -periodic:

$$\begin{aligned} Q(s+T) &= \Omega(s+T)\, B^{\{s+T\}^{-1}} \\ &= \left[\Omega(s)\,\Omega(T)\right]\left[B^{\{s\}}\ B^{\{T\}}\right]^{-1} \\ &= \left[\Omega(s)\,\Omega(T)\right]\left[\Omega(T)^{-1} B^{\{s\}^{-1}}\right] \\ &= \Omega(s)\, B^{\{s\}^{-1}} \\ &= Q(s) \end{aligned} \qquad \text{(F-9)}$$

Therefore, $\Omega(s)$ at any time s can be written in the particular form:

$$\Omega(s) = Q(s)\, B^{\{s\}} \qquad \text{(F-10)}$$

where $Q(s)$ is a T -periodic $n \times n$ non-singular matrix and $Q(0) = I_n$.

Conversely, if $\Omega(s)$ is defined by (F-10) with a T -periodic $Q(s)$ and a constant B,

$$\begin{aligned}\Omega(s+T) &= Q(s+T)\,B^{\{sB+TB\}} \\ &= Q(s)\left[B^{\{sB\}}\;B^{\{TB\}}\right] \\ &= \Omega(s)\,B^{\{TB\}} \\ &= \Omega(s)\,\Omega(T)\end{aligned} \tag{F-11}$$

Thus, any $\Omega(s)$ of the form in (F-10), solves (F-6) and is matrizant of some equation with the form of (F-2) with T -periodic $A(s)$.

This proves a special case of the Floquet-Lyapunov Theorem:

Theorem: $\Omega(s)$ is the matrizant of (F-2) if and only if $\Omega(s)$ is of the form of (F-10), where $Q(t)$ is a T -periodic $n \times n$ non-singular continuous matrix function with integrable piecewise-continuous derivative and such that $Q(0) = I_n$, and B is a constant $n \times n$ matrix.

The above theorem can be rephrased so as to refer to any arbitrary full-rank fundamental matrix $\delta Z_1(s)$ of (F-3) $\left(n = m, \delta Z_1(0) \neq I_n, \det \delta Z_1(0) \neq 0\right)$. We have:

$$\begin{aligned}\delta Z_1(s) &= \Omega(s)\,\delta Z_1(0) \\ &= Q(s)\,B^{\{s\}}\;\delta Z_1(0) \\ &= \left[Q(s)\,\delta Z_1(0)\right]\left[\delta Z_1(0)^{-1}\;B\;\delta Z_1(0)\right]^{\{s\}}\end{aligned} \tag{F-12}$$

Thus,

$$\delta Z_1(s) = Q_1(s)\,B_1^{\{s\}} \tag{F-13}$$

where

$$Q_1(s) = Q_1(s+T) = Q(s)\,\delta Z_1(0)$$
$$B_1 = \delta Z_1(0)^{-1}\; B\; \delta Z_1(0) \qquad \text{(F-14)}$$

So the above theorem is true for any fundamental matrix $\delta Z_1(s)$. Elaborating on (F-12), for a set of vectors as columns of $\delta Z_1(0)$, we have:

$$\begin{aligned}\delta Z_1(s) &= Q(s)\, B^{\{s\}}\; \delta Z_1(0) \\ &= Q(s)\, B^{\{T\}\frac{s}{T}}\; \delta Z_1(0) \\ &= Q(s)\, \Omega(T)^{\frac{s}{T}}\; \delta Z_1(0)\end{aligned} \qquad \text{(F-15)}$$

In particular, at $s = kT$,

$$\begin{aligned}\delta Z_1(kT) &= Q(kT)\, \Omega(T)^k\, \delta Z_1(0) \\ &= Q(0)\, \Omega(T)^k\, \delta Z_1(0) \\ &= \Omega(T)^k\, \delta Z_1(0)\end{aligned} \qquad \text{(F-16)}$$

Therefore, propagation of any arbitrary set of vectors, $\delta Z_1(0)$, in the system of (F-2) will be according to (F-16) and all we need to know is $\Omega(T)$, the monodromy matrix.

6.7 References

Anderson, J. L., B. Wyman, S. Zhang, and T. Hoar, 2005: Assimilation of surface pressure observations using an ensemble filter in an idealized global atmospheric prediction system. *J.*

Atmos. Sci., **62**, pp 2925-2938.

Daley, R., 1991: *Atmospheric Data Analysis*. Cambridge University Press, UK, p 457.

Fillion, L., 2002: Variational Assimilation of precipitation data and gravity wave excitation. *Mon. Wea. Rev.*, **130**, pp 357-371.

Fisher, M., 2002: Assimilation techniques (2-5): Approximate Kalman filters and singular vectors. *Meteorological Training Course Lecture series, ECMWF*.

Gauthier, P., and J. N. Thépaut, 2001: Impact of the digital filter as a weak constraint in the preoperational 4DVAR assimilation system of Météo-France. *Mon. Wea. Rev.*, **129**, pp 2089-2102.

Henon, M., 1976: A two-dimensional mapping with a strange attractor. *Comm. Math. Phys.*, **50**, pp 69-77.

Jaeger, L., and H. Kantz, 1997: Homoclinic tangencies and non-normal Jacobians - Effects of noise in non-hyperbolic chaotic systems. *Physica D*, **105**, pp 79-96.

Kraut, S., and C. Grebogi, 2004: Escaping from nonhyperbolic chaotic attractors. *Phys. Rev. Lett.*, **92**, number 23, 234101.

Molteni, F., R. Buizza, T. N. Palmer, and T. Petroliagis, 1996: The new ECMWF ensemble prediction system: Methodology and Validation. *Quart. J. Roy. Meteor. Soc.*, **122**, pp 73-119.

Neef, L. J., S. M. Polavarapu, T. G. Shepherd, 2006: Four-dimensional data assimilation and

balanced dynamics. *J. Atmos. Sci.*, **63**, pp 1840-1858.

Rabier, F., J. F. Mahfouf, M. fisher, H. Järvinen, A. Simmons, E. Andersson, F. Bouttier, P. Courtier, M. Hamrud, J. Haseler, A. Hollingsworth, L. Isaksen, E. Klinker, S. Saarinen, C. Temperton, J-N. Thépaut, P. Undén, and D. Vasiljević, 1997: Recent experimentation on 4dVar and first results from a Simplified Kalman Filter. *ECMWF Tech. Memo. 240.*

Robert, C., K. T. Alligood, E. Ott, and J. A. Yorke, 2000: Explosions of chaotic sets. *Physica D*, **144**, pp 44-61.

Saad, Y., 1992: *Numerical methods for large eigenvalue problems*. Manchester University Press, UK, pp 183-185.

Schroer, C. G., E. Ott, and J. A. Yorke, 1998: Effect of noise on nonhyperbolic chaotic attractors. *Phys. Rev. Lett.*, **81**, pp 1397-1400.

Wee, T. K., and Y. H. Kuo, 2004: Impact of a digital filter as a weak constraint in MM5 4DVAR. *UCAR COSMIC Project*, Boulder, USA.

Yakubovich, V. A. and V. M. Starzhinskii, 1975: Linear differential equations with periodic coefficients, *John Wiley & Son Inc.*, New York, USA, pp 70-91.

6.8 Figures

Figure 6-1: Henon attractor (cyan) and its basin of attraction (white), with parameters $(a,b) = (1.4,0.3)$. Ensemble members without dynamic model error (black) remain on the attractor. Same initial ensemble members follow different trajectories with dynamic model error; some leave the basin of attraction within 10 time steps (red), while the rest still converge (blue).